

REPORT DOCUMENTATION PAGE			Form Approved OMB NO. 0704-0188		
<p>The public reporting burden for this collection of information is estimated to average 1 hour per response, including the time for reviewing instructions, searching existing data sources, gathering and maintaining the data needed, and completing and reviewing the collection of information. Send comments regarding this burden estimate or any other aspect of this collection of information, including suggestions for reducing this burden, to Washington Headquarters Services, Directorate for Information Operations and Reports, 1215 Jefferson Davis Highway, Suite 1204, Arlington VA, 22202-4302. Respondents should be aware that notwithstanding any other provision of law, no person shall be subject to any penalty for failing to comply with a collection of information if it does not display a currently valid OMB control number.</p> <p>PLEASE DO NOT RETURN YOUR FORM TO THE ABOVE ADDRESS.</p>					
1. REPORT DATE (DD-MM-YYYY) 15-04-2013		2. REPORT TYPE Final Report		3. DATES COVERED (From - To) 1-Jan-2012 - 31-Dec-2012	
4. TITLE AND SUBTITLE Novel Task Functionalized Biopolymers for Enhanced Change Detection in Support of C-IED Operations			5a. CONTRACT NUMBER W911NF-12-1-0033		
			5b. GRANT NUMBER		
			5c. PROGRAM ELEMENT NUMBER 1620BP		
6. AUTHORS Gary M. Nijak Jr., Jeffrey W. Talley			5d. PROJECT NUMBER		
			5e. TASK NUMBER		
			5f. WORK UNIT NUMBER		
7. PERFORMING ORGANIZATION NAMES AND ADDRESSES SecureNet, LLC SecureNet, LLC 75 W. Baseline Rd, Ste 32 Gilbert, AZ 85233 -			8. PERFORMING ORGANIZATION REPORT NUMBER		
9. SPONSORING/MONITORING AGENCY NAME(S) AND ADDRESS(ES) U.S. Army Research Office P.O. Box 12211 Research Triangle Park, NC 27709-2211			10. SPONSOR/MONITOR'S ACRONYM(S) ARO		
			11. SPONSOR/MONITOR'S REPORT NUMBER(S) 60778-CH-DRP.1		
12. DISTRIBUTION AVAILABILITY STATEMENT Approved for Public Release; Distribution Unlimited					
13. SUPPLEMENTARY NOTES The views, opinions and/or findings contained in this report are those of the author(s) and should not be construed as an official Department of the Army position, policy or decision, unless so designated by other documentation.					
14. ABSTRACT A novel fluorophore tagged exopolysaccharide (TEPS) was developed, synthesized, and tested for its potential implications toward locating Improvised Explosive Device (IEDs). Our TEPS exhibited unique and substantial properties that lend well to current change detection processing techniques and allows for significantly improved detection of objects implanted into the natural landscape. When coupled with a novel image processing package, or Automated Disturbance Detection System (ADDS), that automatically processes images, and creates a map of areas					
15. SUBJECT TERMS Change Detection, Counter IED, Polymers, IED, Automation Software					
16. SECURITY CLASSIFICATION OF:			17. LIMITATION OF ABSTRACT UU	15. NUMBER OF PAGES	19a. NAME OF RESPONSIBLE PERSON Gary Nijak, Jr.
a. REPORT UU	b. ABSTRACT UU	c. THIS PAGE UU			19b. TELEPHONE NUMBER 000-000-0000

## Report Title

Novel Task Functionalized Biopolymers for Enhanced Change Detection in Support of C-IED Operations

### ABSTRACT

A novel fluorophore tagged exopolysaccharide (TEPS) was developed, synthesized, and tested for its potential implications toward locating Improvised Explosive Device (IEDs). Our TEPS exhibited unique and substantial properties that lend well to current change detection processing techniques and allows for significantly improved detection of objects implanted into the natural landscape. When coupled with a novel image processing package, or Automated Disturbance Detection System (ADDS), that automatically processes images, and creates a map of areas of interest (AOIs) that relate to the detection of a hidden object, TEPS has shown great success. For example, in pilot scale field testing it was able to accurately and automatically identify large (larger than 12”) implanted devices nearly 100% of the time and smaller objects (between 1” and 12”) 87.5% of the time from an aerial platform. Furthermore, the system only falsely detected one terrestrial disturbance for every fourteen that it correctly identified. An additional benefit of our TEPS system is that its computational requirements will be about 75% less than comparable systems because computationally intense preprocessing algorithms are unnecessary. The combined TEPS and ADDS technologies can rapidly produce maps of AOIs, which would ultimately allow for greater and safer movement of troops in dangerous areas.

---

**Enter List of papers submitted or published that acknowledge ARO support from the start of the project to the date of this printing. List the papers, including journal references, in the following categories:**

**(a) Papers published in peer-reviewed journals (N/A for none)**

Received

Paper

**TOTAL:**

**Number of Papers published in peer-reviewed journals:**

---

**(b) Papers published in non-peer-reviewed journals (N/A for none)**

Received

Paper

**TOTAL:**

**Number of Papers published in non peer-reviewed journals:**

---

**(c) Presentations**

**Number of Presentations:** 0.00

**Non Peer-Reviewed Conference Proceeding publications (other than abstracts):**

<u>Received</u>	<u>Paper</u>
1	1
2	2
3	3
4	4
5	5
6	6
7	7
8	8
9	9
10	10
11	11
12	12
13	13
14	14
15	15
16	16
17	17
18	18
19	19
20	20
21	21
22	22
23	23
24	24
25	25
26	26
27	27
28	28
29	29
30	30
31	31
32	32
33	33
34	34
35	35
36	36
37	37
38	38
39	39
40	40
41	41
42	42
43	43
44	44
45	45
46	46
47	47
48	48
49	49
50	50
51	51
52	52
53	53
54	54
55	55
56	56
57	57
58	58
59	59
60	60
61	61
62	62
63	63
64	64
65	65
66	66
67	67
68	68
69	69
70	70
71	71
72	72
73	73
74	74
75	75
76	76
77	77
78	78
79	79
80	80
81	81
82	82
83	83
84	84
85	85
86	86
87	87
88	88
89	89
90	90
91	91
92	92
93	93
94	94
95	95
96	96
97	97
98	98
99	99
100	100

**TOTAL:**

---

**Number of Non Peer-Reviewed Conference Proceeding publications (other than abstracts):**

**Peer-Reviewed Conference Proceeding publications (other than abstracts):**

<u>Received</u>	<u>Paper</u>
-----------------	--------------

**TOTAL:**

**Number of Peer-Reviewed Conference Proceeding publications (other than abstracts):**

**(d) Manuscripts**

<u>Received</u>	<u>Paper</u>
1	1
2	2
3	3
4	4
5	5
6	6
7	7
8	8
9	9
10	10
11	11
12	12
13	13
14	14
15	15
16	16
17	17
18	18
19	19
20	20
21	21
22	22
23	23
24	24
25	25
26	26
27	27
28	28
29	29
30	30
31	31
32	32
33	33
34	34
35	35
36	36
37	37
38	38
39	39
40	40
41	41
42	42
43	43
44	44
45	45
46	46
47	47
48	48
49	49
50	50
51	51
52	52
53	53
54	54
55	55
56	56
57	57
58	58
59	59
60	60
61	61
62	62
63	63
64	64
65	65
66	66
67	67
68	68
69	69
70	70
71	71
72	72
73	73
74	74
75	75
76	76
77	77
78	78
79	79
80	80
81	81
82	82
83	83
84	84
85	85
86	86
87	87
88	88
89	89
90	90
91	91
92	92
93	93
94	94
95	95
96	96
97	97
98	98
99	99
100	100

**TOTAL:**

**Number of Manuscripts:**

## Books

<u>Received</u>	<u>Paper</u>
-----------------	--------------

**TOTAL:**

### Patents Submitted

POLYMERS AND TASK FUNCTIONALIZED POLYMERS FOR ENHANCED CHANGE DETECTION

---

### Patents Awarded

---

### Awards

---

### Graduate Students

NAME

PERCENT SUPPORTED

FTE Equivalent:

Total Number:

### Names of Post Doctorates

NAME

PERCENT SUPPORTED

FTE Equivalent:

Total Number:

### Names of Faculty Supported

NAME

PERCENT SUPPORTED

FTE Equivalent:

Total Number:

### Names of Under Graduate students supported

NAME

PERCENT SUPPORTED

FTE Equivalent:

Total Number:

### Student Metrics

This section only applies to graduating undergraduates supported by this agreement in this reporting period

The number of undergraduates funded by this agreement who graduated during this period: ..... 0.00

The number of undergraduates funded by this agreement who graduated during this period with a degree in science, mathematics, engineering, or technology fields:..... 0.00

The number of undergraduates funded by your agreement who graduated during this period and will continue to pursue a graduate or Ph.D. degree in science, mathematics, engineering, or technology fields:..... 0.00

Number of graduating undergraduates who achieved a 3.5 GPA to 4.0 (4.0 max scale): ..... 0.00

Number of graduating undergraduates funded by a DoD funded Center of Excellence grant for Education, Research and Engineering:..... 0.00

The number of undergraduates funded by your agreement who graduated during this period and intend to work for the Department of Defense ..... 0.00

The number of undergraduates funded by your agreement who graduated during this period and will receive scholarships or fellowships for further studies in science, mathematics, engineering or technology fields: ..... 0.00

### Names of Personnel receiving masters degrees

NAME

Total Number:

### Names of personnel receiving PhDs

NAME

Total Number:

### Names of other research staff

NAME

PERCENT SUPPORTED

FTE Equivalent:

Total Number:

### Sub Contractors (DD882)

### Inventions (DD882)

5 POLYERS AND TASK FUNCTIONALIZED POLYMERS FOR ENHANCED CHANGE DETECTION

Patent Filed in US? (5d-1) Y

Patent Filed in Foreign Countries? (5d-2) Y

Was the assignment forwarded to the contracting officer? (5e) N

Foreign Countries of application (5g-2): Israel, United Kingdom, Canada, Australia, Japan

5a: Gary M Nijak Jr

5f-1a: Environmental Technology Solutions

5f-c: 6793 W Willis Rd

Chandler AZ 85226

5a: Christopher Griggs

5f-1a: US Department of Army

5f-c:

5a: Steven Larson

5f-1a: US Department of Army

5f-c:

5a: Jeffrey W Talley

5f-1a: Environmental Technology Solutions

5f-c:

**Scientific Progress**

**Technology Transfer**

Novel Task Functionalized Biopolymers for Enhanced Change Detection  
in Support of C-IED Operations

Final Technical Report  
PI: Gary M. Nijak, Jr.  
Previous PI: Dr. Jeffrey Talley  
Environmental Technology Solutions LLC/SecureNet LLC  
Jan 2012-Dec 2012  
DARPA Grant W911NF121033

## Table of Contents

1. Abstract.....	3
2. Introduction .....	3
a. Statement of Need.....	3
b. Literature Review.....	4
c. Background Approach and Rationale .....	6
3. Synthesis of Novel TEPS Materials .....	8
d. Tag Selection .....	10
e. TEPS Synthesis-Tosylation Method 1 .....	11
f. TEPS Synthesis- Tosylation Method 2.....	13
g. TEPS Synthesis-Tosylation Method 3.....	13
h. TEPS Synthesis-Amination Method.....	13
i. TEPS Synthesis-Amination and Tosylation Method .....	13
j. TEPS Synthesis Results .....	14
4. Bench and Pilot Scale TEPS Testing.....	18
k. Small Plots- Rapid Testing and Set Up.....	18
l. Large Pilot Scale Plots .....	19
5. ADDS Development.....	20
n. Image Analyses .....	20
o. A-Forge.NET .....	22
p. Inaccuracy Vector Score .....	22
6. ADDS and TEPS Field Testing.....	24
7. Conclusion .....	31
8. References .....	33
9. Appendix .....	35
q. Appendix A- Cost Analysis of the Materials.....	35
s. Appendix C- Alternative Synthesis Method.....	36
t. Appendix D- Chemical Elucidation/Characterization .....	37
u. Appendix E- Small Plot Testing Results .....	41
w. Appendix F- Large Plot Testing Results.....	61



## 1. Abstract

A novel fluorophore tagged exopolysaccharide (TEPS) was developed, synthesized, and tested for its potential implications toward locating Improvised Explosive Device (IEDs). Our TEPS exhibited unique and substantial properties that lend well to current change detection processing techniques and allows for significantly improved detection of objects implanted into the natural landscape. When coupled with a novel image processing package, or Automated Disturbance Detection System (ADDS), that automatically processes images, and creates a map of areas of interest (AOIs) that relate to the detection of a hidden object, TEPS has shown great success. For example, in pilot scale field testing it was able to accurately and automatically identify large (larger than 12") implanted devices nearly 100% of the time and smaller objects (between 1" and 12") 87.5% of the time from an aerial platform. Furthermore, the system only falsely detected one terrestrial disturbance for every fourteen that it correctly identified. An additional benefit of our TEPS system is that its computational requirements will be about 75% less than comparable systems because computationally intense preprocessing algorithms are unnecessary. The combined TEPS and ADDS technologies can rapidly produce maps of AOIs, which would ultimately allow for greater and safer movement of troops in dangerous areas.

## 2. Introduction

### *a. Statement of Need*

Improvised explosive devices (IEDs) are the number one cause of death for United States troops in Afghanistan (Shaughness, 2012). As detection technologies have advanced, so have the approaches by enemy combatants to implant these devices. A simple pressure activated switch became a very effective tool utilized by combatants. The equivalent of a roller pin was developed to counter this, hoping to destroy a non-material portion of a convoy rather than the primary vehicle where soldiers were. In response to this, enemy combatants developed the delayed pressure activated explosive. When combatants came up with a way to remotely detonate charges using cellular technologies, the military implemented cellular jamming technologies. In response to this, short range communications were utilized that are not easily jammed. The perpetual game of cat and mouse has become an ordinary part of modern warfare.

This has left the military attempting to resolve the issue by several primary outlets: chemical detection of the explosive components of the IEDs, physical detection of the materials of construction of the IEDs, visual identification of the devices (which currently is tied to image processing analysis). All of these approaches require relatively close proximity to the devices. A recent development in IEDs is charge directed explosives where the enemy combatants predict the relative proximity of those trying to detect the devices and detonate the explosives in that direction. Approaching any type of explosive device unduly puts lives at risk. There is a need for the ability to remotely and autonomously detect devices that have been implanted.

Out of all of the detection modalities, only visual/image identification can detect and identify devices at long range stand-off conditions. Detection profiles of chemicals dissipates rapidly unless able to be identified by remote spectroscopic technologies (currently none of which exist) and physical measurements rely on either Infra Red (IR) or other analysis that are complex and require advanced signal processing. Current technologies require very robust amounts of data to be collected in the field, processed, and then analyzed. As computational

power increases, the amount of information that can be processed increases, but rapid advanced instruments in the future will only increase the amount of information collected to identify the device, resulting in a net zero gain in overall computational delivery effectiveness. Therefore, the military would greatly benefit from a technology that would rapidly and effectively detect terrestrial disturbances, remotely, using practical, cheap, and available platform mounted computational systems.

#### *b. Literature Review*

Most currently employed ADDSs comprise a complex variety of approaches with varying success rates (Wilson, 2006) and they are often cost prohibitive and achieve low success rates (Dekker, 2010). One growing area of research due to improved optics capability, computational processing and bandwidth, and algorithm development is aerial, remote change detection. Processes such as ground penetrating radar (Ma, 2007), as well as image change analysis in novel view synthesis (NVS) (Buchanan, 2009) are being examined in light of their ability to improve change detection in support of the C-IED fight. While these technologies represent some of the most advanced methods of change detection, their sensitivity is often less than desired and are subject to error due to natural and man-made changes to the monitored areas.

IED detection can be generally classified into four categories-

- 1) *Chemical Sensing*- sensing related to the explosive or components of manufacturing such as Gas Chromatographing
- 2) *Physical Sensing*- sensing related to the materials of construction such as metal detectors and more complex versions
- 3) *Image Change Detection*- comparison of images to determine difference and thus disturbance such as hyperspectral imaging or visual imaging
- 4) *Electromagnetic Detection*- variation on physical sensing where magnetic properties of metals are exploited for detection such as microwave detection of metals

All of these can be effective within known limitations. Standoff detection is generally poorer in chemical sensing, and strongest in image change detection, but image change detection is currently limited by the realities of technology and computational power. Any addition of new platforms to the currently utilized arsenal of sensors on mobile units in the military will likely prevent the use of a technology unless sufficient justification exists. Current platforms on mobile units do include imaging technologies and IR (thermal) sensing technologies. Use of current platforms would more rapidly and effectively ensure utilization of any newly developed technologies.

All Optronics, LLC of Tucson, AZ received a Small Business Innovation Research (SBIR) grant to develop dispersed fluorescent compounds to detect IEDs. The project showed much promise, but there was no mention in the report about how to maintain the compounds in the natural environment for extended periods of time (SBIR, 2004). Lockheed Martin attempted to use fluorescent-tagged antibodies to detect trace levels of certain explosives (Stevens et al., 2012). This particular project falls under the ‘chemical sensing techniques’ and because of the complexity and the lack of ruggedness of these systems, they are practically useless. A patent granted in 2010 discloses the use of hyperspectral imagery and lasers to identify implanted IEDs,

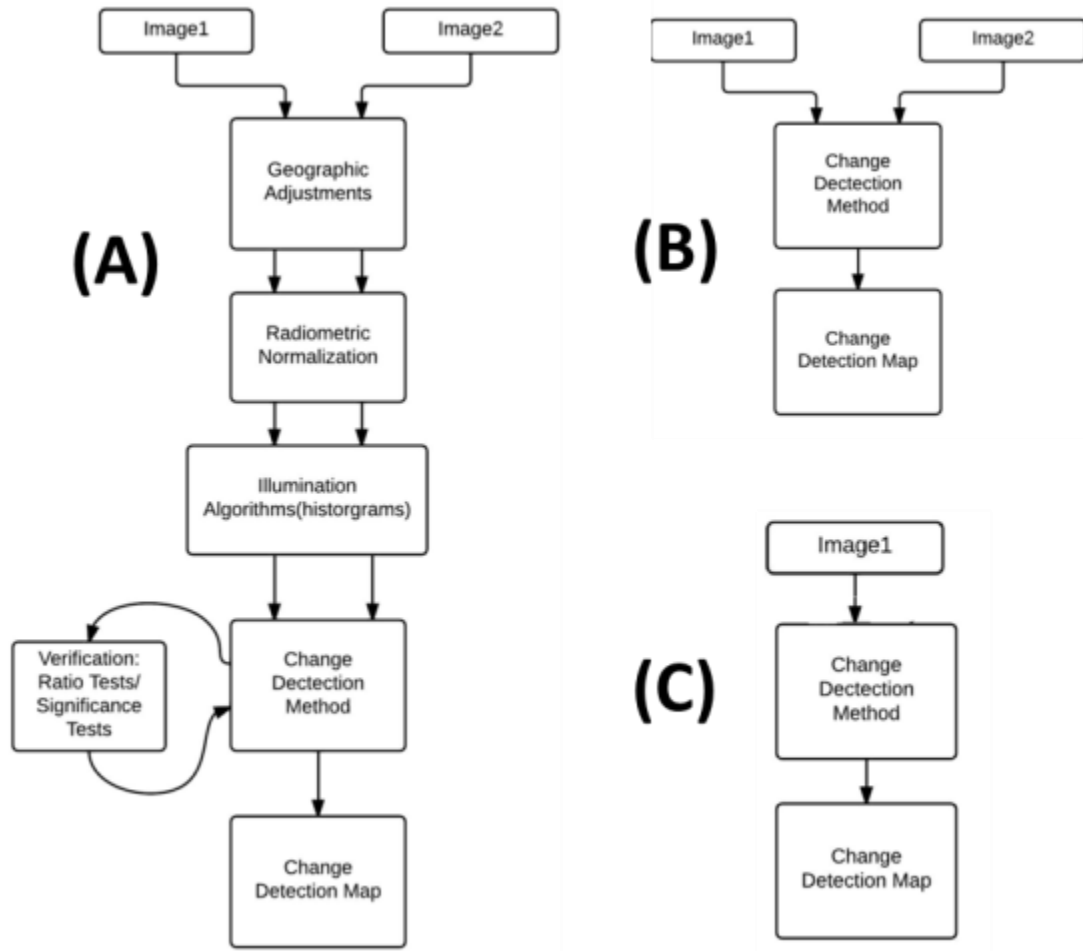
but the resolution is limited by the scanning rate of the laser and the collection of the incident light from the reflection of the laser on the AOI (Treado et al., 2010).

One method to improve these processes could be by the novel use unique, artificial ground surfaces and signatures. These signatures can mitigate natural environmental changes that make detection difficult, and help create uniform surfaces where disturbances are readily identifiable. These polymers possess the ability to assist in a number of device detection modalities such as radar (Coderre and Smith, 2008), ground penetrating radar (Davy et al., 2006) and Light Detection and Ranging (LIDAR) (Binstock and Minukas, 2010). The changes between two images that might correspond to a small implanted device are not significant enough to withstand the litany of environmental factors that might also introduce natural changes between images. Pre-alignment and pre-processing filters, currently necessary in ADDSs, require significant calculations before a pair of corresponding pixels can be compared between images. Various methods for pre-alignment and pre-processing include normalization, homographic filtering, illumination modeling and linear transformation modeling. These cumbersome preprocessing calculations prevent widespread implementation of ADDSs in the C-IED field. *Preprocessing Algorithms* commonly employed to suppress or filter insignificant image aberrations before detecting actual significant change, include:

- A. *Geometric Adjustments* –filters out camera movement, aligns images in to same coordinate frame. -
- B. *Intensity Adjustments* - Attempt to pre-compensate for illumination variations between images. (not always in preprocessing Algorithms)
  - i. *Methods*
    - a. Normalization
    - b. Homographic Filtering
    - c. Illumination Modeling
    - d. Linear transformation Modeling

One way to eliminate the need for preprocessing algorithms in ADDSs is to convert the image to a Lambertian Surface, which is one that appears to have a similar reflective light intensity regardless of the angle and direction from which the surface is observed. The process converts surfaces with significant contour and depth into planar, two-dimensional (2D) objects. A Lambertian Surface has particular known qualities by which it can be analyzed. Furthermore, if it is a homogeneous layer, i.e. consisting of only one light intensity or color that has a uniform and equal distribution, any modification to that surface results in an easily distinguishable feature that indicates change. This creates an artificial background with known parameters. This significantly reduces any computations required. Rather than looking for small changes in a complex image that has been processed, modified and converted into a quasi 2D image, rather than a 3D surface, a Lambertian Surface *is* a 2D surface and modifications to that surface are distinct, simple, and easy to detect.

The only currently utilized method to achieve a Lambertian surface is through enrichment of the soil by using IR emitting compounds, generally trace metals from the actinide or lanthanide series. Use of these metals causes long-term liability and environmental issues, due to very high acute toxicity levels, and they are expensive. A cheap, non-toxic material that can achieve more effective results would be ideal.



**Figure 1.** (A) Image change detection processing(B) Elimination of background noise and environmental factors (C) Creation of a homogeneous Lambertian Surface in the natural environment

### *c. Background Approach and Rationale*

Explosive devices are hidden in a variety of locations; under other objects, in the road, on the shoulders of roads, behind bushes- the locations are endless. In remote areas devices are hidden in the surrounding soil of areas of interest. It is often in these areas that convoy routes are restricted in their movement by the time it requires route clearance teams to certify that a particular stretch of road is safe to travel. This can significantly slow the advance of supplies and rations necessary to advance a mission. Best available technologies require painful step-by-step clearance of areas by a variety of means. Automating IED detection would tremendously increase the speed of clearance and a route clearance team to rapidly move from one AOI to another.

Because of the limitations associated with image change detection, several materials were tested for their impact on current change detection techniques, and a novel material was conceptualized, developed, and tested properties that approximate a homogenous Lambertian

surface. Several commercially available materials were selected that have known cohesive properties to the soil matrix and could provide at a minimum a homogeneous layer that would resist environmental factors such as wind and weather related phenomena. Because of this need for an effective system to endure harsh environmental factors, this project focused on materials already used for soil stabilization and erosion control. Of the commercial synthetic polymers currently available, only a few have functional properties that allow them to be readily chemically modified. Several factors were considered in selecting polymeric material to be tagged for use in an ADDS;

- 1) It must be functional in the natural environment for soil stabilization
- 2) It must be chemically modifiable while maintaining its soil stabilization properties
- 3) It must be non-toxic and pose no ongoing environmental hazards
- 4) It must be readily identifiable by spectroscopic techniques while maintaining its soil stabilization properties

Three materials were identified that warranted further investigation- 1) chitosan, a highly functional, widely available naturally produced biopolymer extracted from the shells of shellfish, 2) EPS produced by a soil bacterial species, *Rhizobium tropici*(RTEPS) and 3) polyacrylamide, a synthetic polymer that is considered the standard for soil stabilization. Chitosan and polyacrylamide were tested in their native form and RTEPS was chemically conjugated to an optical tag that may allow for the creation of a homogenous Lambertian Surface. Chitosan, while an interesting natural biopolymer, has bio-pesticidal properties and has regulated use in the natural environment (EPA, 2001). It was tested as a baseline material but no further modifications to the material we performed. Polyacrylamide (PAM) was tested as a baseline for conventional soil stabilization materials but this material again has known toxicities, especially if there are unpolymerized monomeric units (Ortiz et al., 2000). Generally these PAM materials are stable, but their tremendous stability in the natural environment means that they have extremely long degradation timeframes. As such, these materials were tested but no further modification to the commercially available materials was performed.

*R. tropici* is a catalogued symbiotic nodulator of leguminous plants, such as *Phaseolus vulgaris* L. (common beans) and *Leucaena spp.* trees, and it is known for its excessive production of gel-like, RTEPS (Dudman et. al, 1983a, Dudman et. al, 1983b, Franzén et. al, 1983). The natural functions of the EPS include adhesion between bacterial cells (biofilms), adhesion between bacterial cells and plant root nodules, water retention and nutrient accumulation around roots (Laspidou and Rittmann, 2002). Because *R. tropici* produces excessive amounts of biopolymer, it can be produced relatively quickly and cost effectively on a large scale and its chemical properties make it an ideal candidate for use in an ADDS. A method of RTEPS production was developed in collaboration with the United States Army Corps of Engineers that produced a highly functional RTEPS which formed a cross-linked, soil matrix that was exceptionally stable.

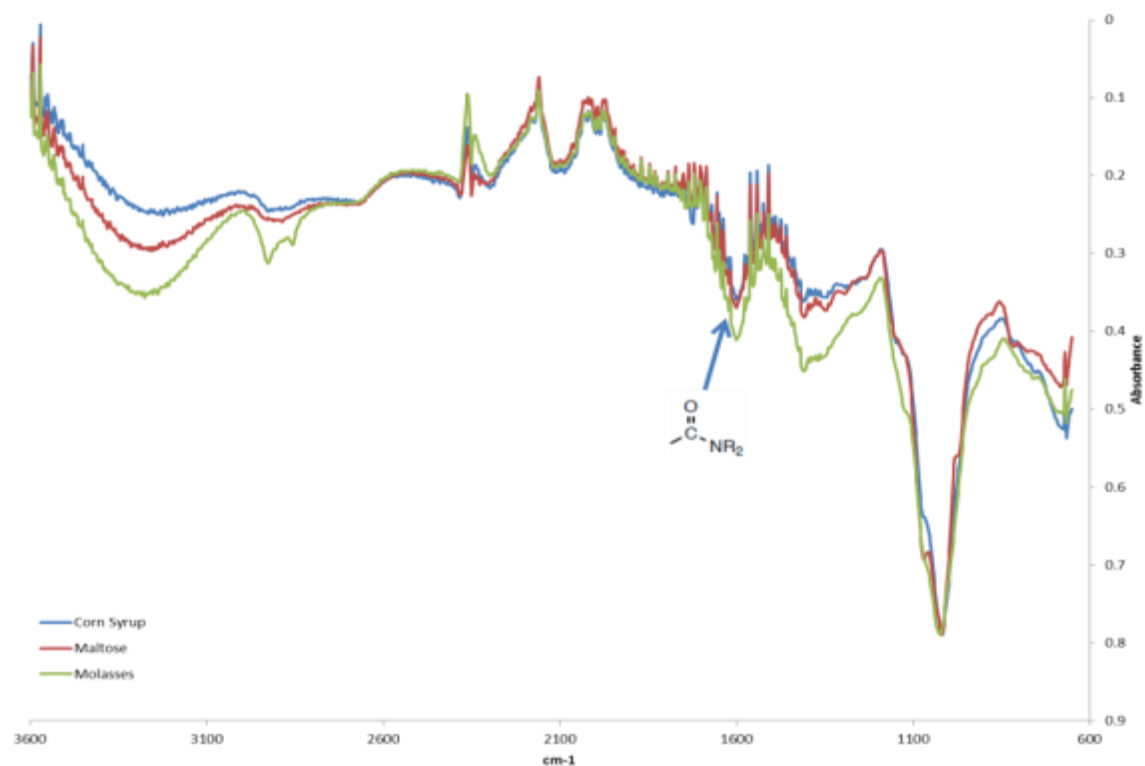
RTEPS has gained attention for its unique chemical and structural properties that are potentially beneficial in numerous applications. As mentioned, it can act as a soil stabilizing agent, with application to dust suppression and erosion control. In the context of this project, RTEPS has a number of uniquely useful qualities. Among the most significant of these is its heterogeneous structure that includes amine groups that can be conjugated to fluorescent tags which can potentially create homogeneous Lambertian surfaces. Additionally, because RTEPS

is produced by a living organism, its effects on the environment are potentially much less than other synthetic polymers traditionally used for these applications.

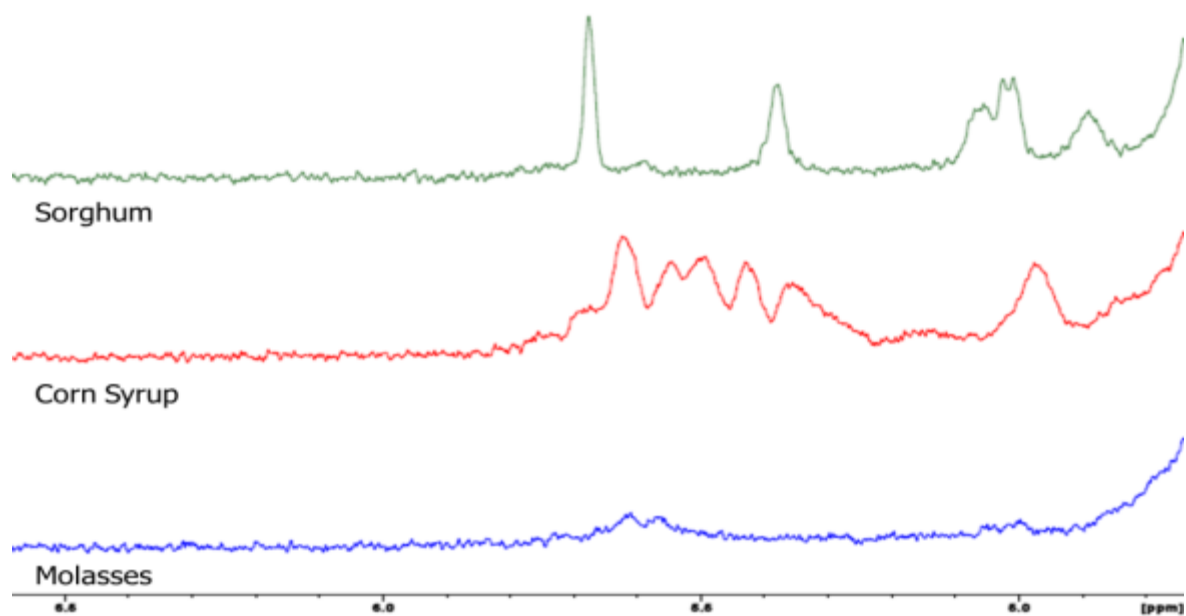
### 3. **Synthesis of Novel TEPS Materials**

RTEPS can be created by a variety of different reaction or fermentation processes that result in different RTEPS chemical structures and nutrient input is the reaction process that seems to have the greatest impact. For example, three different versions of the RTEPS were synthesized from three different carbon sources; molasses, corn syrup, and sorghum. Of these, the molasses-based RTEPS was the most effective on a variety of levels, including its ability to bind to and stabilize soil matrix.

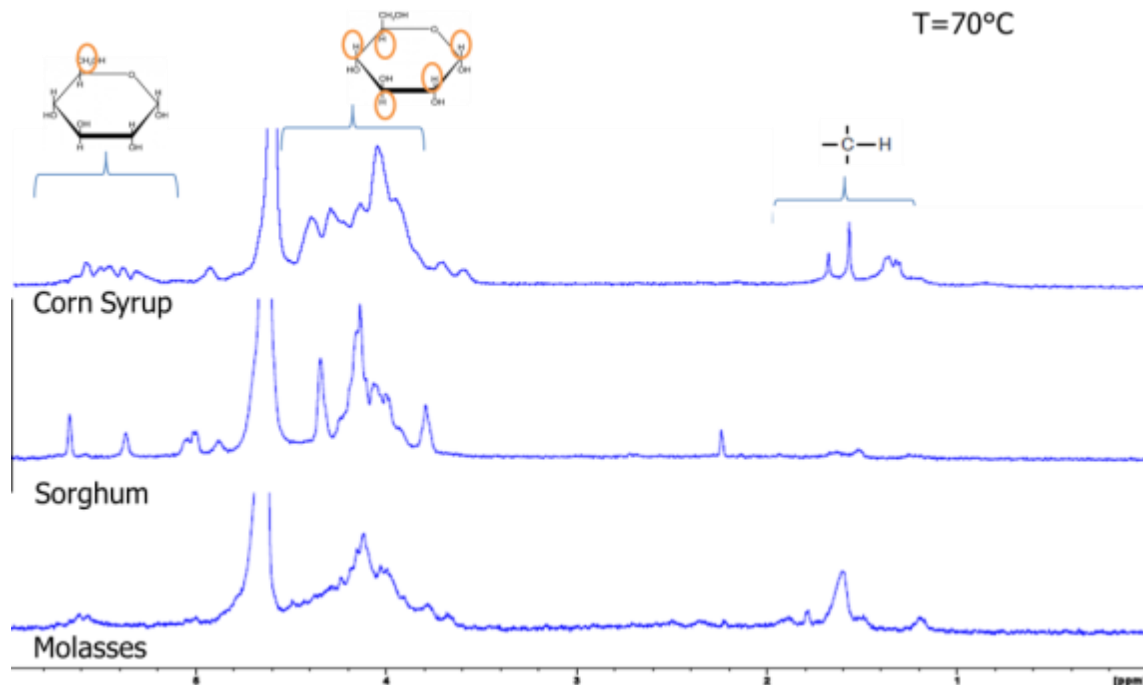
The molasses based biopolymer also appeared to have the greatest ability to be chemically modified, toward the formation of a TEPS, while still maintaining its bulk soil properties. Fourier Transform Infrared Spectroscopy (FT-IR) spectra were obtained with the use of an attenuated total reflectance unit for solid-state analysis for the infrared region from 3600-600  $\text{cm}^{-1}$ . Functional group stretches and peaks observed through these analyses include: hydroxyl groups stretches (above 3300  $\text{cm}^{-1}$ ), carboxylic acid stretches (3000-3300  $\text{cm}^{-1}$ ), fully reduced carbon-hydrogen bond peaks (2850-2960  $\text{cm}^{-1}$ ), ketone carbonyl peaks (1710  $\text{cm}^{-1}$ ) and amide peaks (1650  $\text{cm}^{-1}$ ). Based on the monomeric units of the sugars utilized by the microbes, it was expected that there would be an abundance of alcohol and carboxylate groups and these expectations were confirmed by the FT-IR (Figure 2) and  $^1\text{H}$  NMR (Figure 3) analyses. Especially significant, and not as easily explained, is the observation that the molasses-based RTEPS has higher content of amine groups (FT-IR stretch near 1600  $\text{cm}^{-1}$ ), which endows this RTEPS with the most useful chemical properties. Additionally, the molasses-based biopolymer had significantly reduced moisture retention and soil binding properties, especially in soils that had higher clay contents, which further increased the utility of this RTEPS variant in this context. Therefore, the molasses-based RTEPS was used in all subsequent studies, so all further mention of RTEPS refers to the molasses-based form.



**Figure 2.** FT-IR spectra of RTEPS synthesized by *R. tropici* grown on different carbon sources: corn syrup (blue), maltose (red), and molasses (green).



**Figure 3.** Fingerprint region of <sup>1</sup>H NMR spectra of RTEPS synthesized by *R. tropici* grown on different carbon sources: sorghum (green), corn syrup (red) and molasses (blue).



**Figure 4.** Near field  $^1\text{H}$  NMR spectra of RTEPS produced by *R. tropici* grown on different carbon sources: corn syrup, sorghum, and molasses.

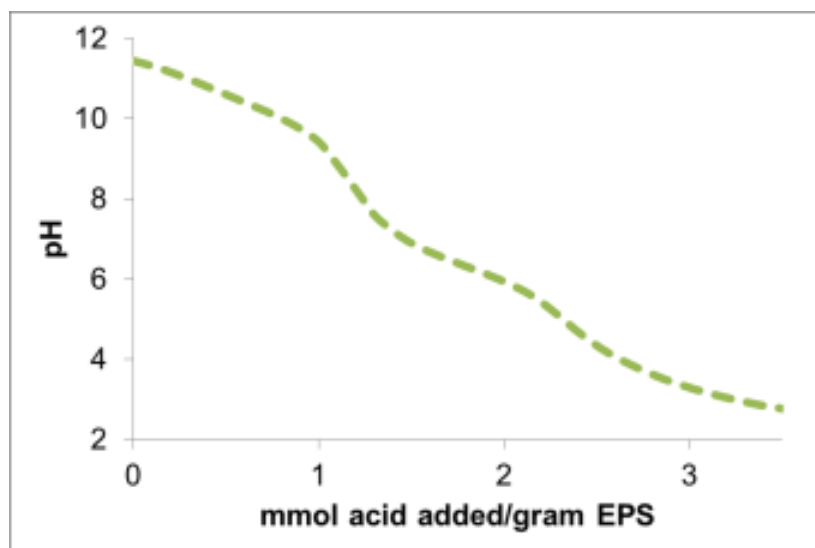
Several commercially feasible synthesis routes were tested to produce a fluorescently-labeled molasses-based RTEPS that would maintain its soil stabilization properties.

#### *d. Tag Selection*

A wide variety of fluorescent tags were identified because of their known optical properties and their relative ease of synthesis and chemical availability. Further, to this end, several types of tags were selected- those with brominated leaving groups that allowed for relative ease of synthesis of tags with alcohol groups or amine-based nucleophilic groups on the biopolymer. Many brominated, optically active compounds are commercially available and several of these were tested for reactivity with RTEPS.

Additionally, a modified titration of the biopolymer was performed to give an indication of how much fluorophore to utilize during the reaction process and to determine the relative basicity of the RTEPS. First, the pH of a purified RTEPS solution was raised to about 12.00, with NaOH, to fully deprotonate any functional groups that would be reactive at physiological pH, and then it was titrated with HCl. The results in Figure 5 demonstrate a  $\text{pK}_a$  at 6.30, which is similar to the basicity of imidazole and other physiological bases. The results of the titration also enabled determination of the concentration of RTEPS samples, such that the fluorescent tag could be added to RTEPS in quantities that were stoichiometrically equivalent to the number of reactive base molecules in the sample.





**Figure 5.** Titration curve of the native EPS material utilized in all of the tagged experiments

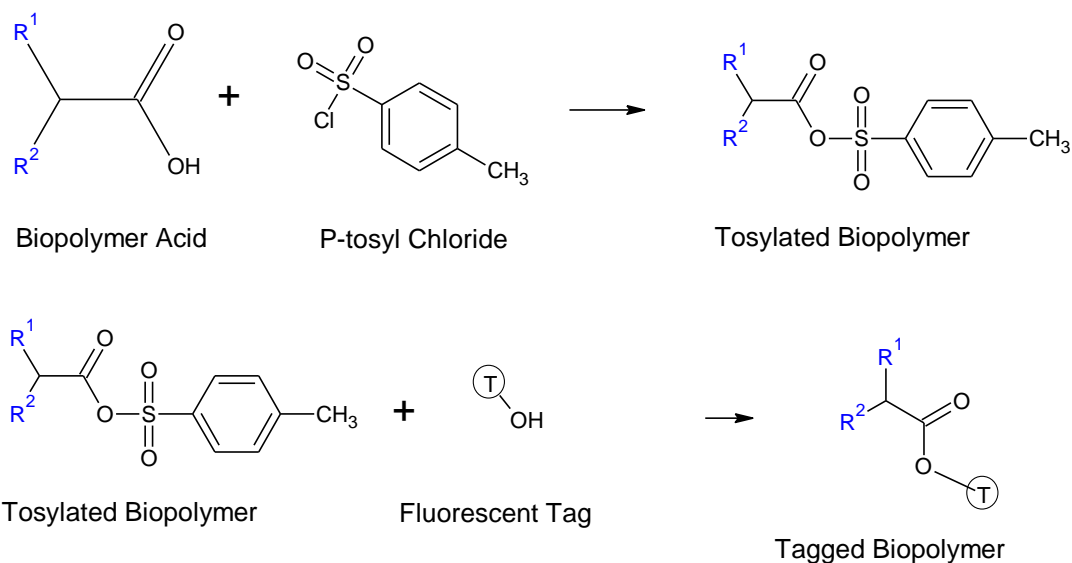
Tosylation of the amines is ideal because the carboxylate functionalities remain that allow the biopolymer to entrain in the soil matrix.

Three synthesis routes utilizing tosylation were performed, one route via amination, and one route that combined amination and tosylation. The native biopolymer was chemically characterized to determine how reaction mechanisms would proceed and from this the multiple routes were selected. While there is extensive work on synthesis of polymers, there is little work on functionalization of complex natural polymers. Because of this, synthesis routes were selected based upon closest available knowledge rather than known synthesis routes.

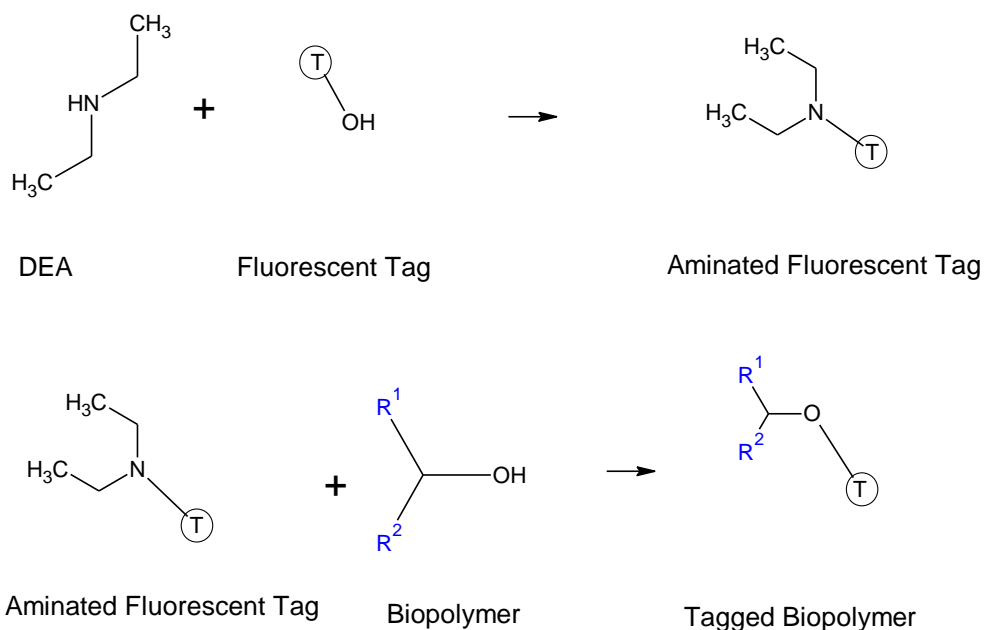
#### *e. TEPS Synthesis-Tosylation Method 1*

In a 100 mL beaker, 1 g of exopolysaccharide (EPS) biopolymer was dissolved in 40 mL of water. To this solution, 0.2 g of 4-toluenesulfonyl chloride (TosCl) was added and allowed to stir for at least 1 hour under low heating (60°C). To this mixture after allowing proper reaction of the EPS biopolymer, 0.4 g of 4-methylumbelliferone (MU) was added. This mixture was allowed to stir at elevated temperatures (60°C) for 3 hours. After this period the reaction was considered completed. The resultant products were washed with methylene chloride to remove the unreacted MU. After the material was washed, the aqueous phase was separated from the organic phase. To the aqueous phase 100 mL of alcohol was added. The resultant reactants precipitated out of solution. The precipitate was centrifuge and collected. The material was allowed to dry at low temperatures (40°C) for at least 24 hours. To utilize the material, it is resolubilized in water and then applied to soils.

To the collect aqueous phase 40 mL ethanol was added to the solution causing the functionalized biopolymer to precipitate out of the solution. Excess solvent was decanted and then the remaining sample was filtered and dried.



**Figure 6.** Mechanism by which the carboxylic portion of the biopolymer is tosylated with p-tosyl chloride (TosCl) then further functionalized with a fluorescent tag that contains a hydroxyl group. The resulting product is an optically tagged biopolymer.



**Figure 7.** Proposed reaction mechanism whereby the fluorescent tag is functionalized to make it more amenable towards functionalizing the biopolymer by attachment of a favorable leaving group and then reacted with the native biopolymer to result in a ether tagged fluorescent biopolymer

*f. TEPS Synthesis- Tosylation Method 2*

1 g of biopolymer was dissolved into 40 mL toluene. To this solution, 0.2 g of Tos was stirred in for 20 minutes. This was followed by 0.4 g MU. This mixture was allowed to stir with constant heating at 100°C for 8 hours. Once it had cooled to room temperature, the product was diluted with 40 mL ether. 50 mL of a 10% sodium bicarbonate solution was added to the solution, causing a phase separation. The aqueous phase was extracted twice with 20 mL of methylene chloride washes. Organic phase extracts were further dried over sodium sulfate and then solvent was evaporated off.

*g. TEPS Synthesis-Tosylation Method 3*

A 1 M NaOH solution was prepared and 1 g biopolymer was stirred into a 40 mL aliquot in a 250 mL beaker. After adding 0.2 g TosCl, the solution was stirred for 20 minutes. 0.4 g MU were added and the solution was chilled to 0°C while stirring for 1 hour. The temperature was raised to ambient and stirring occurred for another 3 hours. After the reaction had completed, the material was washed with methylene chloride. The aqueous phase is separated from the organic phase and to this is added 40 mL ethanol causing the functionalized biopolymer to precipitate out of the solution. Excess solvent was decanted and then the remaining sample was filtered and dried.

*h. TEPS Synthesis-Amination Method*

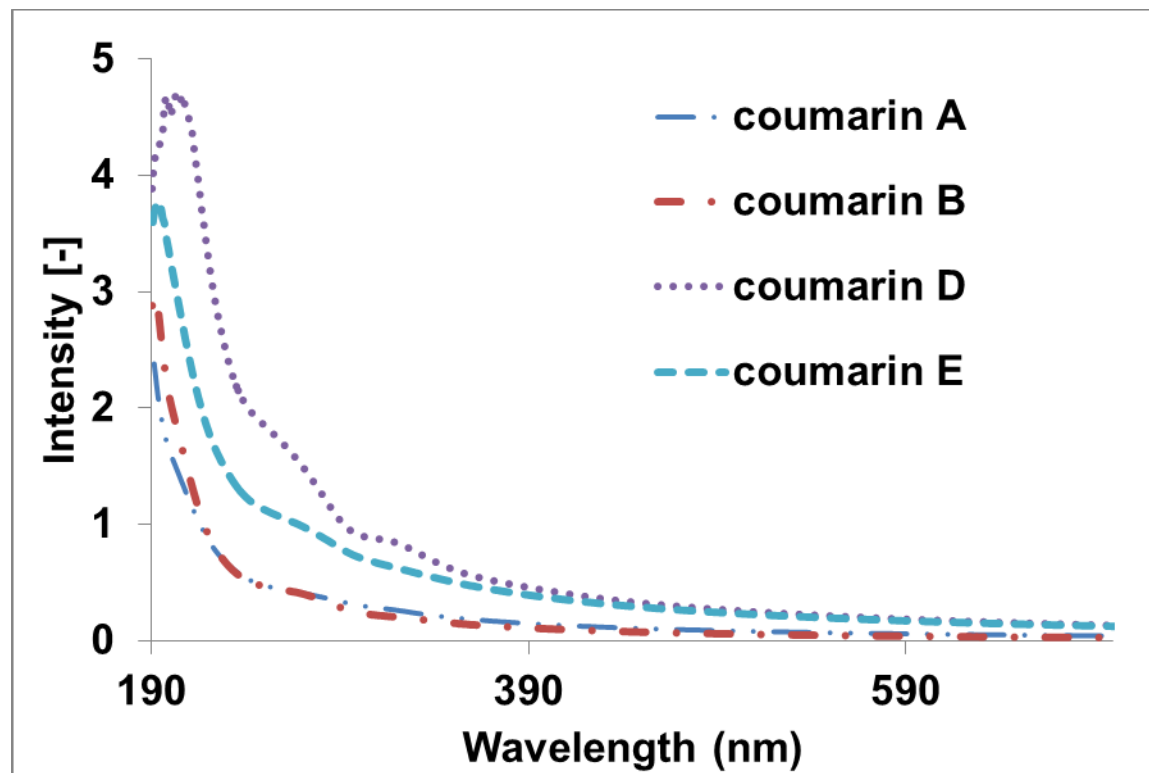
The purpose of this example is to demonstrate biopolymer functionalization through Amination. To 0.4 g of MU, 100 mL diethylamine (DEA) was added and allowed to react for an hour. After the fluorophore had been functionalized, 1 g biopolymer was added and stirred for several hours at an elevated temperature (60°C). After the reaction had completed, the mixture was washed with methylene chloride, the aqueous phase was collected and the resultant product was precipitated using 40 mL of ethanol. This results in a final functionalized biopolymer.

*i. TEPS Synthesis-Amination and Tosylation Method*

The purpose of this example is to demonstrate biopolymer functionalization through Amination and Tosylation. 40 mL of DEA were placed in a 100 mL beaker and 2.5 g biopolymer were dissolved into solution. This was stirred at 50°C for 1 hour, and then cooled to room temperature. In a 50 mL beaker, 5 g Tos were dissolved in 10 mL of water. This was added dropwise to the cooled solution. In a 250 mL beaker, 1 g MU was dissolved in 100 mL DEA. The two solutions were combined and stirred at 50°C for 1 hour. The product was allowed to cool to room temperature and then 100 mL. The resultant product was washed using benzene. The aqueous phase was collected. To this solution, ethanol was added to the solution causing the functionalized biopolymer to precipitate out of the solution. Excess solvent was decanted and then the remaining sample was filtered and dried.

### j. TEPS Synthesis Results

Analytical techniques such as  $^1\text{H}$  NMR show the attachment of the desired tags or compounds to the biopolymer spine by the reactions in Figures 6 and 7. For example, the proton signal at approximately 3ppm, in Figure 11, corresponds to a proton in the fluorophore in MU, the tag attached to the biopolymer spine by the reaction in Figure 7. Other variants of the tagged biopolymer were formed and verified by  $^1\text{H}$  NMR, IR and UltraViolet/Visible (UV/Vis) spectroscopies. The UV/Vis spectra of four of these variants are shown in Figure 8.



**Figure 8.** UV/Vis spectra of four coumarin-based brominated fluorophores after attachment to RTEPS.

All of the coumarin-based fluorophores exhibited significant fluorescence, individually, but when incubated with RTEPS under the conditions described above, all lost their ability to fluoresce. Determining which synthesized compounds would retain their spectroscopic properties was based on hypothesis and tested empirically. NMR techniques were used to verify the attachment of the particular tags. Several coumarin derivatives were tested due to their known fluorescence and wide range of commercial availability, but all but one of the fluorophores when attached to the EPS still exhibited fluorescence.

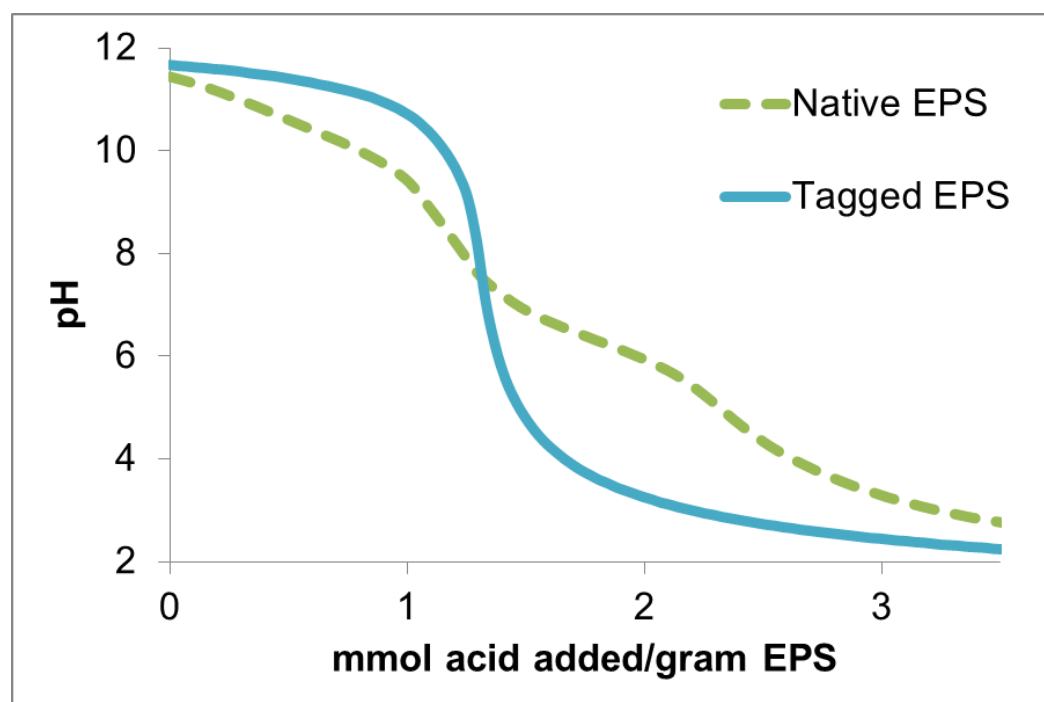
The MU-BP was further characterized with  $^{13}\text{C}$  NMR,  $^1\text{H}$  NMR, UV/Vis and FTIR spectroscopies. Magic-angle spinning NMR enabled solid state analyses of MU-BP.  $^1\text{H}$  NMR was utilized to identify glycoside bonds, which form the cross linkages in the RTEPS. saccharide molecules and had shifts in the range of 3-5 ppm. Alkyl carbon protons were identified at shift of

0.5-1.5 ppm, anomeric fingerprint proton shifts characteristic of polysaccharides were noticed from 3.3-4.8 ppm and extra-hemiacetal pyranosidic protons had a shift at 4.8-5.8 but were difficult to elucidated due to the solvent peak of water at approximately 4.8 ppm.

The tested halogenated coumarins have a rapid ease of synthesis and were confirmed via NMR but of the halogenated fluorophores tested they all lost their fluorescent properties once attached to the biopolymer spine. The most promising variant has involved tagging biopolymer with a functional bromine or iodine group on the coumarin but outside of the aromatic portion of the molecule. Additionally, other compounds such as fluorescein (another fluorescent ringed coumarin commonly used for fluorescence) and its derivatives can be utilized as optical tags. Since much of the tagged compound remains in a similar electronic state as compared to the non-tagged compound prior to chemical attachment, NMR readily and easily identifies synthesis of the desired compound.

$^{13}\text{C}$  NMR was used to identify major functionalities to be expected in the NMR of the materials of carbonylic carbon atoms at a shift of 170-190 ppm, Identification of carbon atoms contained in glycosidic linkages shifted at 100 ppm, Confirmation of functionalization through the elimination of carboxylic acid peaks at 140 ppm and the introduction of a sulfonyl peak from 60-65 ppm. Confirmation of processing steps through the liberation of amide moieties shown in peaks shifted from 20-30 ppm.

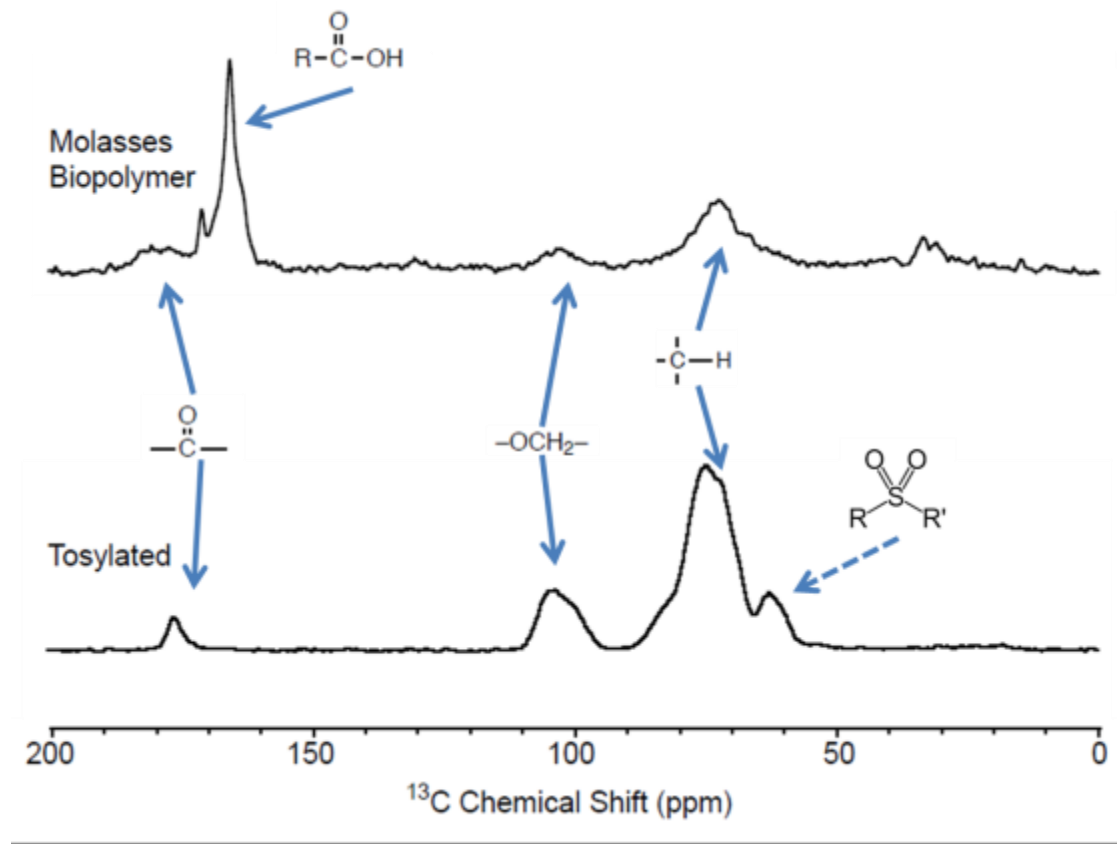
In the titration of the tagged EPS as compared to the native EPS, there is a modification of in equivalence points on the curve that shows the existence of a modified material (and successful modification of the native biopolymer with the optical tag).



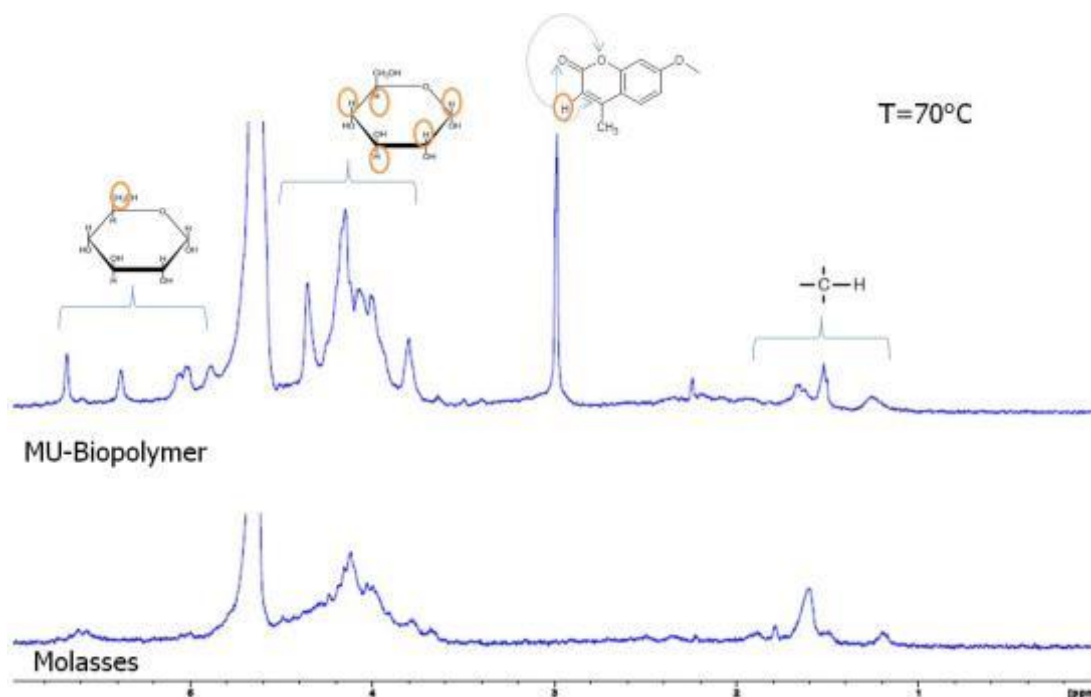
**Figure 9.** Comparison of the titration of the native EPS versus the EPS tagged with the fluorophore methylumbelliferyl (MU-RTEPS).

The MU biopolymer was the most promising TEPS material as it had the best reaction product (from a single pot synthesis), maintained fluorescent properties after synthesis and had fluorescent properties when applied to the soil. Many of the other materials failed to produce fluorescent properties when attached to the native EPS and some of the reaction products failed to properly attach to the biopolymer under the reaction conditions tested.

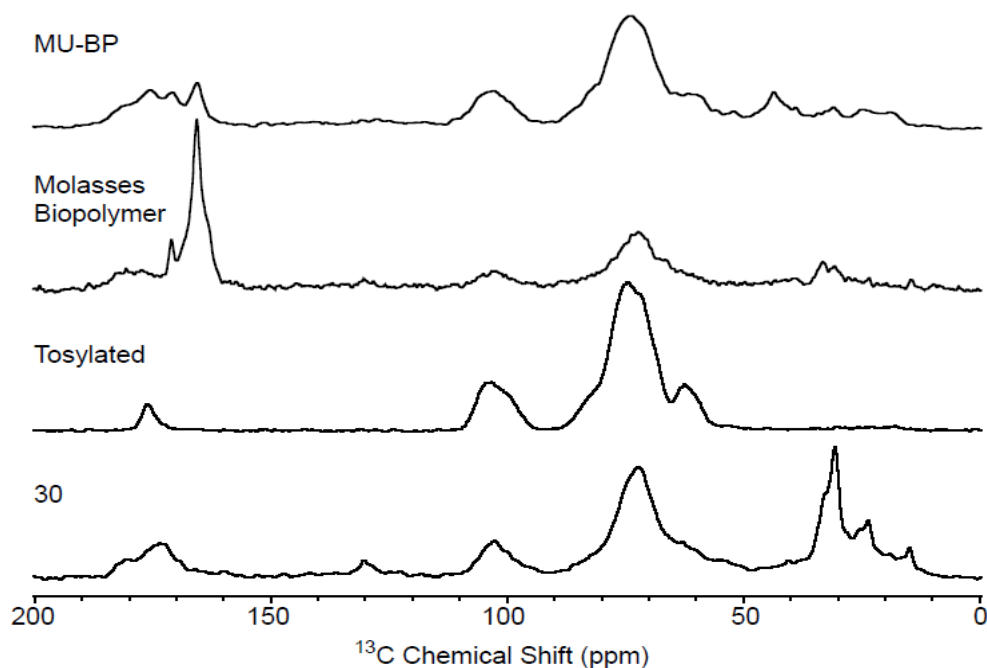
There are several readily identifiable differences between the two spectra of the native biopolymer and the MU-biopolymer (MU-BP or MU-EPS) including a distinct peak that corresponds to the proton in the fluorophore indicating successful and complete chemical synthesis of the MU-BP complex (Figure 11). Because of the optical features of the MU-BP complex and the relative ease of synthesis, this material was utilized in all further bench and pilot scale testing.



**Figure 10.**  $^{13}\text{C}$  NMR spectra of the molasses-based RTEPS before (above) and after tosylation (below).



**Figure 11.**  $^1\text{H}$  NMR spectra of the molasses-based native biopolymer and MU-BP



**Figure 12.** Comparison of four  $^{13}\text{C}$  NMR of varying materials, where MU-BP is the optically tagged native biopolymer with methylumbelliferyl, the fluorophore, the native molasses biopolymer, the tosylated biopolymer intermediate in a two step reaction process to synthesize the fluorescent tagged biopolymer, and a fractionated molasses biopolymer showing only the higher molecular weight biopolymers (labeled 30).

#### **4. Bench and Pilot Scale TEPS Testing**

Chemical synthesis of a variety of tagged biopolymer complexes resulted in one particular complex with the most desirable properties, a methylumbelliferone tagged biopolymer complex. This material exhibited fluorescent properties when applied to the soil and had a relatively minimal shift in its fluorescent properties when conjugated to the biopolymer. All other tested fluorophores lost their optical properties when conjugated and thus were not tested further. Additional compounds could be synthesized in the future but for the purposes of the proof of concept, only the MU conjugated biopolymer was tested.

All materials tested, PAM, chitin, the native biopolymer, and the MU conjugated biopolymer, were applied in small soil plots consisting of a variety of different types of soils. The soils tested were an Arizona soil (a clay sand type of soil), a clay with slight sand mixture, a loam mixture, and a sandy soil with minimal other materials. Each of these soils was tested to exhibit their varying properties. Some TEPS tests plots, because of time restrictions, used an unconjugated MU to demonstrate proof of concept. Optimization of the conjugated materials requires more extensive testing and development of materials that can be detected with less energy at long range detection.

PAM was applied to the soils at conventional soil stabilization rates derived from the erosion and soil stabilization industries (approximately 150 kg of PAM per acre). Rates for chitosan, since they were unknown, were tested at several application rates using a previously conducted soil stabilization study as a minimum amount and increasing the rate to determine if effectiveness could be achieved. The native biopolymer was tested at similar rates as chitosan, which were determined from complementary work that attempted to use the native biopolymer for dust control and soil erosion (Larson et al., 2012, Nijak, 2012).

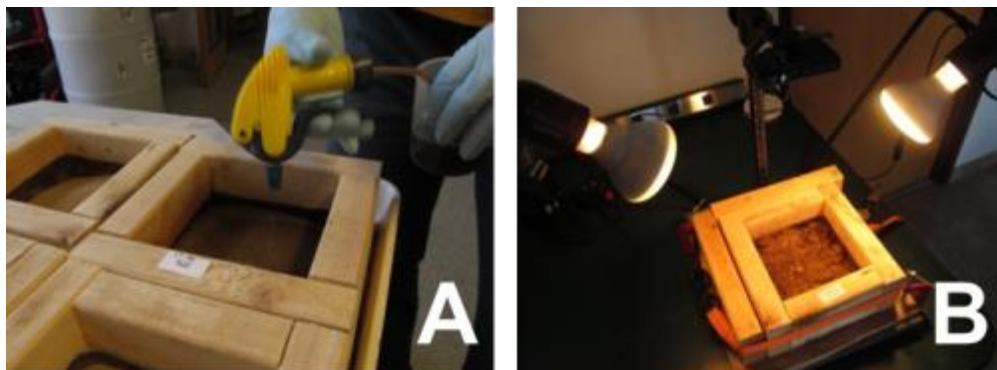
##### *k. Small Plots- Rapid Testing and Set Up*

After materials were applied to the test plot soils, a baseline image or pre-disturbance image was captured. The soils were then physically disturbed by implanting a metal disk. The disk was then covered up. The size of the disturbance was minimized to ensure that no more than 15% of the test plot was disturbed. The images were then compared to determine changes between the background and disturbed image and the accuracy of the automated detection system was monitored and optimized for each particular stabilization material.

Boxes sized 0.5 sq. ft were constructed and filled with 400 ml of a specific soil type (sand, silt, clay or loam). Each Soil amendment was tested at the application rates 50, 75, 100 and 150 kg/acre chitosan, PAM or TEPS to determine the minimal application rate that would produce images that were readable by our ADDS. 200 mL of each product was applied at the aforementioned rate in two steps. 100 mL was first applied evenly using a hand sprayer, the area was scarred and then the remaining 100 mL of solution was applied in the same manner.

Images were captured in an Illuminated Camera Stand (Figure 13) before and after a circular metal washer (0.75" diameter) was buried in it using a standard CCD array off-the-shelf camera. Photos of the un-tampered and tampered soil boxes were then analyzed to determine the location of the disturbances caused by implanting the objects.





**Figure 13.** (A) Soil amendments applied by hand to small test boxes for rapid test and comparisons between varying types of materials to be tested. (B) Stand utilized for base testing of a variety of materials in a controlled environment to develop an optimized score for disturbance.

### *1. Large Pilot Scale Plots*

Four raised soil plots were constructed that were approximately 9' x 9' filled with 10" of soil (Figure 14). Four soil types (sand, silt, clay and loam), one in each plot, were used to test the effectiveness of three soil amendments (native biopolymer, polyacrylamide and chitosan) and 5-MU in soil disturbance detection. Each of the four plots was separated into eight areas to test each of the four disturbance-detection compounds alongside a control (untreated) plot. Each of the amendments was applied at 125 kg/acre and MU-EPS was applied at 17 kg/acre (to simulate the 'effective' rate when conjugated to the biopolymer).

A large A-frame (Figure 14) was constructed to hold a wide angle camera 14 feet above the plot. An initial photo of the un-tampered plot was taken before 3-5 objects, varying in size from 1.25" x 1.25" to 12" x 6", were buried on each side for eight objects in total, four on each side. A final photo of the tampered plot was then taken. Photos of the un-tampered and tampered plots were then analyzed to determine the location of the disturbances caused by burying the objects. The location of objects was automatically determined by computer software developed during the rapid test plot research and compared against the known locations of the implanted materials. All materials were imaged during the daytime under natural light except for the UV tagged materials which were taken under a UV emitting bulb. Data for both sets of images were collected through the same camera. Further work should utilize a UV camera rather than a full spectrum CCD array. Most commercially available CCD based cameras have UV filters on the lenses to protect the array from unwanted damage, as did the camera utilized in this project.



**Figure 14.** Frame used to support aerial camera used to take photos of un-tampered and tampered soil plots. The size of the implanted or disturbed area could be modified to simulate detection at locations from 1 foot to 200 ft above the ground, depending on the implanted object size and distance of the A frame from the plots

## 5. ADDS Development

### *m. Approach and Rationale*

Current approaches to image comparison are typically focused on eliminating background noise and variability to align two images in an unspecified time series. Differences between these two images are calculated on a pixel by pixel basis and results in a change map. Generally the differences between the two images are relatively small so all pixels must be accounted for. Additionally, the amount of ‘pre-processing’ is a rate limiting step and is computationally intensive. Several methods were attempted- 1) a comparison with conventional detection techniques using image change analysis and optimized routines 2) simplified image change processing using histogram/blob counter analysis and 3) detection using a single image of optically modified material applied to the soil through the use of a homogeneous Lambertian surface.

### *n. Image Analyses*

The C# image comparison program was employed with Microsoft Visual Studios and an A-Forge.net library for computer vision and image analyses. The first step of the program was to detect differences between two images mark the differences between the two images, and generate a third image, the difference image. The difference map highlights each pixel that is different between pre and post disturbance images. After the change map was created, the shape of the change clusters was analyzed and interpreted using an A-forge.net edge detection and blobcount class counter). The third step was to score the performance of each amendment or 5-MU at producing a difference map with accurate detection of the hidden object. This latter step

was executed by comparing the location of the object predicted by the system with the actual location of the object as defined by the program user. Finally, the quantified features of interest in each difference map were loaded into the variables of the a feature vector, which calculated a final output score for the application. The magnitude represents accuracy of detection, where a smaller magnitude represents a better accuracy.

Given a pair of images “before” and “after” a disturbance, the system compares a pair of corresponding pixels. Each pixel contains a **R**ed, **G**reen and **B**lue (RGB) value. The differences between the RGB values are taken between the selected pixels. The sum of the new R, G and B values are then added together and stored in place holder  $S_{jk}$  with the original pixel location in  $j$  (x-location) and  $k$  (y-location).

As shown in Equation 1, the value of P1 represents the information value from image 1, while P2 holds the information value from image 2. A threshold value (T) is chosen for each soil amendment to accommodate the lighting, shadowing and angle differences in the difference image. This T is compared against each pair of before and after pixels. Pixel differences above the T are considered to be "different" and represent a tampered area of the plot (Figure 17C). The image comparison program then divides the images into sections and gives them a section number (W). A concentration ratio is created for each section of the image, and is defined as the number of "different" pixels divided by the total number of pixels in the section. If a section is found to have a ratio over the established concentration threshold (V) the different pixels within that section are considered to be "significantly different" (Figure 17D).

$$\text{Equation 1} \quad S_{jk} = (P1jkR - P2jkR) + (P1jkG - P2jkG) + (P1jkB - P2jkB) \quad (1)$$

When the sum of all pixel changes  $\sum S_{jk}$  is divided by the sum of all the pixels in the windows  $\sum P_{jk}$  it is compared against threshold value V. The T (threshold) is set by the user and determines how much change must be detected in the window before it declares the area as significant (Fig 15). The threshold value was optimized for each particular material that was tested to minimize the inaccuracy score. The optimized threshold values were determined in small box test and utilized through the rest of the testing. If the significance ratio is less than (V), a value of 0, meaning that the pixel differences are "non-significant", is assigned to the section. If the concentration ratio is greater than (V), a value of 1 is assigned to the section, meaning that the pixel differences in the section are "significant". Each ‘optimum’ threshold for each of the materials was determined by an optimization program that minimized the score obtained for each of the practice test boxes in ideal conditions.

$$\text{Equation 2} \quad B = \begin{cases} 0 & \text{if } \frac{\sum_w S_{jk}}{\sum_w P_{jk}} < V \\ 1 & \text{if } \frac{\sum_w S_{jk}}{\sum_w P_{jk}} > V \end{cases} \quad (2)$$

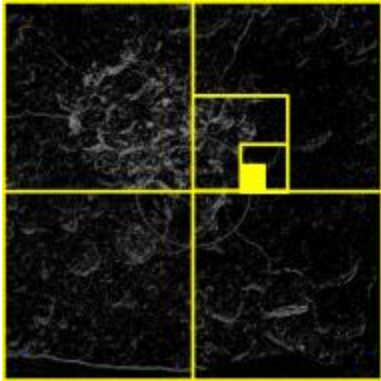
After the difference image was created, a midpoint formula was utilized on all "different" pixels marked as changed by taking the sum of the x and y locations and dividing by the total number of changed pixels. This midpoint calculates an approximate area of the tampered area. This is also used with all area marked as significant, but only uses those areas determined to be

significant. Equation 3 uses  $M$  to represent Points of interest,  $j$  and  $k$  represent the  $x$  and  $y$  location.

Equation 3 
$$\left( \frac{\sum M_j}{\text{TotalM}}, \frac{\sum M_k}{\text{TotalM}} \right) \quad (3)$$

*o. A-Forge.NET*

A “class blob counter” counts and extracts standalone objects in images using connected components labeling algorithm. This algorithm treats all pixels with values less or equal to a Background Threshold as background, but pixels with higher values are treated as objects' pixels. When the standalone objects are extracted the size and density is then determined to assess the possibility that the disturbance might be a source of concern. Areas of possible disturbance that did not provide a 50% confidence interval for a possible AOI were not labeled. Areas above 50% were marked with a yellow box and areas above 75% were marked with a red box.



**Figure 15.** Histogram approach utilized to minimize computational intensity of determining significant change areas. Large areas were analyzed using an average of changed pixels over the whole area. If no change was noticed within that area, the next area was analyzed. Maximum and minimum size areas were analyzed.

*p. Inaccuracy Vector Score*

An 8-tuple feature vector was created where each component represents a major characteristic of a difference image. In Equation 4 each component is normalized based on a set of training examples which represented a perfect disturbance indicator with minimal noise. The magnitude of the feature vector is then determined where the smaller the magnitude the closer the characteristics match that of the training examples and the lower the inaccuracy score. The higher the inaccuracy the higher the risk associated with utilizing the material in disturbance and change detection.

$$t_{\hat{k}} = \frac{\hat{k} - k_0}{s.e.(\hat{k})}$$

Equation 4. Normalization of each vector component.

Where  $k_0$  = Target Value,  $\hat{k}$  = Quantized Value, s.e ( $\hat{k}$ ) = Acceptable Deviation. The detectable object can be determined by the characteristics of each changed pixel, and the concentration of these pixels referred to as significant areas. For each of these two attributes a midpoint was created and a circle drawn with the radius equal to that of the actual disturbed area. All pixels and concentrated areas located outside the circumference of these two circle was counted as noise and weighed depending on its distance from the circumference of their corresponding circle. The concentration of each circle for the pixel and significant area was determined along with the distance from the actual area of the disturbance. These values where then all used in the feature vector in equation 5 to determine a final inaccuracy score.

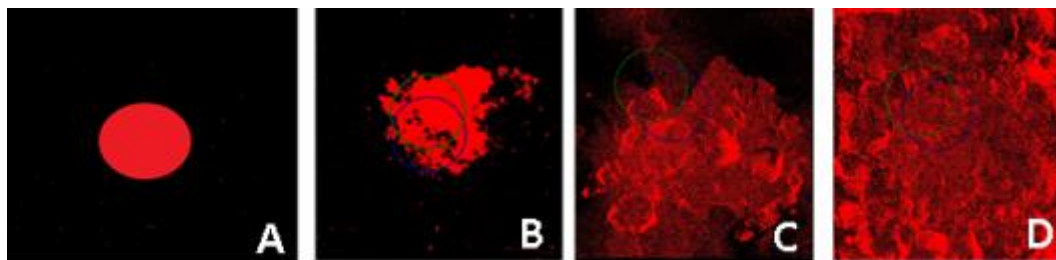
*Equation 5.* Vector employed to determine the final inaccuracy score.

$$\|V_N\| = \sqrt{\left(\frac{\hat{a} - a_0}{s.e.(\hat{a})}\right)^2 + \left(\frac{\hat{b} - b_0}{s.e.(\hat{b})}\right)^2 + \left(\frac{\hat{c} - c_0}{s.e.(\hat{c})}\right)^2 + \left(\frac{\hat{d} - d_0}{s.e.(\hat{d})}\right)^2 + \left(\frac{\hat{e} - e}{s.e.(\hat{e})}\right)^2 + \left(\frac{\hat{f} - f_0}{s.e.(\hat{f})}\right)^2 + \left(\frac{\hat{g} - g}{s.e.(\hat{g})}\right)^2 + \left(\frac{\hat{h} - h_0}{s.e.(\hat{h})}\right)^2}$$

Where a= noise outside pixel circle, b= noise outside concentration circle, c= pixels distance from circumference of pixel circle, d= concentration distance from circumference of concentrated circle, e = accuracy of pixel circle, f = accuracy of concentration circle, g = concentration inside pixel circle, and h = concentration inside concentration circle.

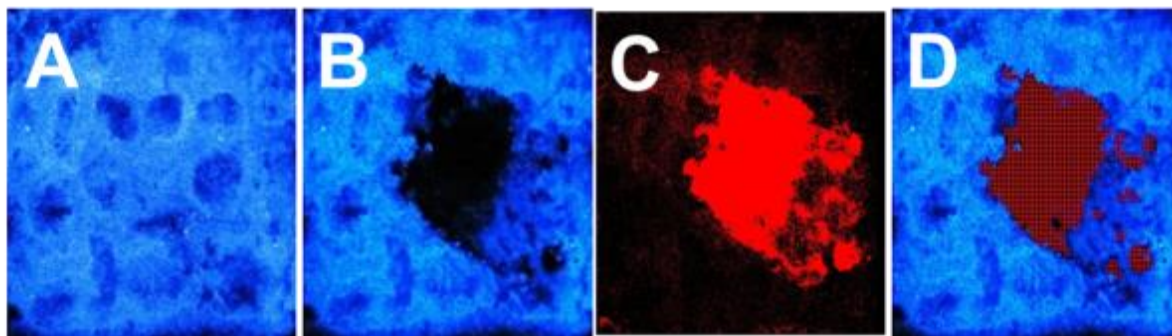
Figure 17 shows one of the training examples used during this experiment followed by a series of difference images with the lowest score starting from the left and increasing to the right and an approximate interval of 500. The best application rate for each product was obtained by finding the average lowest score of each tested products application.

**Figure 16.** Screen shot of vector performance software that shows the scores of the individual components of the performance score calculation.



**Figure 17.** Examples of images and their corresponding calculated inaccuracy scores (A) (perfect detection) score = 0, (B) score = 461, (C) score = 995 and (D) score = 1509.

After development of a method to determine an inaccuracy score, further work was performed to visually create a system that was identify the areas of significant difference above a minimum threshold. Images of changes between two images could be calculated independently or super-imposed upon a final image (see Figure 18, where A is the original image, B is the post disturbance image, C is the change difference image, and D is the change difference super-imposed on the post disturbance image). In a final, field usable technology, Figure 18D would be the resulting product that someone would analyze and use to know where the AOI is located and then further investigate that location.



**Figure 18.** (A) MU treated soil, (B) tampered MU treated soil, (C) the difference between compared photos in A and B and (D) the significant area highlighted in B

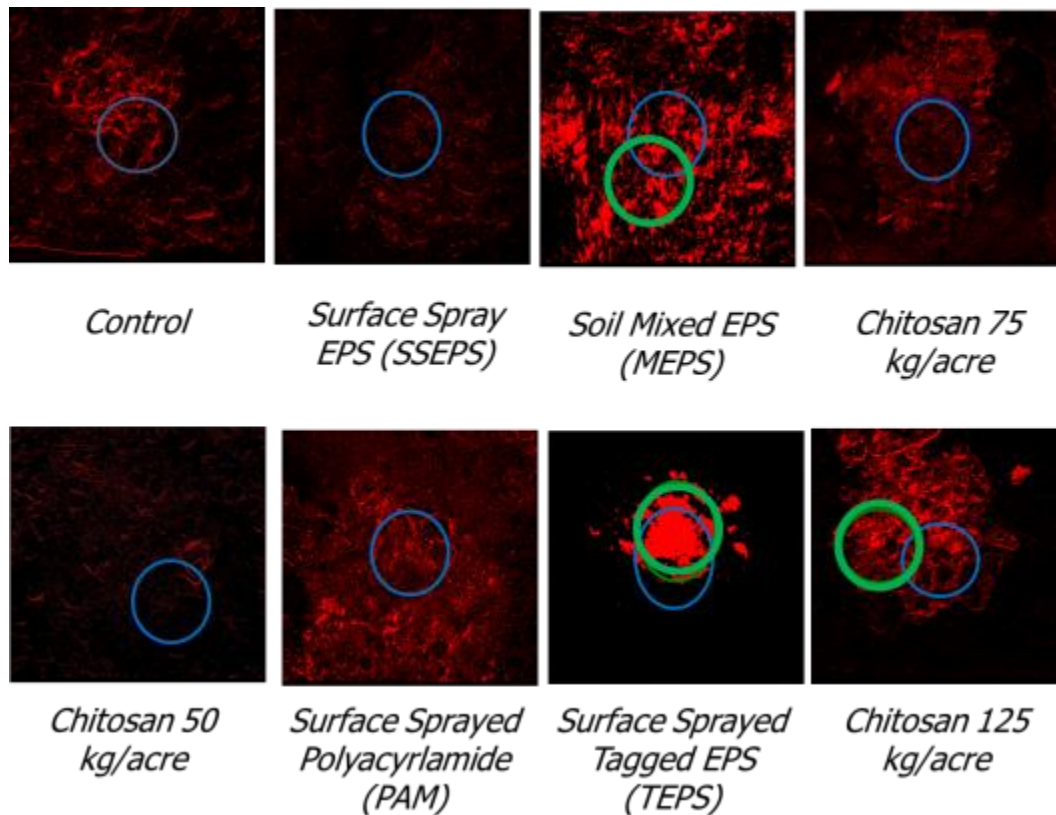
## 6. ADDS and TEPS Field Testing

Small scale bench testing was used to optimize the thresholds for each material. A known object was placed in a known location such that an optimization scheme could be used to minimize the inaccuracy score for each material and thus select the optimized threshold value for each tested material. Figure 19 shows the repeated process where optimization of both the concentrations of the materials used and their thresholds to minimize their inaccuracy scores was tested. The difference between each of the materials tested was readily identifiable. All of the unmodified native materials tested (PAM, Chitosan, and EPS) showed minimal improvements as compared to water in most of the test as shown in Figure 19.

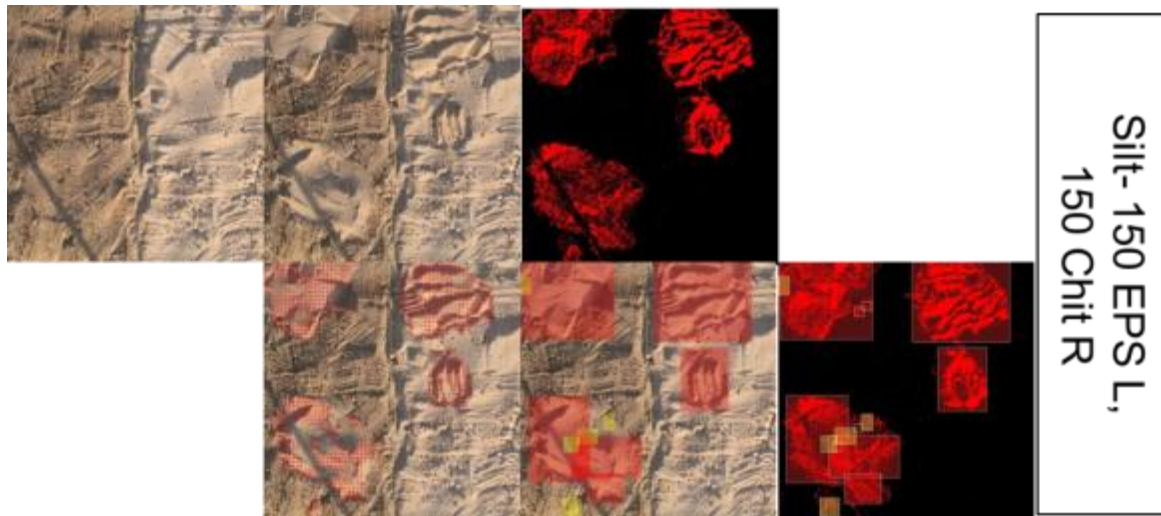
The information gathered in the small box testing was used to improve the application test on a larger scale from larger distances in the larger scale field testing. Two materials were tested simultaneously on several soil types- silt, an Arizona based soil (clay/sand mixture), clay, and loam and implanted with four different objects ranging in size from as small as 1.25" washer



to a 12"x 6" block. Some materials performed better than others using the automated identification program described earlier. One of the biggest issues was sensitivity due to light related issues as shown in Figure 22. One of the researchers accidentally impeded the image by casting a shadow over the plot. Because of the large shadow, none of the implanted objects were identified by the software on the side of the object with the shadow.



**Figure 19.** Several different soil materials that were tested and their change detection images. The blue circle indicates the actual location of the implanted device and the green circle indicates an area of significant change as determined by having a number of pixels inside of the size of the object that indicate a more than 50% change of significant pixels over the area.

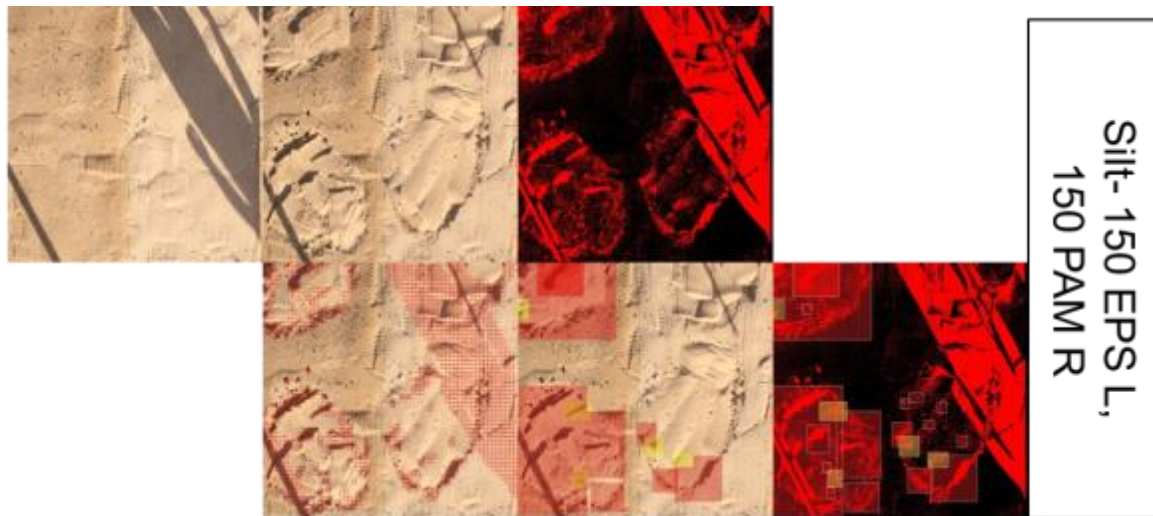


**Figure 20.** Comparison between two different materials applied to the soil with a Chitosan based material (Chit) applied at 150 kg/acre applied to the right side of the plot (150 Chit R) and 150 kg/acre of the EPS material applied to the left side of the plot on a silt based soil.

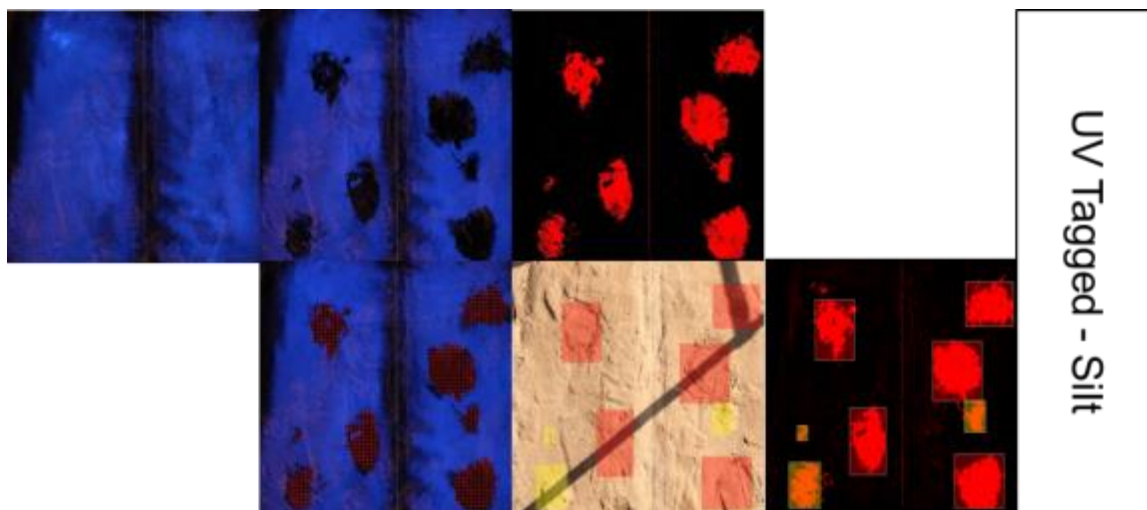


**Figure 21.** large scale testing utilizing both the EPS material at 100 kg/acre and the a water control in the same test plot (EPS on the left, control on the right). Four objects were implanted in each treatment area and the automated detection system attempted to identify the implanted areas automatically.

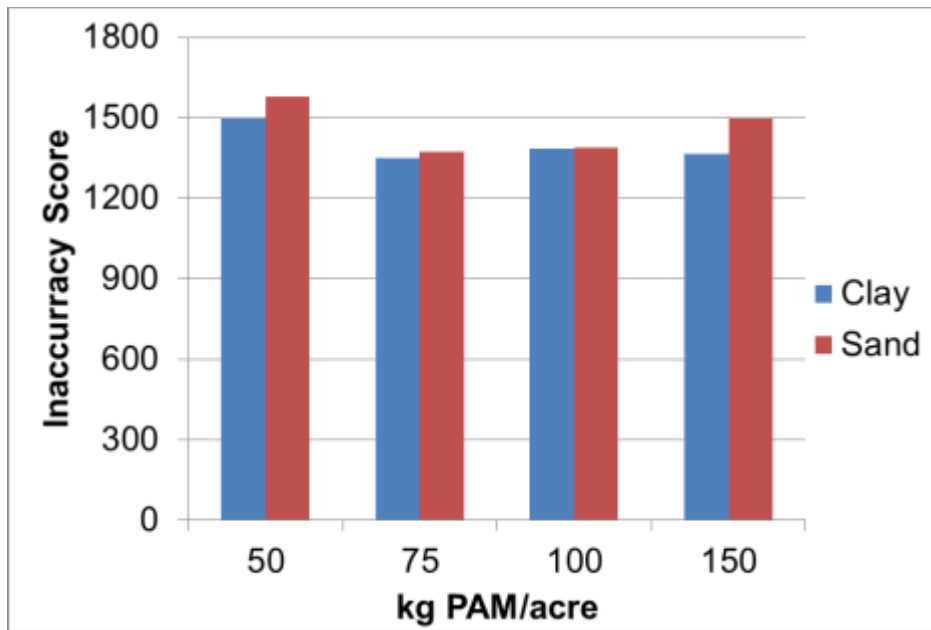




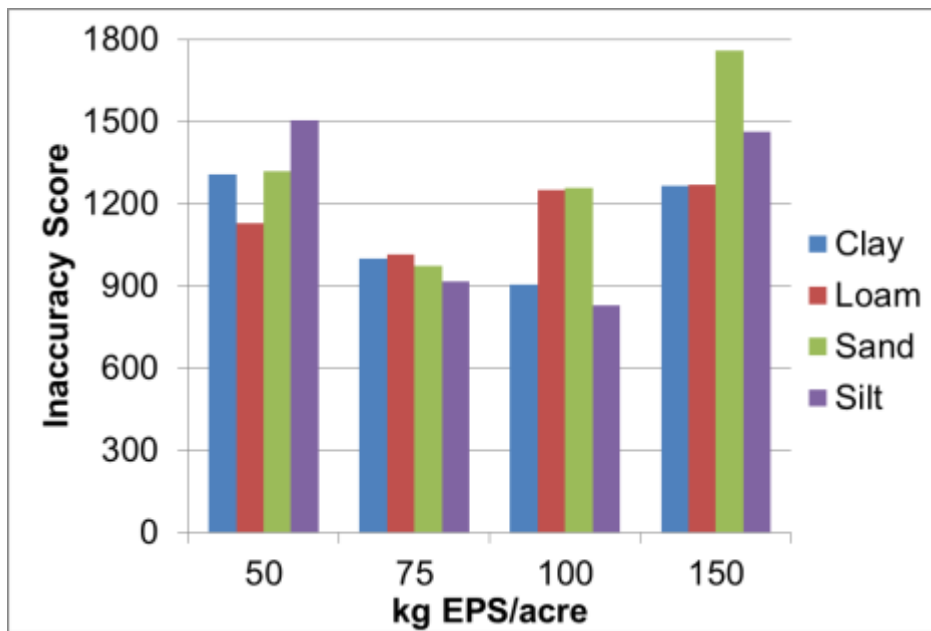
**Figure 22.** large scale testing utilizing both the EPS material and the PAM material in the same test plot (EPS on the left, PAM on the right) both at a rate of 150 kg/acre. Four objects were implanted in each treatment area and the automated detection system attempted to identify the implanted areas automatically.



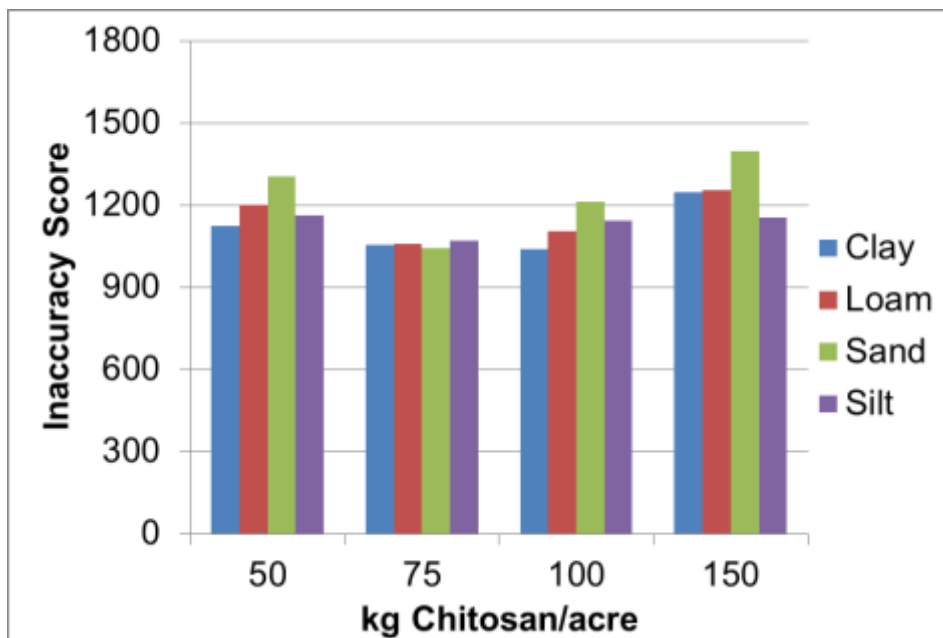
**Figure 23.** UV Tagged EPS material applied to a silt soil where four objects were implanted on each side of the test and an automated detection software was utilized to detect each of the objects, where red indicates a very high level of probable disturbance (above 75% confidence) and yellow indicates a lower level of confidence (above 50%)



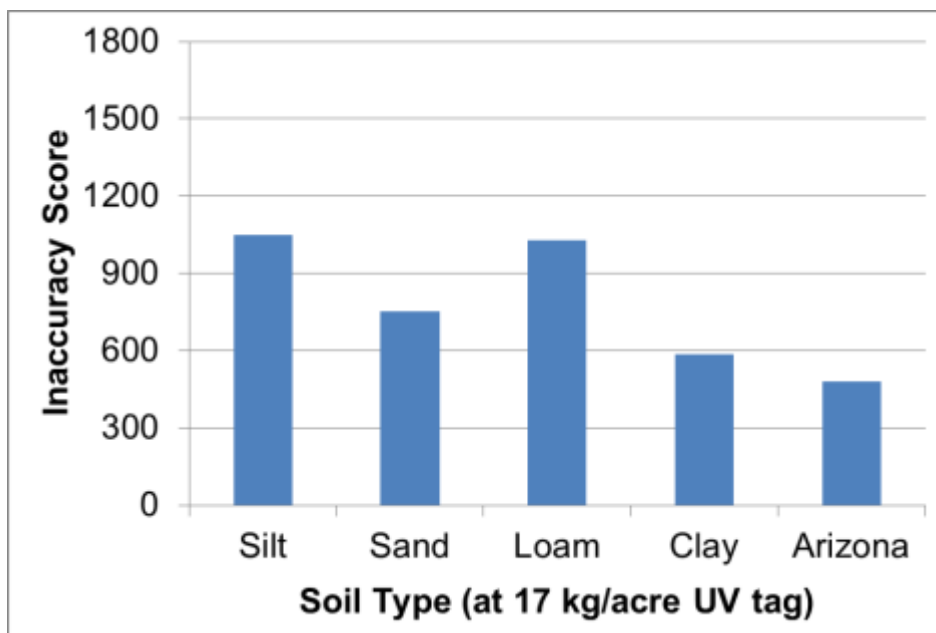
**Figure 24.** Varying rates of PAM applied to two soil types, clay and sand and the inaccuracy score associated with each application rate and soil type



**Figure 25.** varying application rates of EPS applied to four different soil types showed that the lowest inaccuracy score was obtained at the 75 and 100 kg/acre rates.



**Figure 26.** Chitosan based change detection where chitosan was applied at varying rates to varying soil compositions and tested to determine how far from a perfect detection.



**Figure 27.** An optimum rate of a tagged compound was applied to varying compositions of soil to determine the accuracy of detection.

There were some impacts based upon the type of soil utilized. Sand showed generally better results in each of the tests regardless of material type. The native EPS material showed relatively low inaccuracy scores at the 75 kg/acre rate, and some improvement at the 100 kg/acre. Controls (water additions only) averaged an inaccuracy score of 1233 with a STD of

118. The native EPS material on all of the soils were slightly above 900, but significantly better than all of the other native materials. All of the tested PAM application rates were above the water control.

The 75 kg/acre chitosan inaccuracy score, while slightly higher than the EPS score, did perform better than other application rates of chitosan and also significantly better than PAM and some of the higher and lower application rates with Chitosan and EPS. The inaccuracy score for the 75 kg/acre fared better than the silt and loam in the tagged EPS test. There are several potential reasons for this, but the overall ability of the tagged EPS to entrain and immobilize itself in these soils was weak and resulted in a less than homogeneous layer as was desired. Aspects of this could be due to over functionalization of the EPS with the fluorescent tag. Other aspects of this less than homogeneous layer could be due to the incompatibility of the native EPS material with those soils, namely the EPS does not effectively bind with those soils and will wash further into the soil and not remain near the surface to optically view and identified.

When using the automatic detection map software that was created, only the UV based field testing correctly identified the range of size of the objects. The larger objects were easily identified at all, but they were also identified in the controls as well, indicating no improvement over current conventional image change analysis processes. While further reduction of the computational power during this project was not analyzed, it could easily be determined that from the produced results that further optimization would be able to modify the detection algorithms to only search for a homogeneous layer or disturbances, effectively turning the search into a binary rather than realignment then change search. Easily, every pixel calculation could be reduced from a minimum of four calculations to one calculation. Further to that end, the more intense the disturbance appears, the easier it should be to detect and identify objects larger than a minimum size.

**Table 1.** Results of larger scale field testing comparing the control to EPS at two rates (100 kg/acre and 150 kg/acre), PAM (polyacrylamide) at 150 kg/acre, Chitosan (Chit) at 150 kg/acre, and the tagged EPS (UV) at 17 kg/acre

Material	Correct Identification (%)	Incorrect to Correct Ratio	Large Object Found %	Small Object Found (%)	Sample Size
Control	25.00	3.67	50.00	0.00	12
EPS 100	41.67	2.80	83.33	0.00	12
EPS 150	41.67	0.90	79.17	4.17	48
PAM 150	36.36	1.25	72.73	0.00	44
Chit 150	53.57	0.47	92.86	14.29	28
UV	93.75	0.07	100.00	87.50	32

In the UV test on silt and loam, the performance was less than ideal and the 75 kg/acre rate performed better on an inaccuracy score basis, although the detection software did properly identify all of the implanted objects in those soils. This indicates that there may be issues with how the inaccuracy scores are calculated but shows that the UV materials cluster and intensify the signature associated with a disturbance.

When analyzed in terms of identifying large and small objects, chitosan was effective in the large plot testing in identifying large objects (12" from approximately a distance of 14'). Both of the EPS materials performed above 75% of the time on the large object but had very

poor detection rates of the small object. Out of all the currently available commercial materials, chitosan performed the best, with a detection rate of large objects of approximately 93%, but a poor detection rate of 14% on the small objects (1.25"). Only EPS at 150 kg/acre and chitosan at the same rate were able to identify the small implanted objects out of the commercial materials. The EPS material at 150 kg/acre had a high rate of false detections, nearly 1 to 1 for incorrect to correct identifications. This means that anyone utilizing this particular software and chemical combination would have to sort through two objects for each real object. The chitosan material performed better in this regard, with one false identification for every two real identifications.

All of the natural materials failed to perform as well as the tagged UV material. The tagged UV material correctly identified 93.75% of the implanted objects. It identified all of the large objects correctly, but failed to identify some of the small objects properly. The false detection ratio was significantly lower in the UV material than any of the commercial materials. In the UV tagged material, for every false detection there were more than 10 positive detections. While the overall accuracy of the system would need to be higher to ensure that there are no missed objects, or the smallest identifiable object using the software corresponded to the smallest dangerous implanted device, it does indicate that there is the real potential for a project of this type to be optimized and utilized on a wide scale. Further work on how to minimize the amount of computations required to determine the minimal cluster size that corresponds to an actual disturbance would be required. Varying types of disturbances could be correlated to standard practices related to implanting devices. This would require more extensive computational power, but there is plenty of room yet within the software system to further optimize the system to improve both the accuracy and ability of the developed software and chemical.

## **7. Conclusion**

Development of an effective ADDS requires a compound that provides intense signal to noise ratios to facilitate image analyses. The results reported herein indicate that MU provides such characteristics and greatly facilitates the rapid detection and improved automation of change detection by creating a homogenous layer. With the fluorophore tagged to a biopolymer, like EPS, it will have enhanced probability of staying on the surface of the soil once the material is optimized. The critical finding from this work is that MU can much more effectively serve as a detecting molecule in ADDS than any of the traditional and new soil amendments investigated.

The use of the MU-BP material could greatly facilitate reduced computational power requirements for image change detection. When utilized with current methodologies and utilized techniques in change detection, the use of the MU-BP material easily improves upon the ability to clearly and rapidly identify implanted devices. With a sufficient level of fluorescence, all of the preprocessing algorithms that are normally used can be avoided and simplify the computational power required for detection. This reduces any change detection to undisturbed or disturbed, and the image can then be

Overall there exists the real potential for a tagged material like the one demonstrated to greatly assist in coherent change detection. The optimized threshold values for each of the individual materials tested indicated some inherent limitations in several materials. Out of all of the materials tested, the synthetic material PAM performed the worst. There are several further areas that can be investigated with the material but the properties of the material indicate that it does not assist significantly with native soil change detection. Chitosan was only marginally better than PAM and likely not a viable alternative. The native biopolymer on native soil had

surprisingly good results at a middle application rate in the range of 75 to 100 kg/acre indicating some potential. As was noticed though in the large scale field testing where a shadow was inadvertently placed over the area that was to be detected, significant error was introduced and was not filtered by the simple algorithms used. More complex algorithms likely could increase accuracy of the system.

Cominbation of optical chemical development, algorithm and computational optimization, software development, and image processing could significantly take strides towards automating the potential detection of implanted devices. The tagged fluorophore EPS demonstrated herein represents the first potential step towards that type of automation.

## 8. References

Binstock, J., Minukas, M. 2010. Developing an Operational and Tactical Methodology for Incorporating Existing Technologies to Produce the Highest Probability of Detecting an Individual Wearing an IED. Naval Postgraduate School: 55-58.

Buchanan, A. 2009. Novel View Synthesis for Change Detection. 6th The Electro-Magnetic Remote Sensing (EMRS) Defense Technology Centre Technical Conference.

Coderre, M., Smith, I. 2008. The Continuing War Against IEDs. Weapon Systems Technology Information Analysis Center. Quarterly, Vol. 8, No. 2.

Davy, M., Duflos, E., Potin, D., Vanheeghe, P. 2006. An abrupt change detection algorithm for buried landmines localization. IEEE Transactions on Geoscience and Remote Sensing, VOL. 44, NO. 2.

Dekker, A. 2010. Agent-Based Simulation for Counter-IED: A Simulation Science Survey.

Dudman, W.F., Franzén, L.-E., Darvill, J.E., McNeil, M., Darvill, A.G., Albersheim, P., 1983a. The structure of the acidic polysaccharide secreted by *Rhizobium phaseoli* Strain 127 K36. Carbohydr. Res. 117, 141-156.

EPA. 2001. Chitin; Poly-N-acetyl-D-glucosamine (128991) Fact Sheet. USEPA Fact Sheet Bulletin 128991.

----- 1983b. The structure of the acidic polysaccharide secreted by *Rhizobium phaseoli* Strain 127 K87. Carbohydr. Res. 117, 169-183.

Franzén, L.-E., Dudman, W.F., McNeil, M., Darvill, A.G., Albersheim, P., 1983. The structure of the acidic polysaccharide secreted by *Rhizobium phaseoli* Strain 127 K44. Carbohydr. Res. 117, 157-167.

Laspidou, C.S., Rittmann, B.E., 2002. A unified theory for extracellular polymeric substances, soluble microbial products, and active and inert biomass. Wat. Res. 36, 2711-2720.

Larson, S, Griggs, C, Newman, K, Nestler, C, and Beverly, M. 2012. Biopolymers as an Alternative to Petroleum-Based Soil Stabilizers. USACE ERDC Technical Report TR-12-8.

Larson, S., Martin, W., Medina, V., Newman, J., O'Connell, K., Ringelberg, D. "Soluble Salt Produced From a Biopolymer and a Process for Producing the Salt." Patent No.: US 7,824,569 B2. 11/2010.

Ma, Zhenhua 2007. Dissertation. Advanced Feature Based Techniques for Landmine Detection Using Ground Penetrating Radar. University of Missouri. 10-43.

Moron, B., Soria-Diaz, M., Auit, J., Verroios, G., Norre, S., Rodriguez-Navarro, D., Gil-Serrano, A., Thomas-Oates, J. Megias, M., and Sousa, C. 2005. Low pH Changes the Profile of Nodulation Factors Produced by *Rhizobium tropici* CIAT899. *Chemistry and Biology*, 12, 1029-1040.

Nijak, G. 2012. Biopolymers: A Sustainable Approach to Erosion and Sediment Control. IECA Conference Proceedings, San Diego, CA. Feb 11-13, 2013  
<<http://www.ieca.org/conference/annual/TechSessionDetails.asp?Conid=19&SessionId=972>>

SBIR. 2004. All Optronics Technologies to Defeat Improvised Explosive Devices.  
<<http://www.sbir.gov/sbirsearch/detail/84904>>

Shaughness, L. 2012. IEDs top cause of US Afghanistan casualties, CNN.

Stevens, M., Kramer, L, and Pike, R. 2012. Infrared fluorescing optical signature agent for real time change detection. US 8253115 B1.

Treado, P., Nelson, M, Hubble, H, and Neiss, J. 2010. Time and space resolved standoff hyperspectral IED explosives LIDAR detection. US Patent 7692775 B2.

Wilson, C. 2006. Improvised Explosive Devices (IEDs) in Iraq: Effects and Countermeasures. Congressional Research Service Report for Congress.



## 9. Appendix

### *q. Appendix A- Cost Analysis of the Materials*

As with any new technology the economic implications of the technology limit or influence its adoption into the commercial space. Preliminary economics were calculated based upon the performance of the material tagged and untagged polymers for their use in soil stabilization. The following matrix describes the economics associated with the untagged cost on a per acre basis which nominally is the equivalent to 0.706 linear miles of road at 20 ft width.

*Table 2- Cost chart of the cost per acre of each of the materials tested and the rates at which they might be applied*

Material	Rate	Cost Per Acre
<b>Control (water)</b>	800 gal/acre	\$1-200
<b>Chitosan</b>	75 kg/acre	\$2000-5000
<b>EPS</b>	75 kg/acre	\$3000-8000
<b>PAM</b>	75 kg/acre	\$4000-10000
<b>MU-EPS</b>	17 kg/acre	\$7000-14000

The chemically modified and optically tagged material results in a different value proposition if effective use of the material can be determined and implemented. The use of water, while it does not impact change detection, is significantly cheaper than all of the other materials. The UV tagged material in its current form has a relatively high cost of about \$400/kg of material. The remaining cost of the chitosan, EPS, and PAM materials were based upon several available commercial prices.

At a cost of \$7000 per acre (or in excess of \$9000/mile), this type of technology may have implications only in high impact areas. Further work could be done to optimize both the rate and efficacy of the material, but in its current form, economics over a wide spread area would be a significant concern. The lifespan of this material will also factor into

### *r. Appendix B- Leaching of EPS materials in soil matrix*

A brief study was conducted to look at how the biopolymer or EPS material holds itself in the soil matrix. Two test were conducted- one looking at the native soil and its colorimetric leaching, and one looking at a soil that was leached after the tagged EPS material was applied to a soil matrix. There were no significant differences between the native soil and the tagged soil indicating that over the amount of water applied to the soil (verifying that there is a relatively long stability of the material in the soil). Work was preliminary and further work should test a range and variety of soil types and situations.

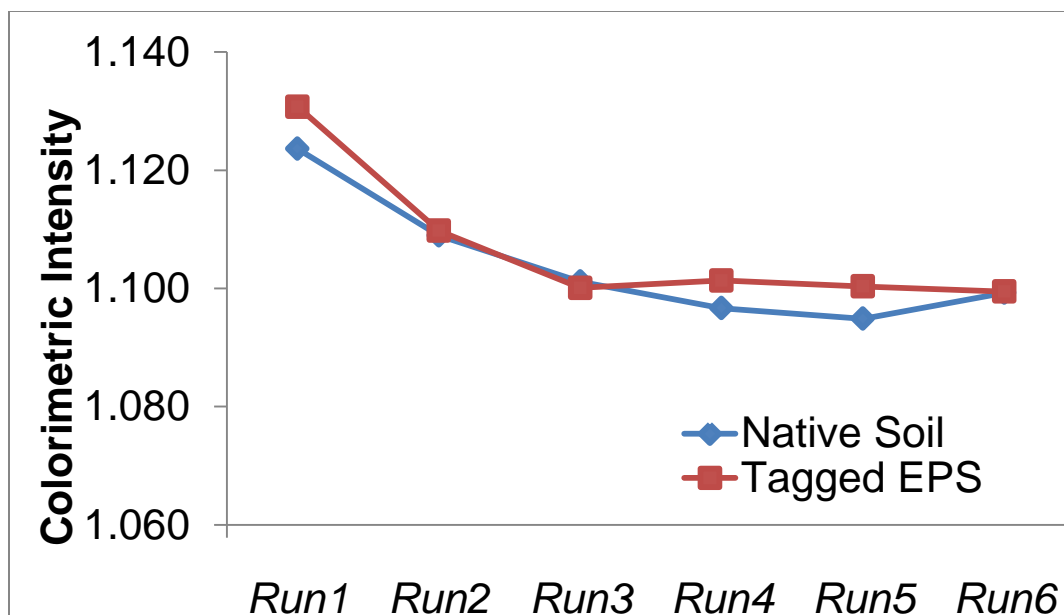


Figure 28- Simulated rain events (each run) where each rain event was 8" of precipitation, simulating approximately 6 years in arid climate or 1 year in a moderate to temperate climate. Shows that little of the material leaches during rain events.

s. Appendix C- Alternative Synthesis Method

There was Synthesis of tagged biopolymer would take place via synthetic routes where the fluorophore, 4-MU (4-methylumbelliferone) is mixed into the microbial mixture. Since the coumarin has a relatively similar structure to the sugars utilized in the microbial mixture to produce the biopolymers. The results were mixed - increased fluorescence but likely due to need for further purification. If the fluorophore could be completely rinsed from the biopolymer mixture all the fluorescence observed likely would dissipate. No further work in this area proposed (leveraged and unfunded work under DARPA)



Figure 29- Alternative tagged EPS synthesis where a fluorophore was mixed into a microbial mixture to determine if the microbes would incorporate the tags into the biopolymer.

*t. Appendix D- Chemical Elucidation/Characterization*

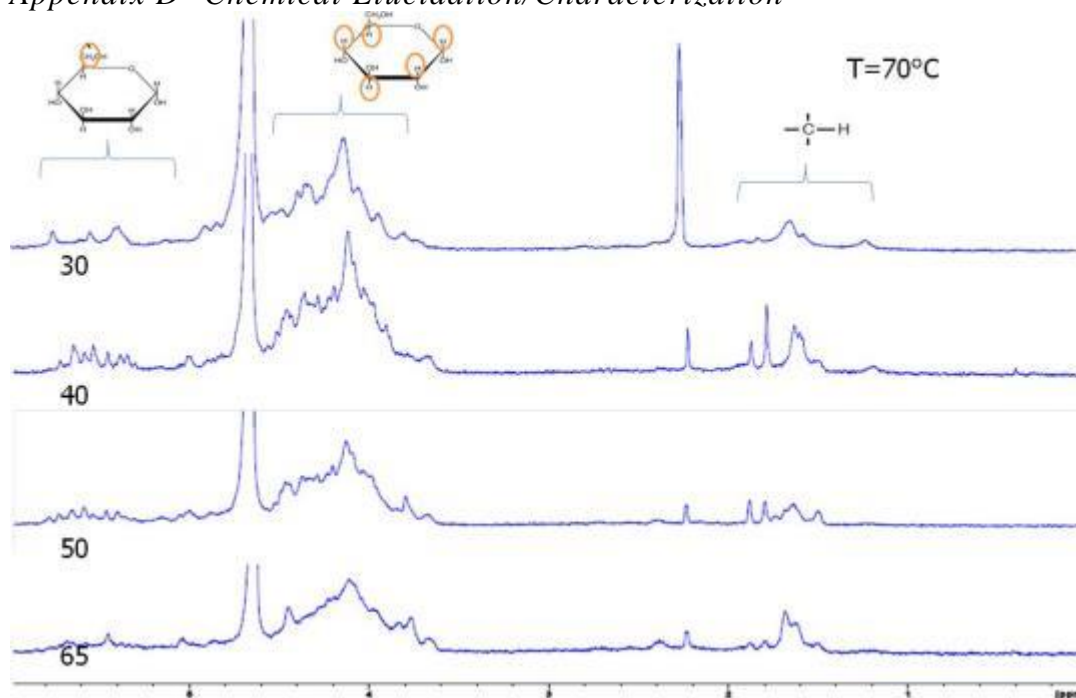


Figure 30- Fractionated biopolymer samples where the largest molecular weights are demonstrated in the lower percentage alcohol fractions (65 indicating 35% alcohol, 65% water).

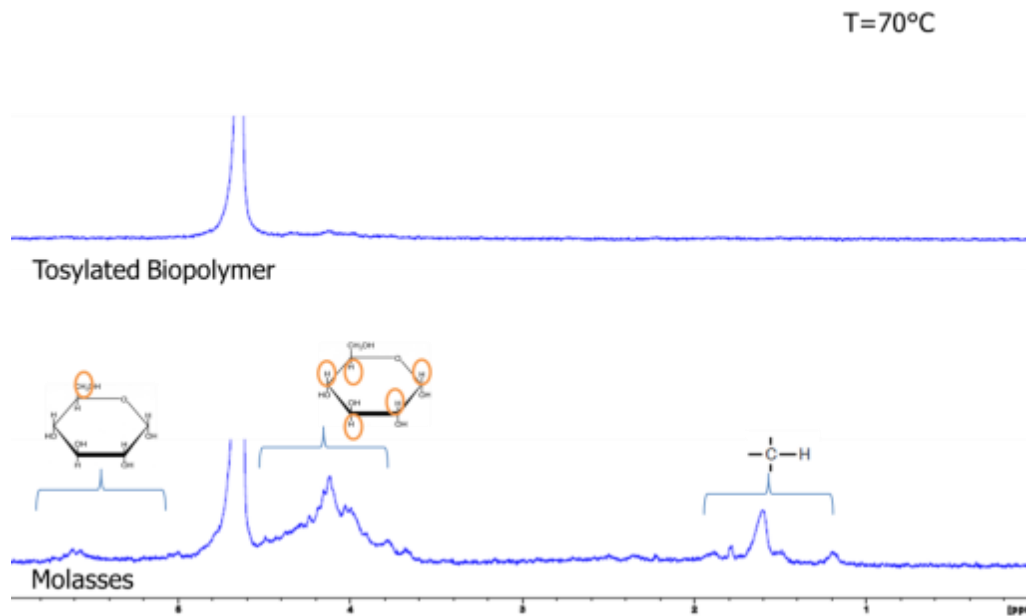


Figure 31-  $^1\text{H}$  solid state magic spinning angle NMR between a tosylated biopolymer and a molasses based biopolymer.

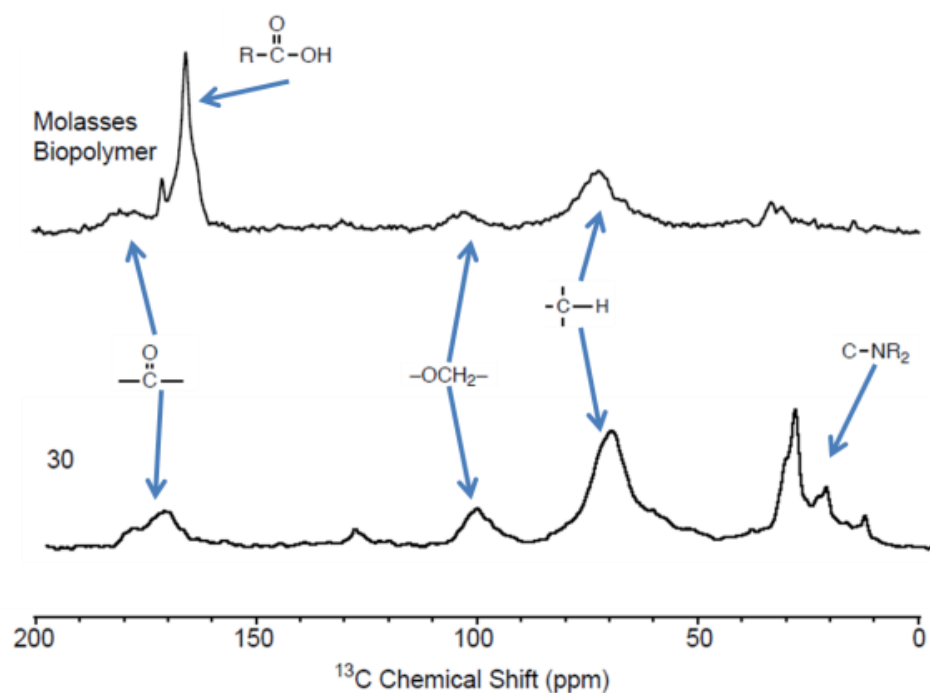


Figure 32-  $^{13}\text{C}$  NMR using magic spinning angle solid state spectrum of a molasses based biopolymer and a large molecular weight separated biopolymer labeled 30.

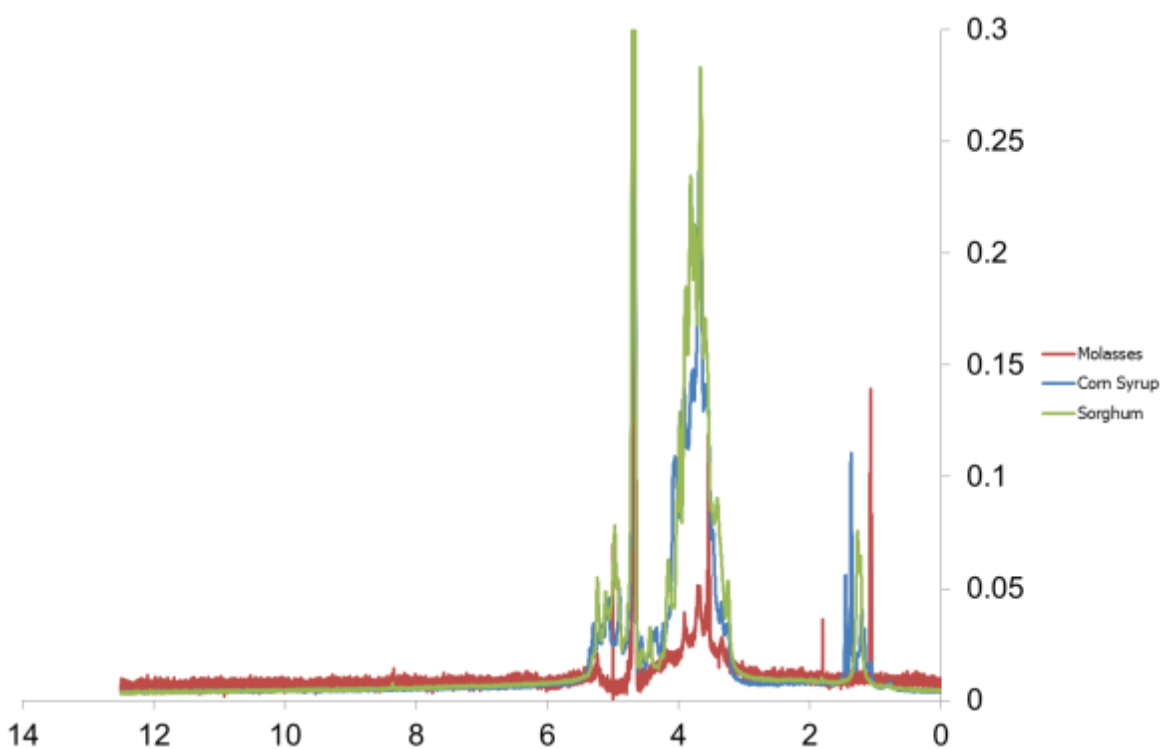


Figure 33-  $^1\text{H}$  NMR comparison of three carbon source biopolymers- molasses, corn syrup, and sorghum.

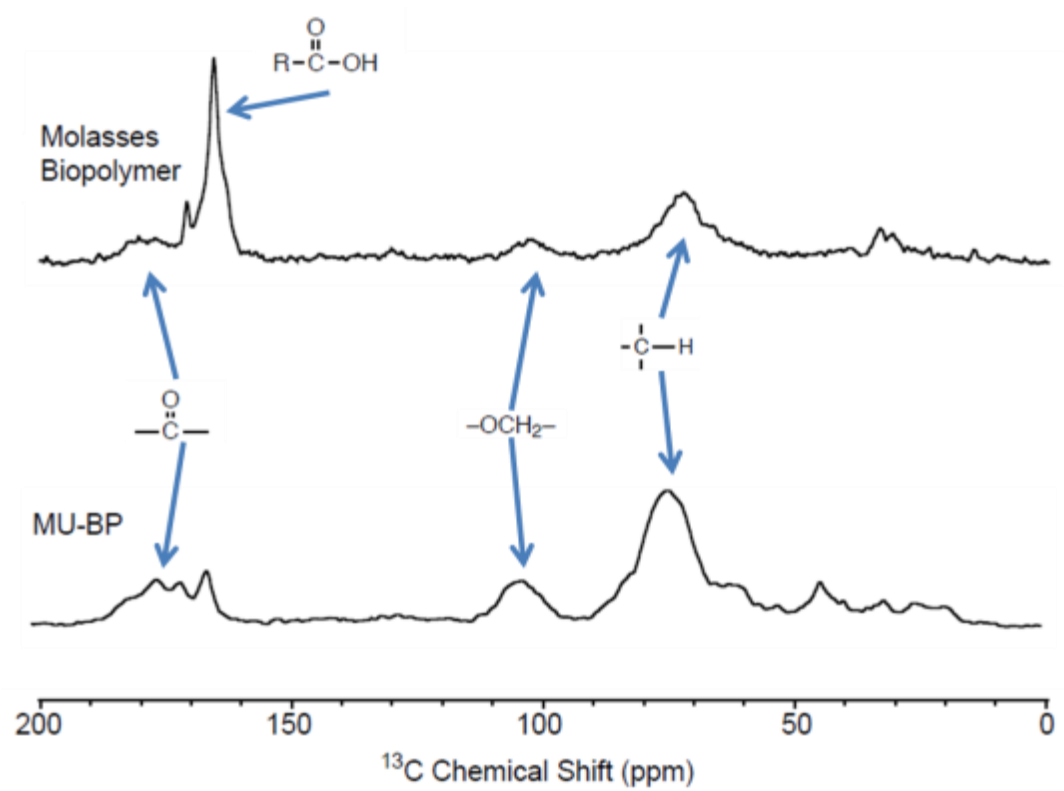
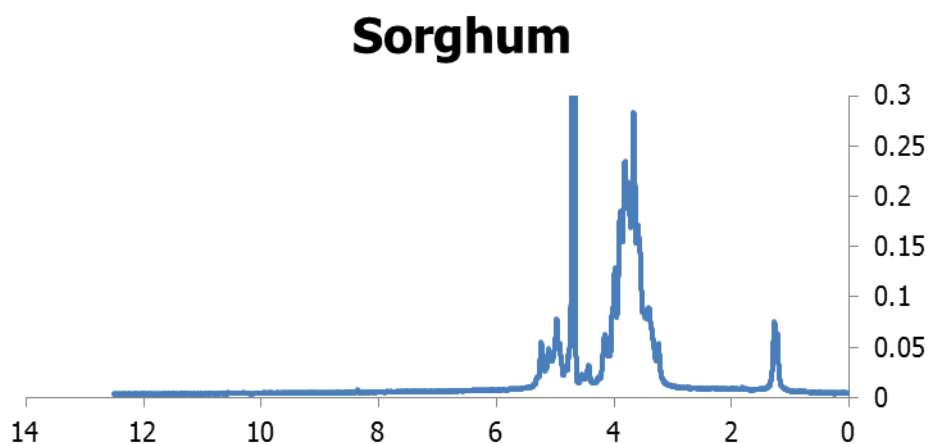
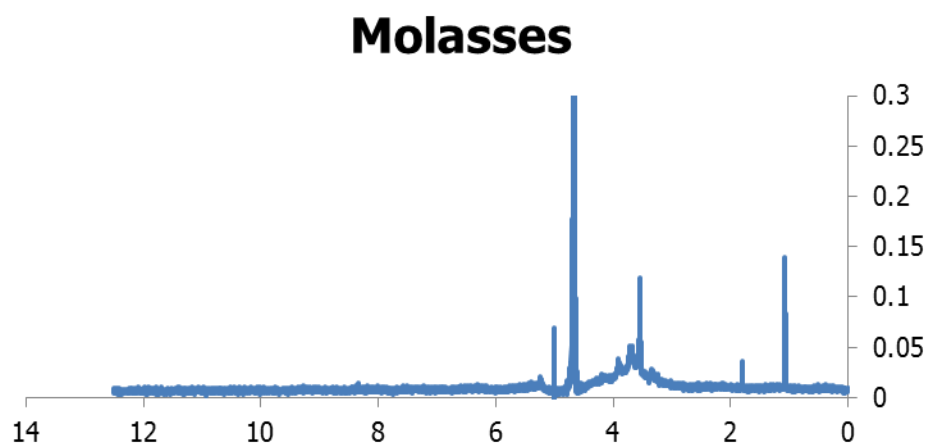
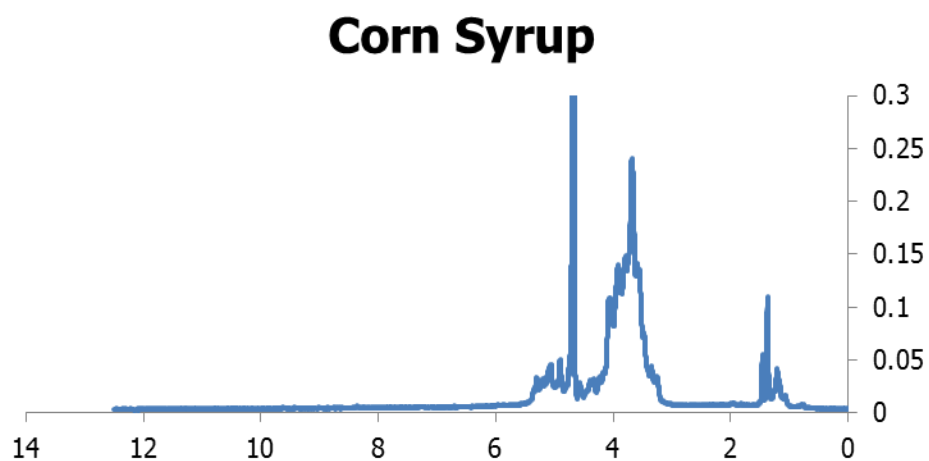


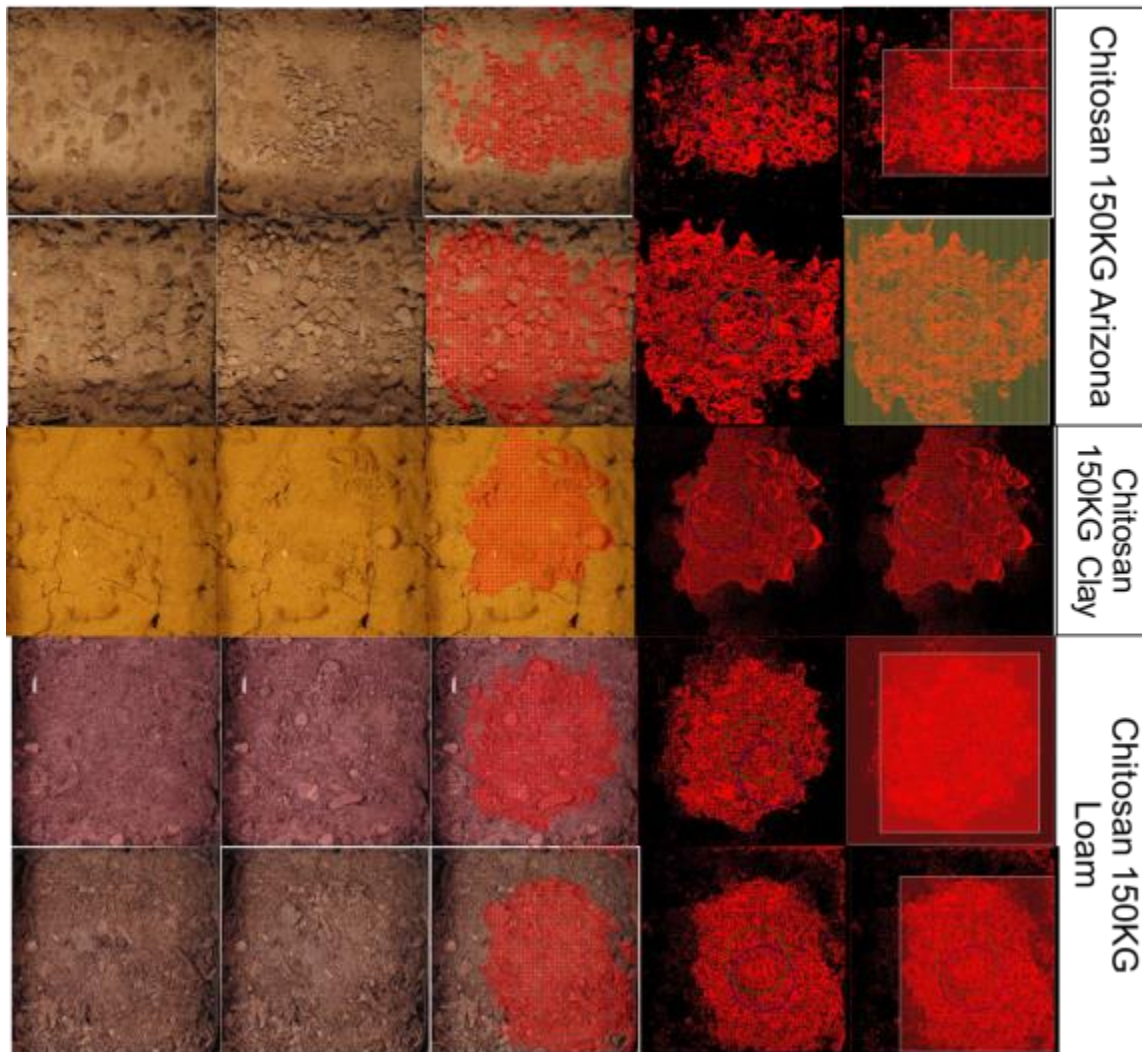
Figure 34-  $^{13}\text{C}$  solid state magic spinning angle NMR of the native molasses biopolymer and the MU tagged biopolymer



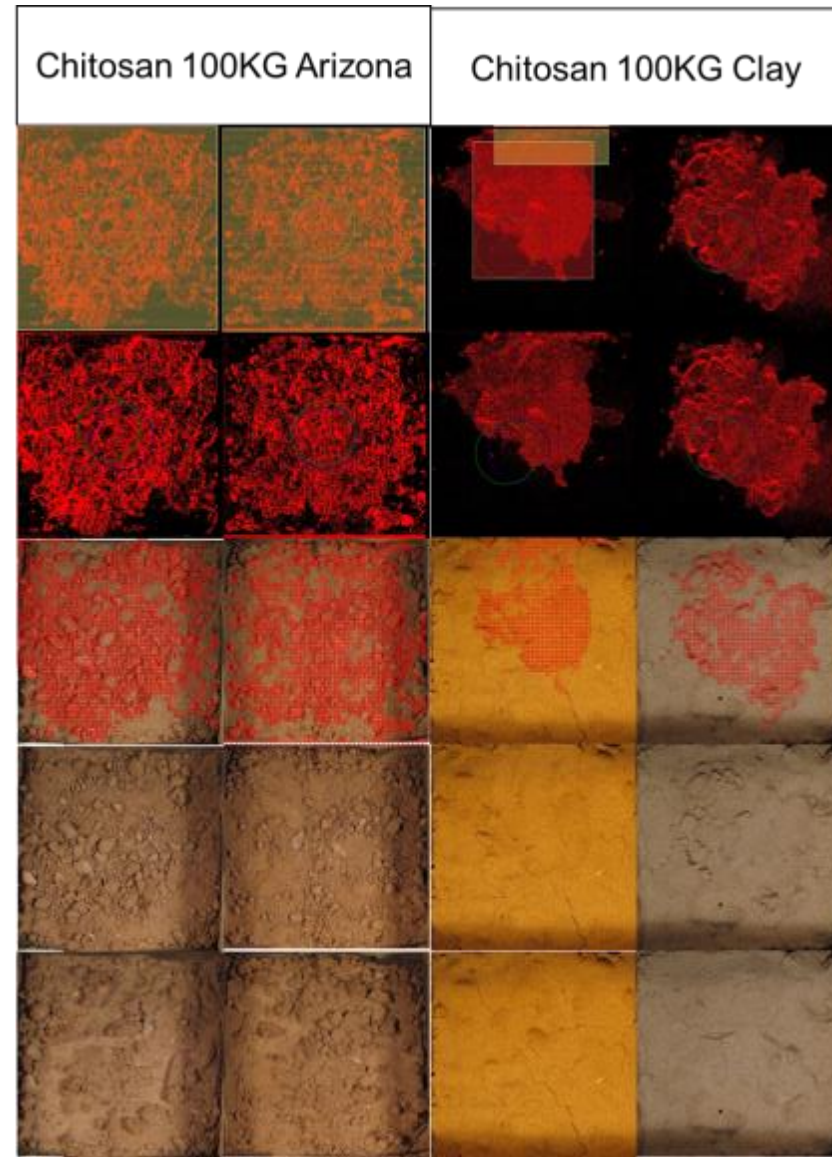
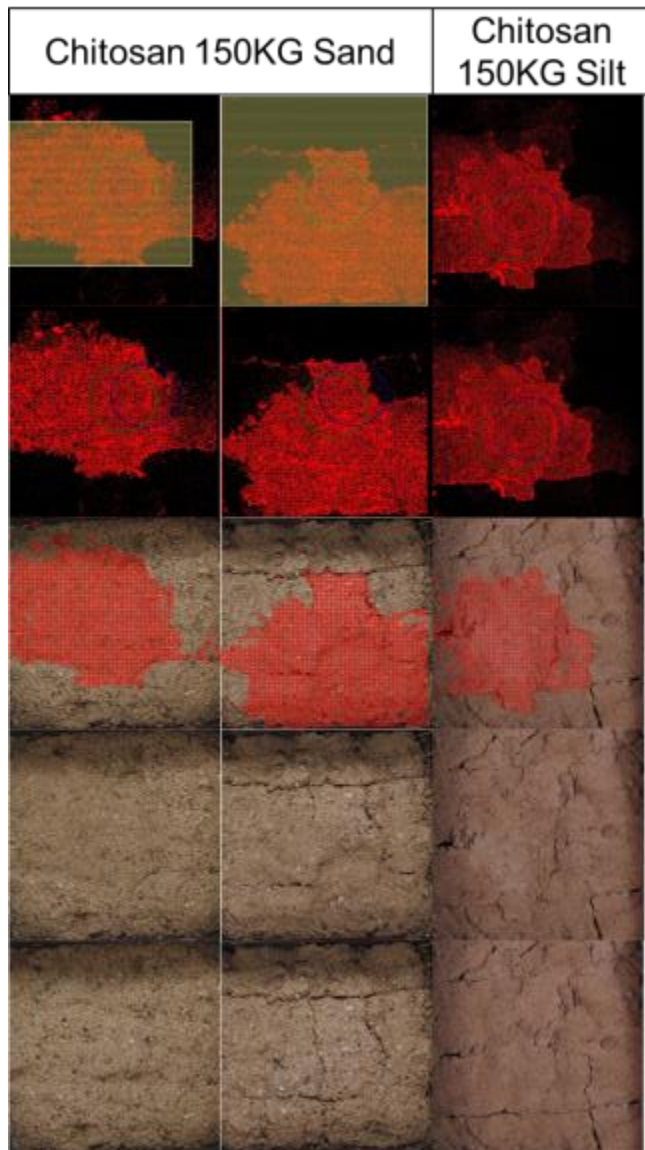
*Figure 35-Comparison of  $^1\text{H}$  NMR spectrum of three native biopolymers, corn syrup, molasses, and sorghum based upon the carbon source utilized in the microbial production process.*

*u. Appendix E- Small Plot Testing Results*

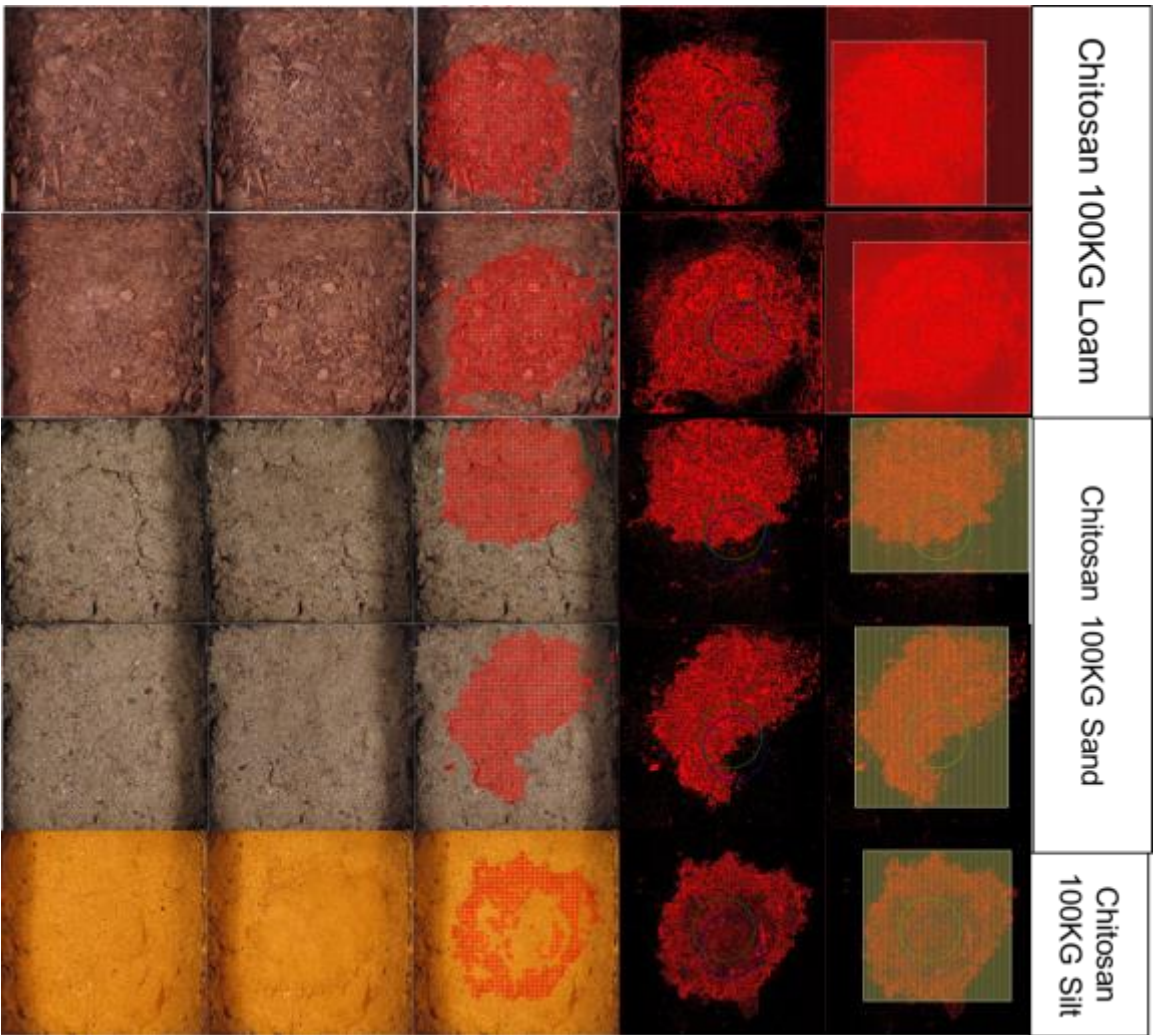
The following sets of images show a progression of images where the first image is the pre-disturbance image, the second image is the post disturbance image, the third image is the post disturbance image with the change difference between image 1 and image 2 overlaid, the fourth image is the change difference by itself, and the fifth image is the change difference significance area calculations showing the areas of significant change where a yellow box indicates an area of 50% significant change and a red box indicates an area of 75% significant change. Both the rates and the soil type and the application amount per area are shown to the right of each series of images.

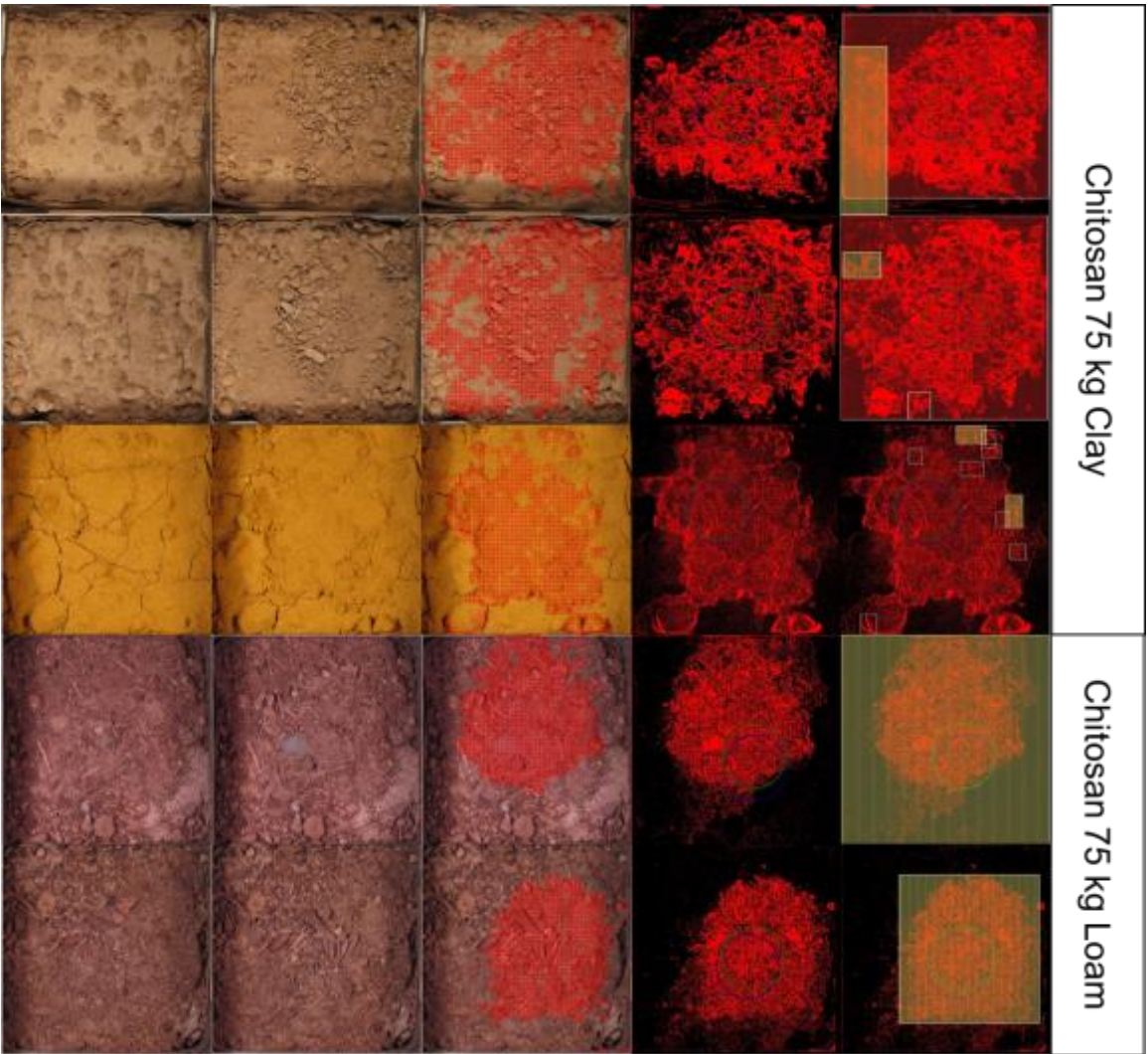


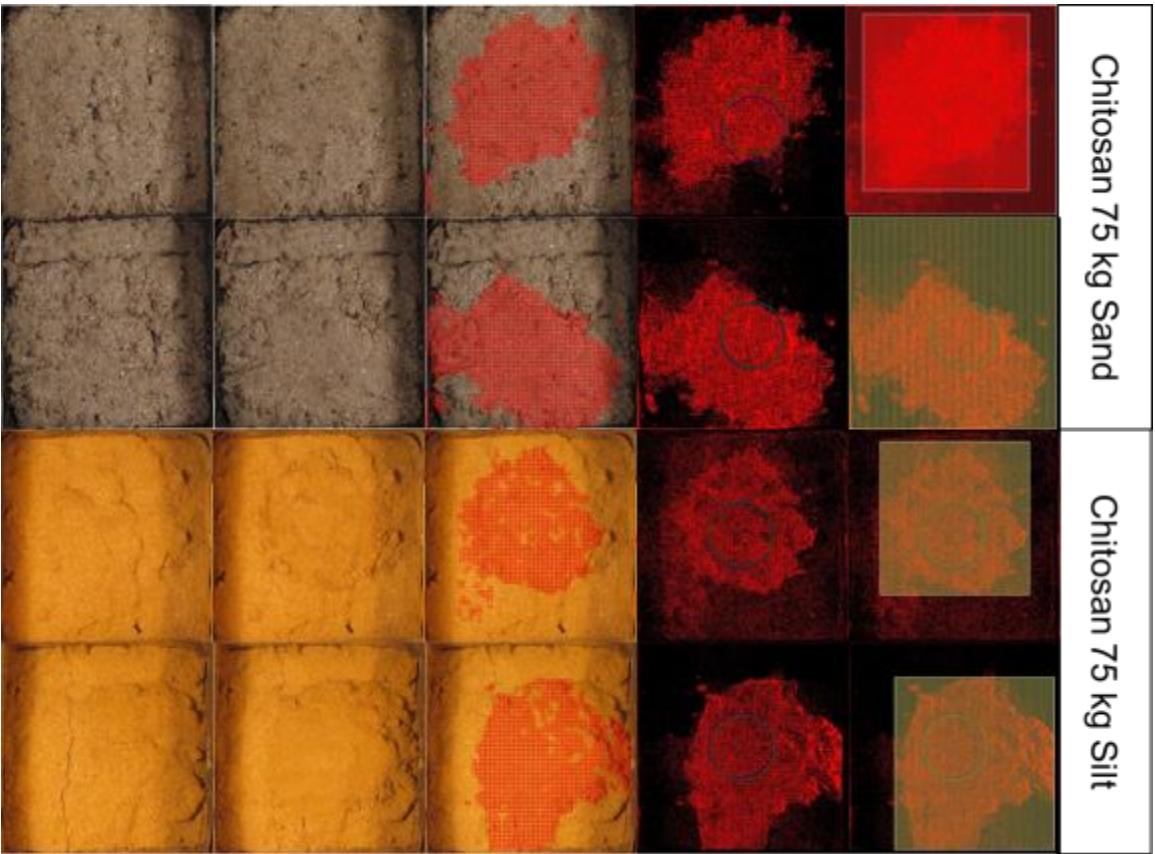




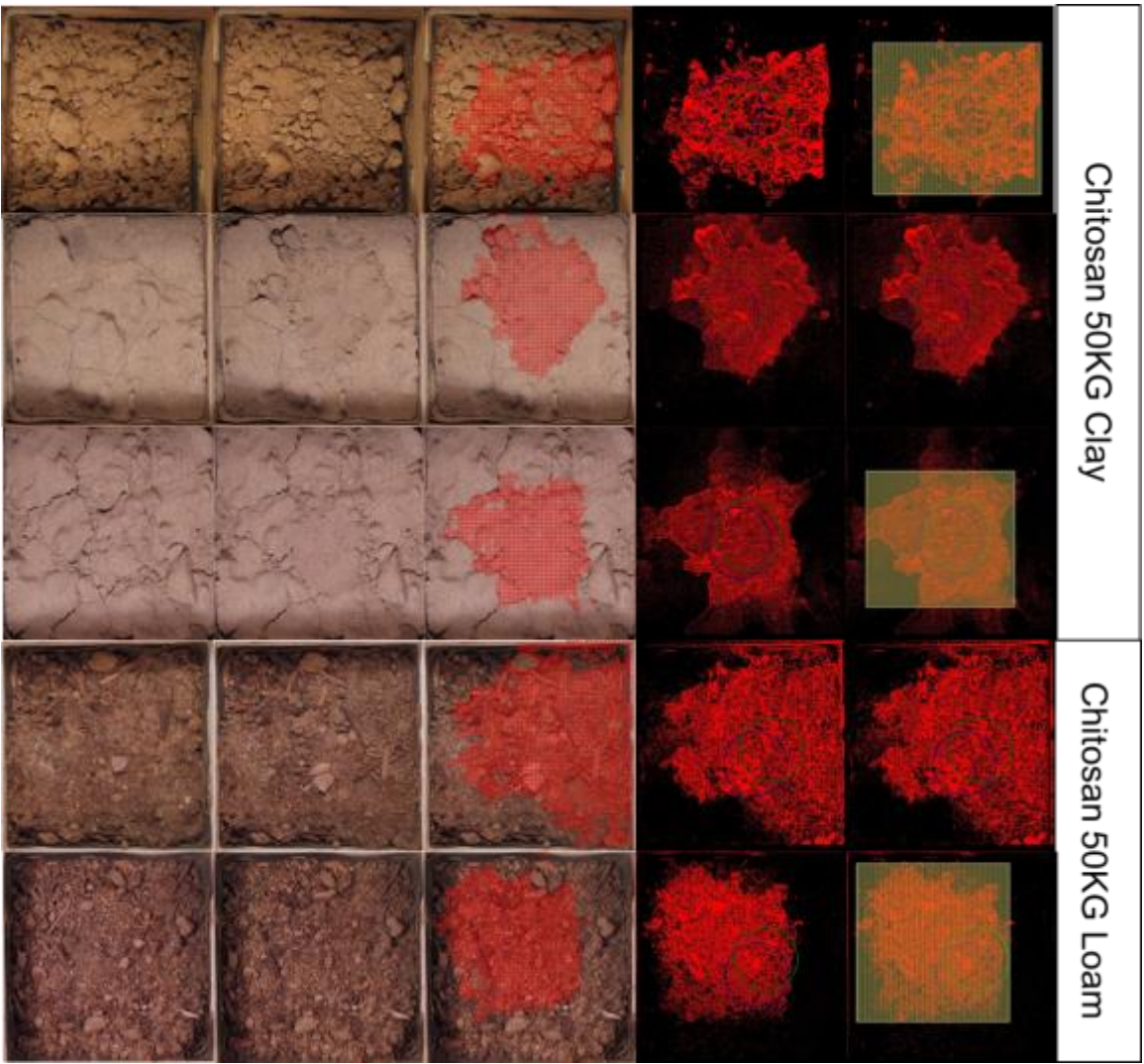


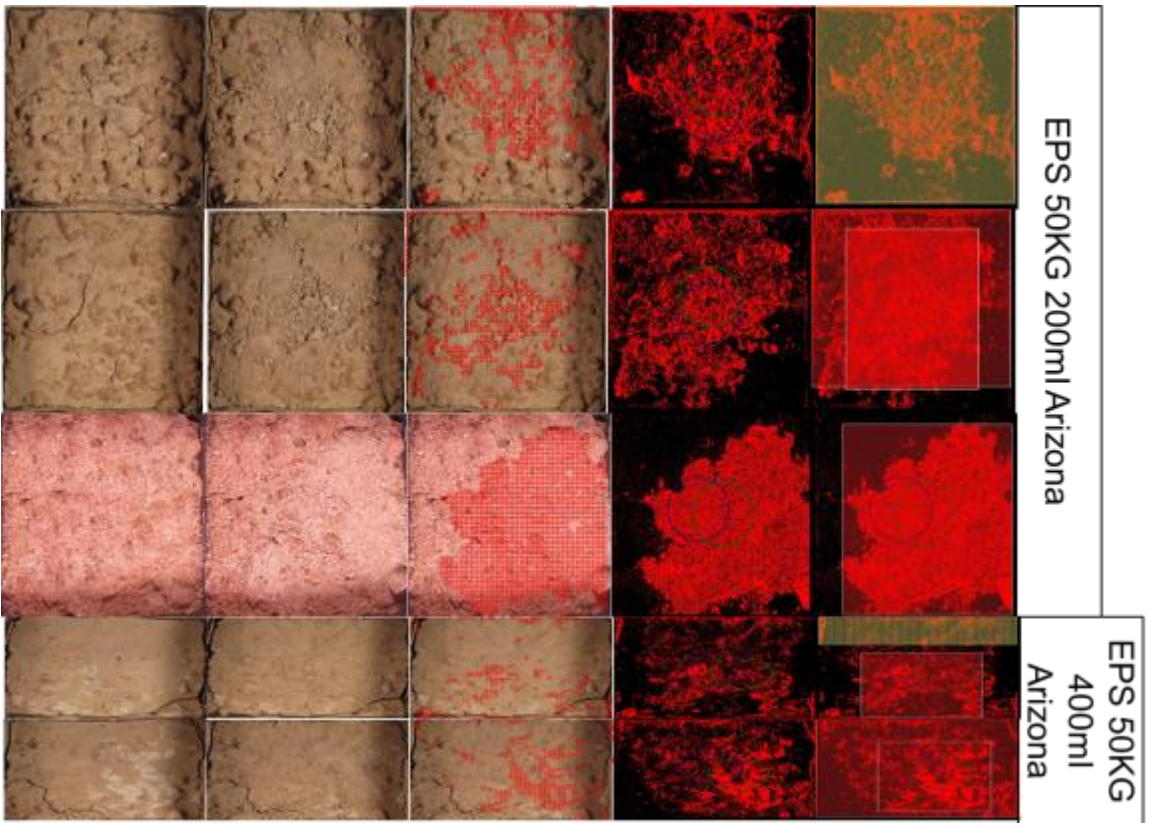
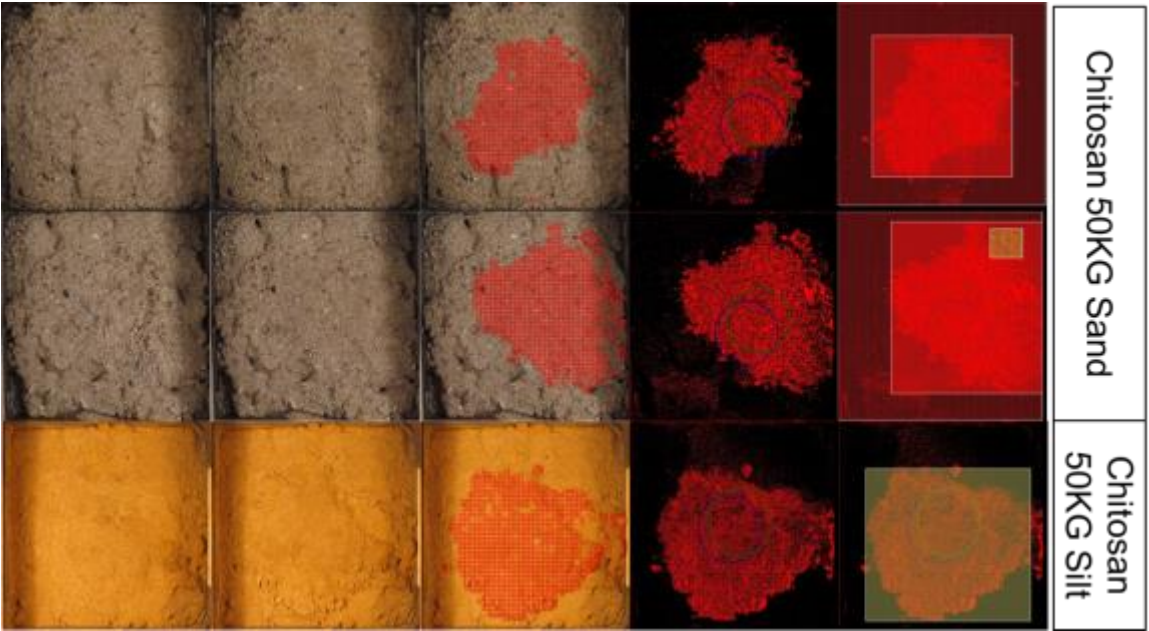




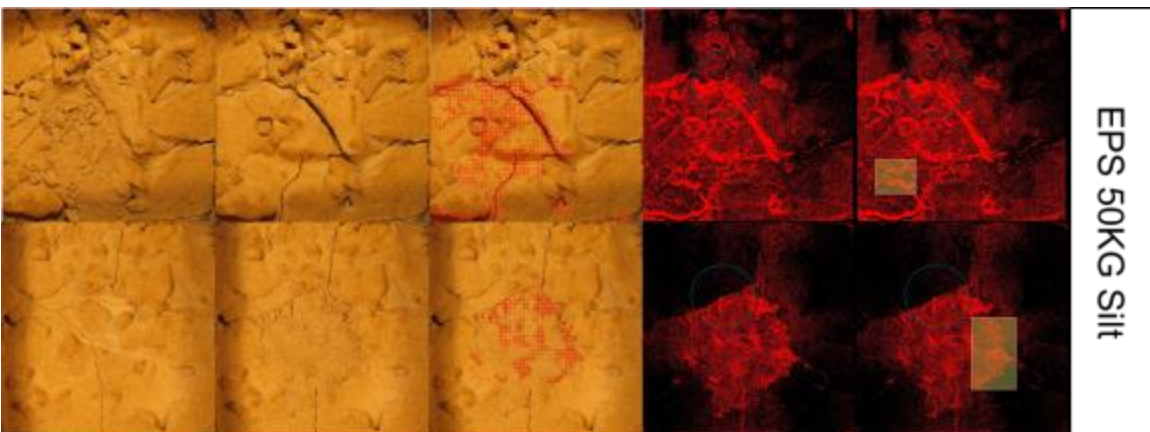
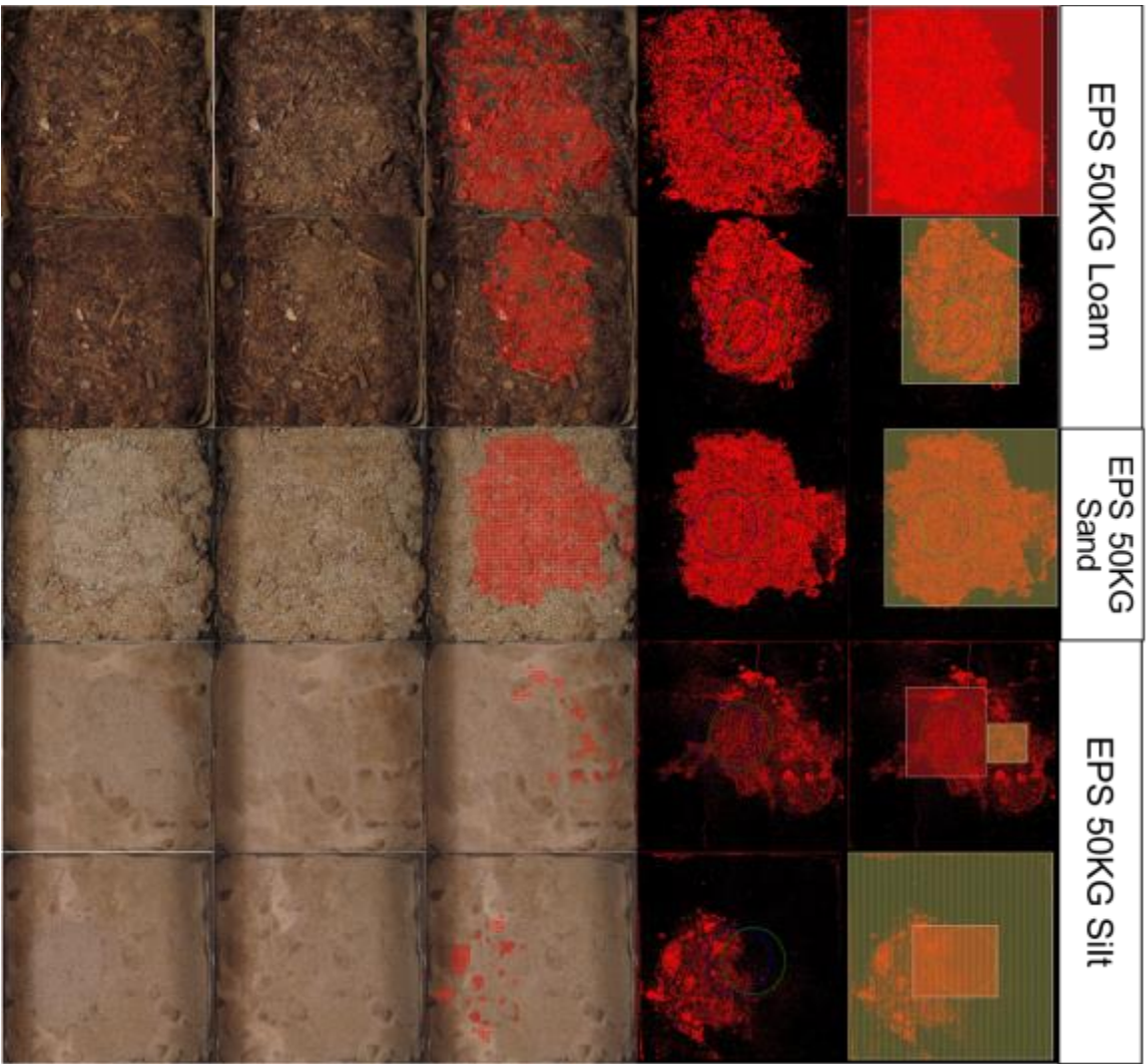





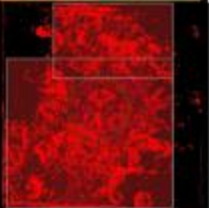
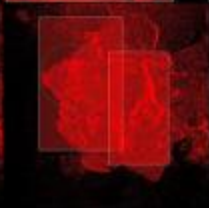





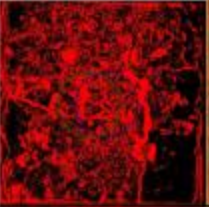

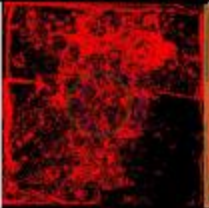

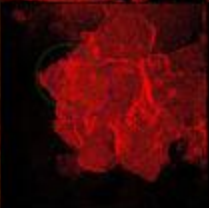
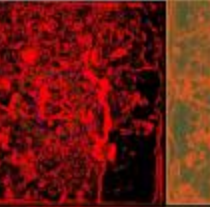
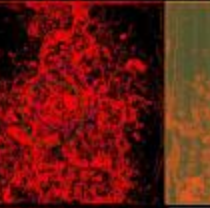
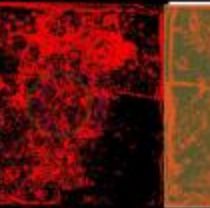
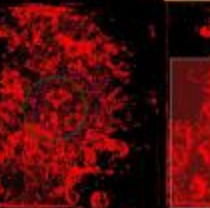
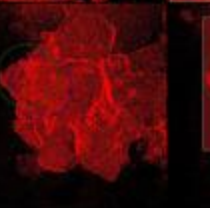






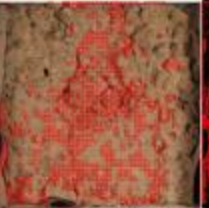


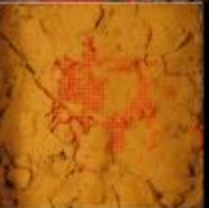















































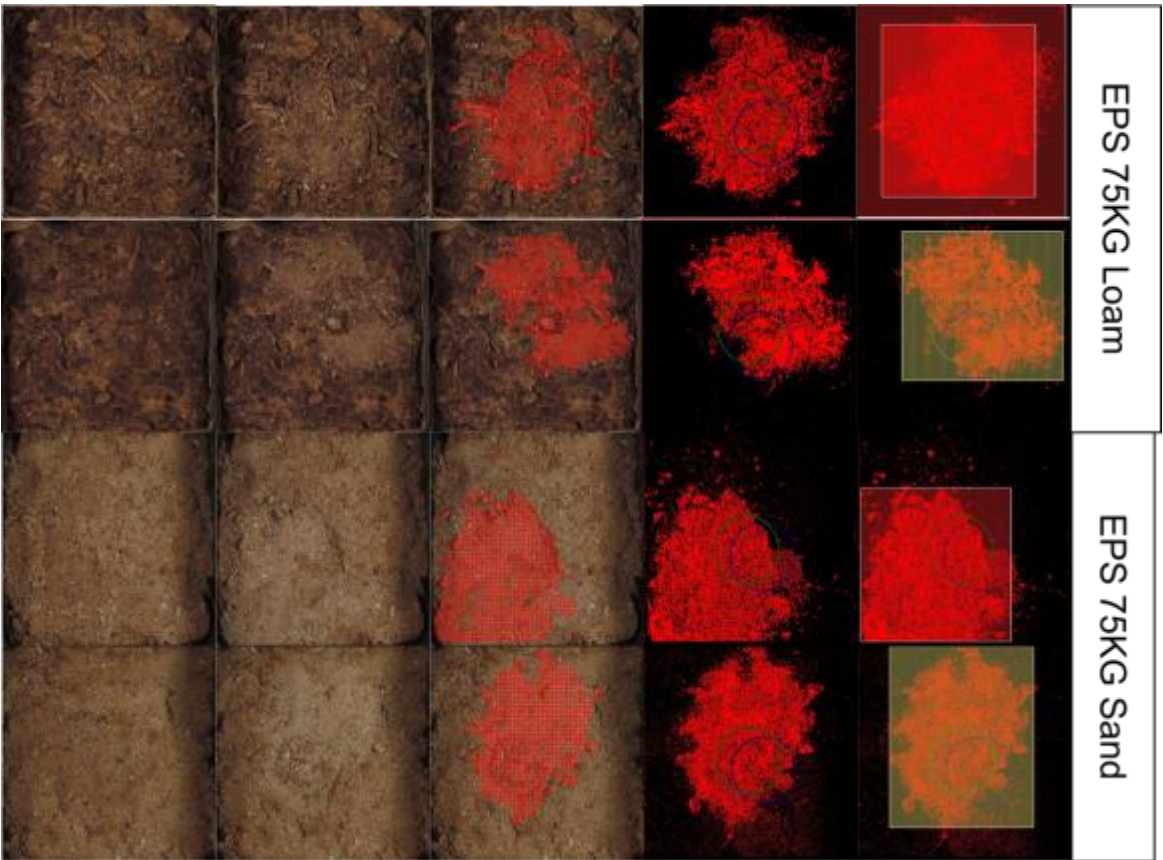




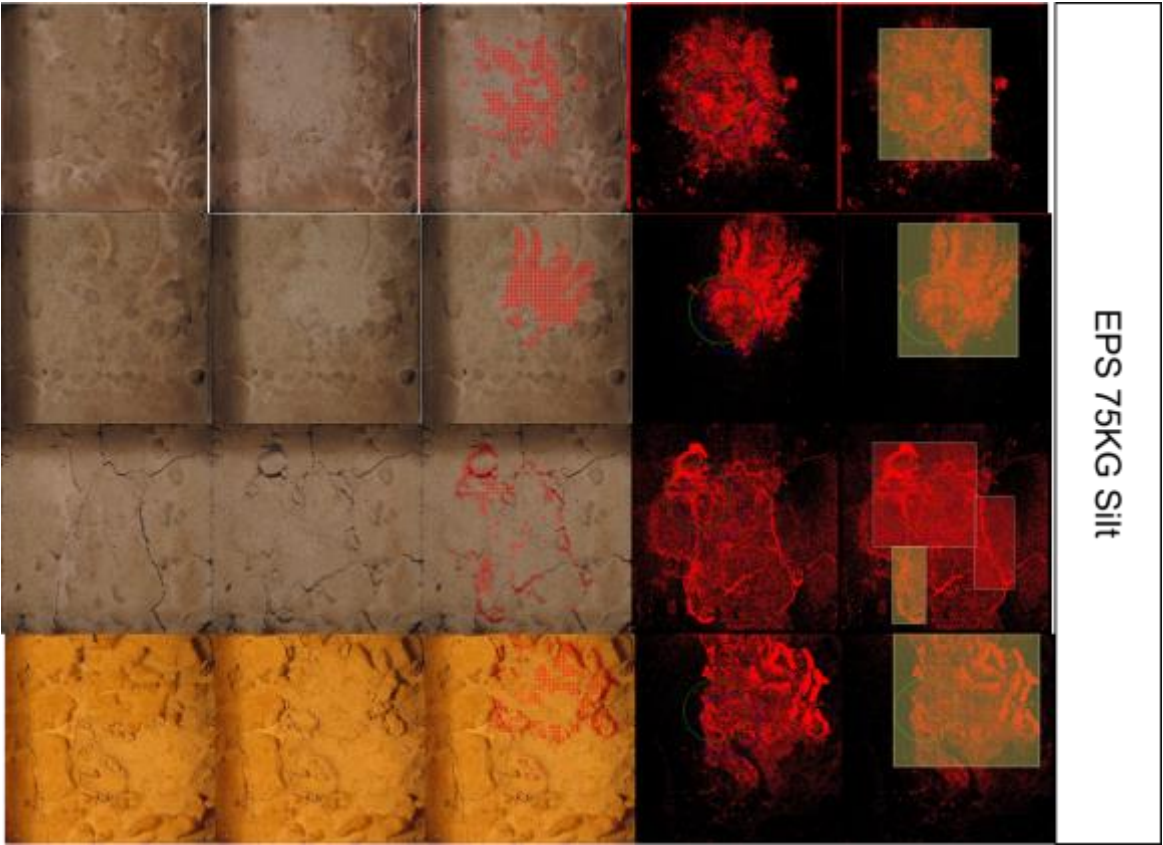


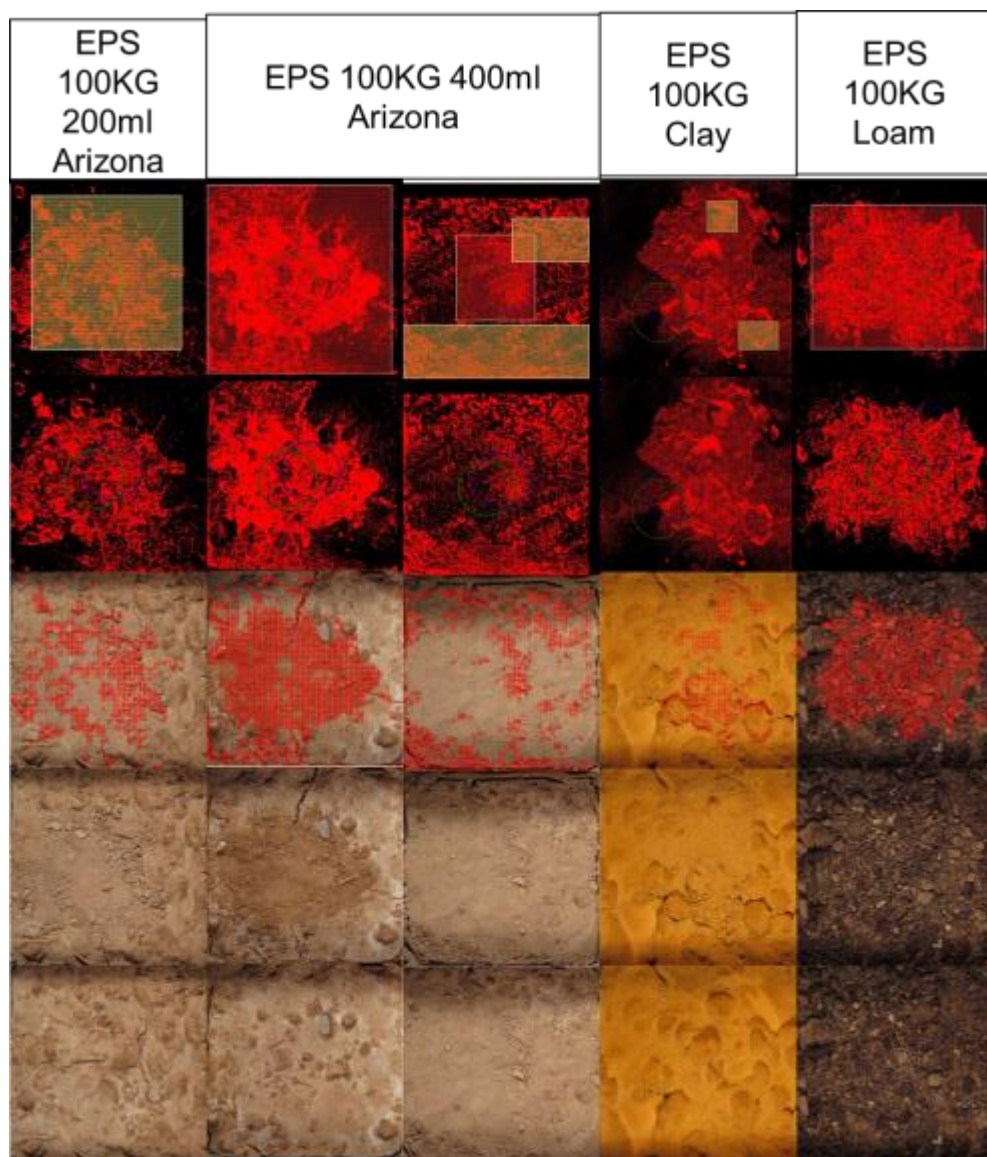


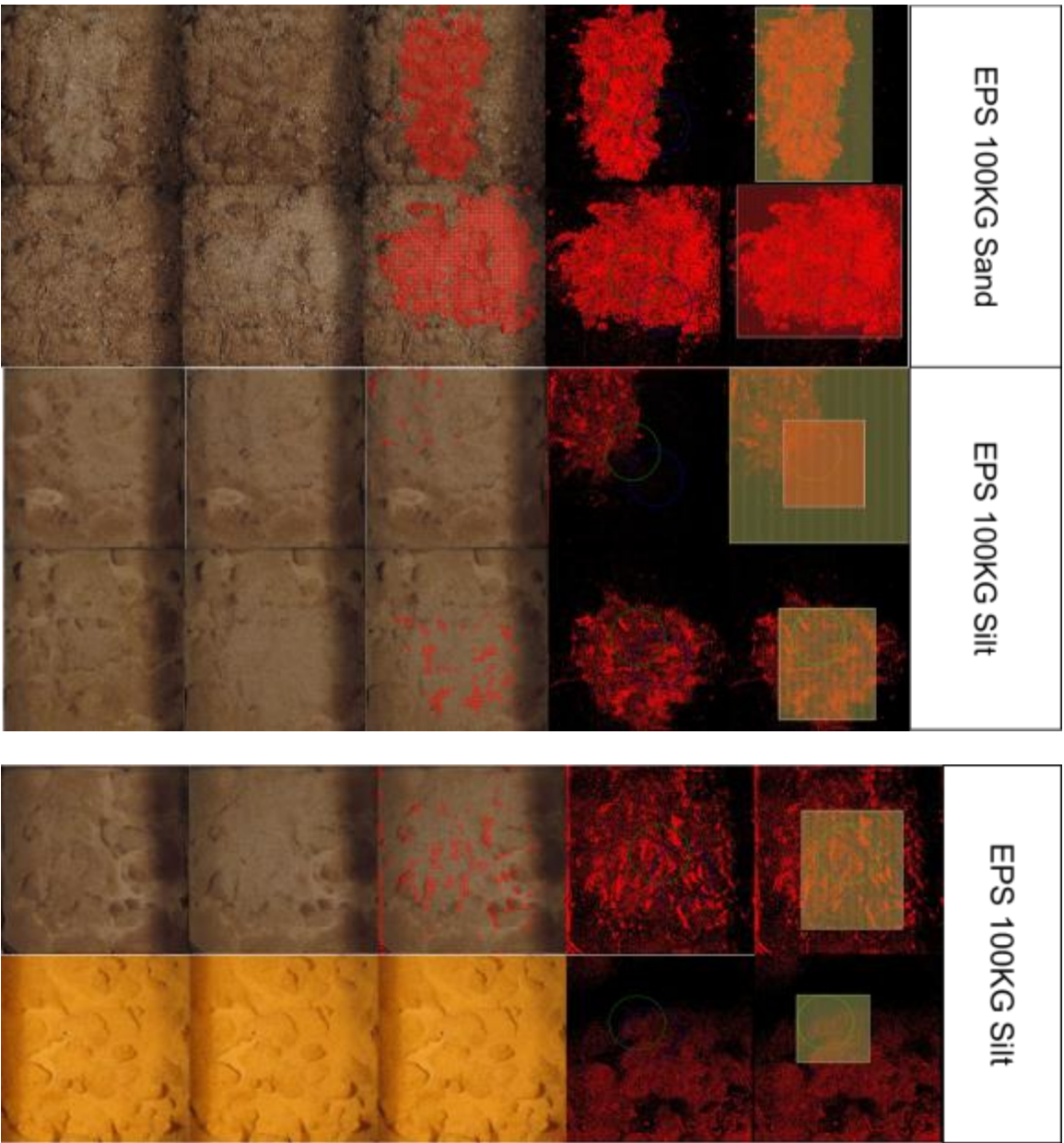
EPS 75KG 200ml Arizona					EPS 75KG 400ml Arizona					EPS 75KG Clay				
														
														
														
														
														







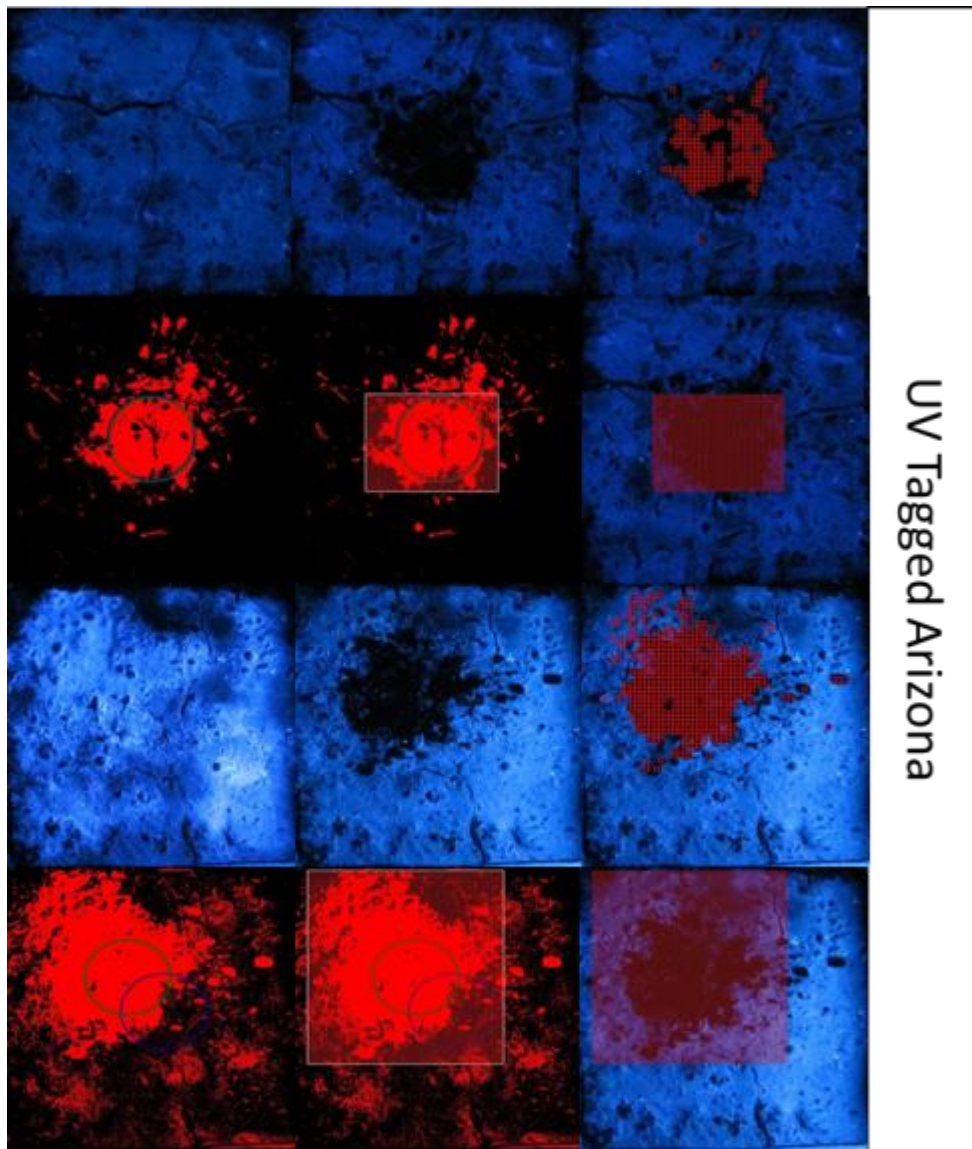




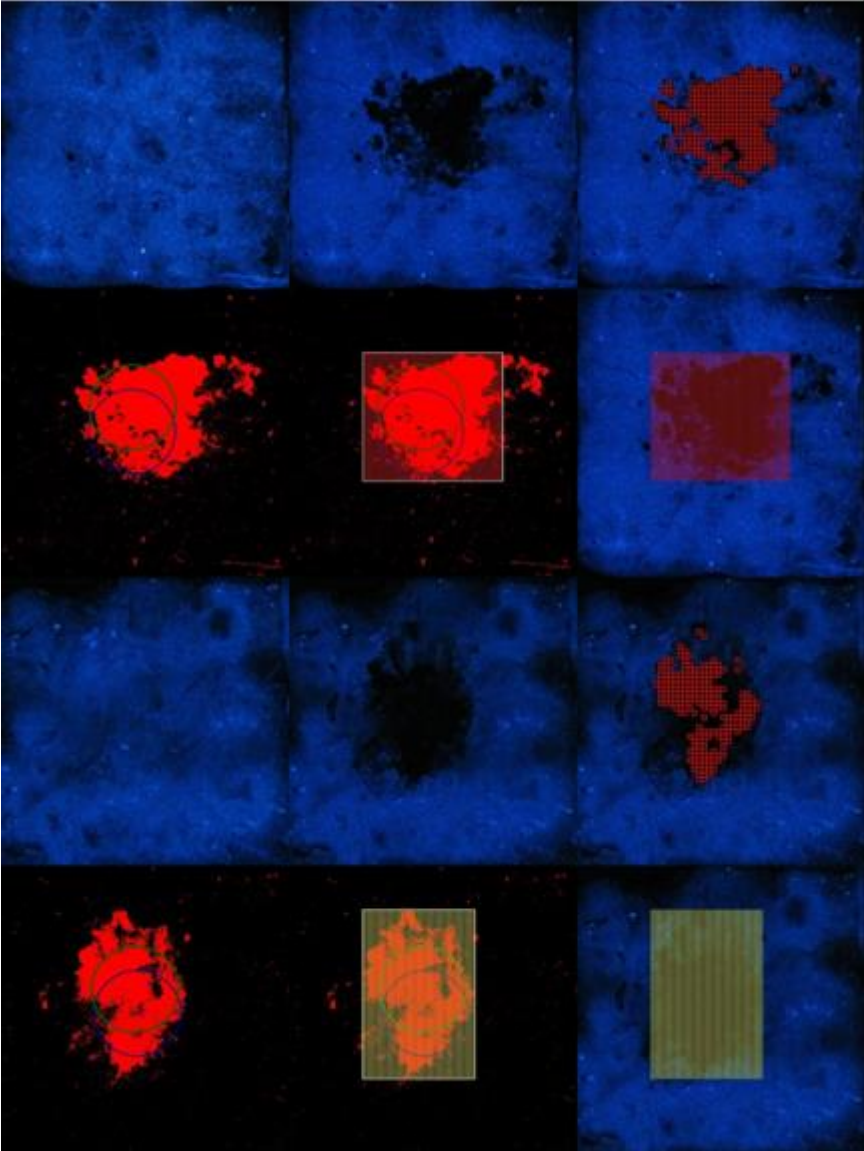


*v. UV Tagged Bench Testing Plots*

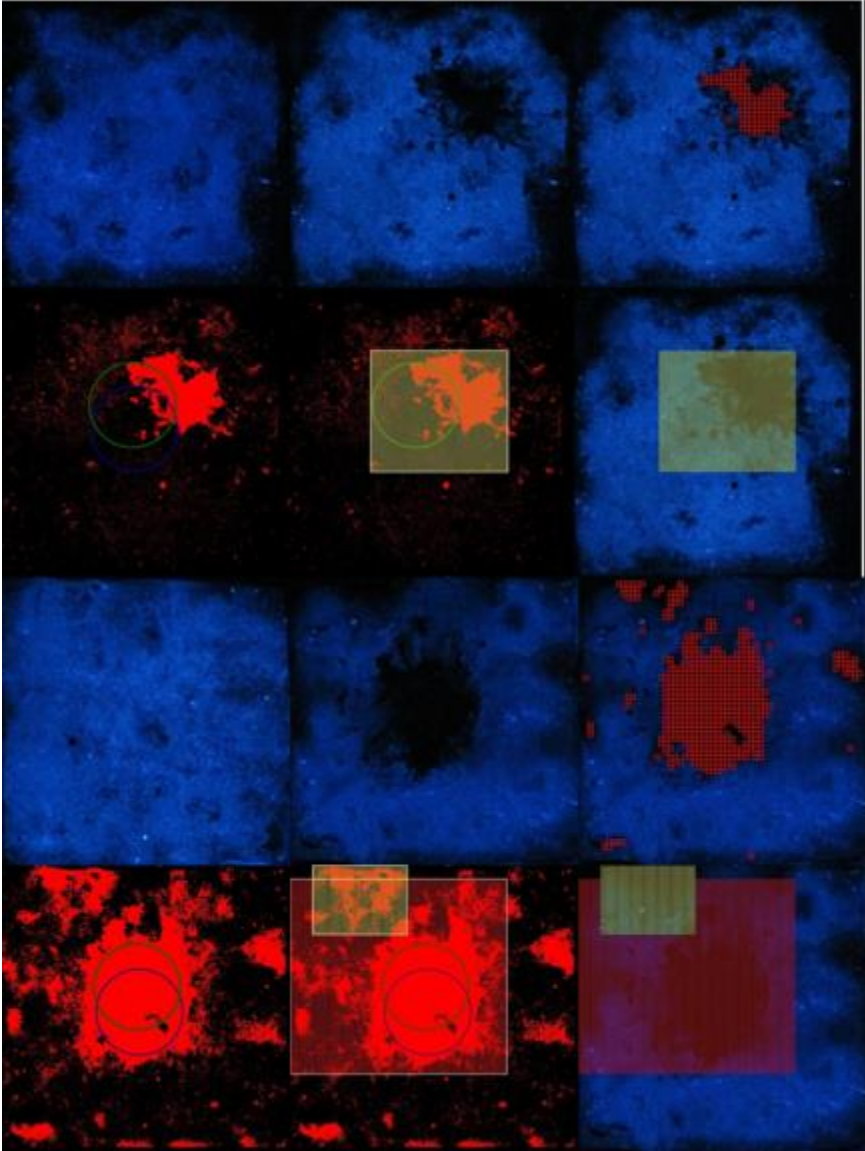
Sets of six images, three images in two rows are shown where the first image is treated only with a UV tagged material, the second image is the disturbance image, the third image is the second image with the change difference overlaid, the fourth image is the change image alone, the fifth image is the ADDS processed change image, and the sixth image is the ADDS detection overlaid on the disturbed image.



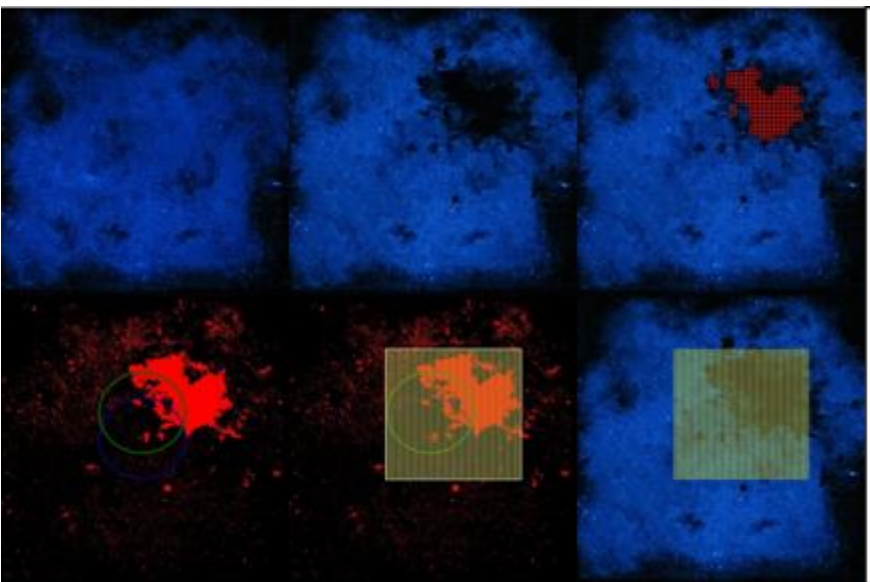
## UV Tagged Clay



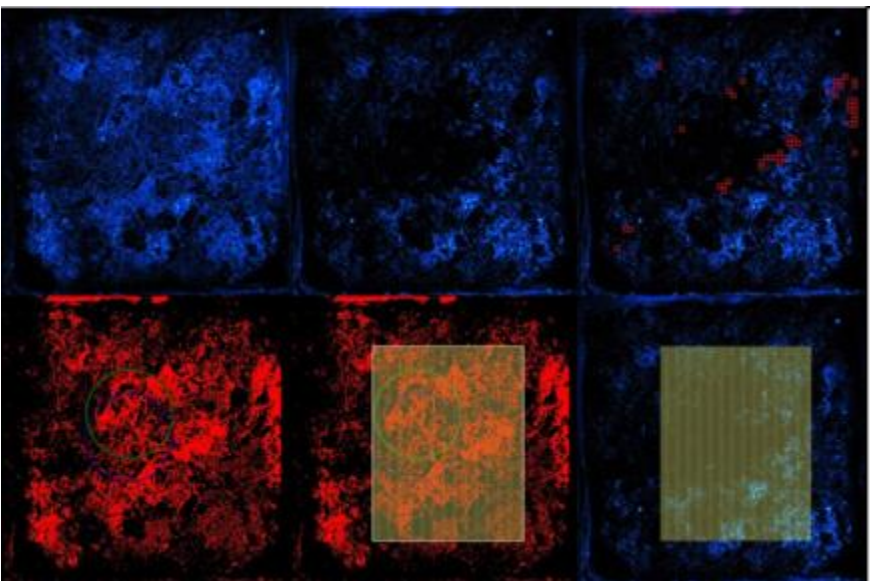
## UV Tagged Clay



UV Tagged Clay

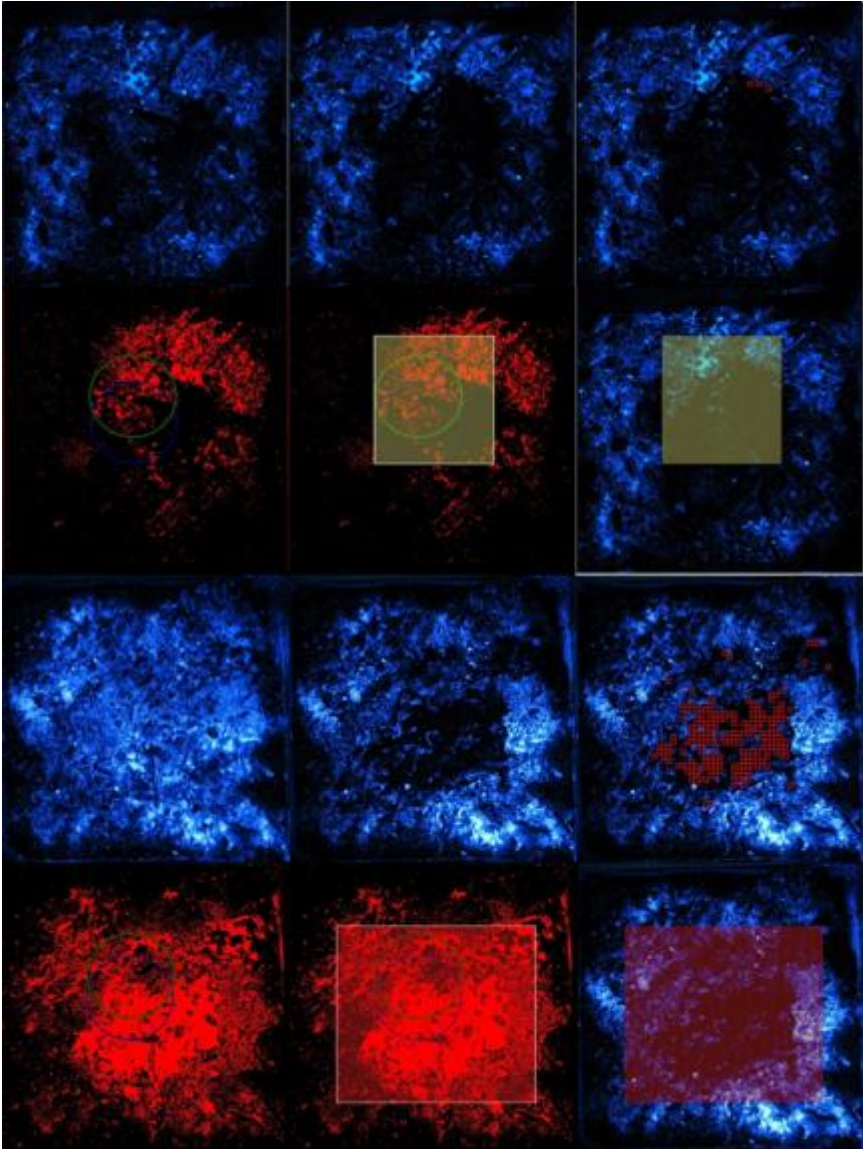


UV Tagged Loam



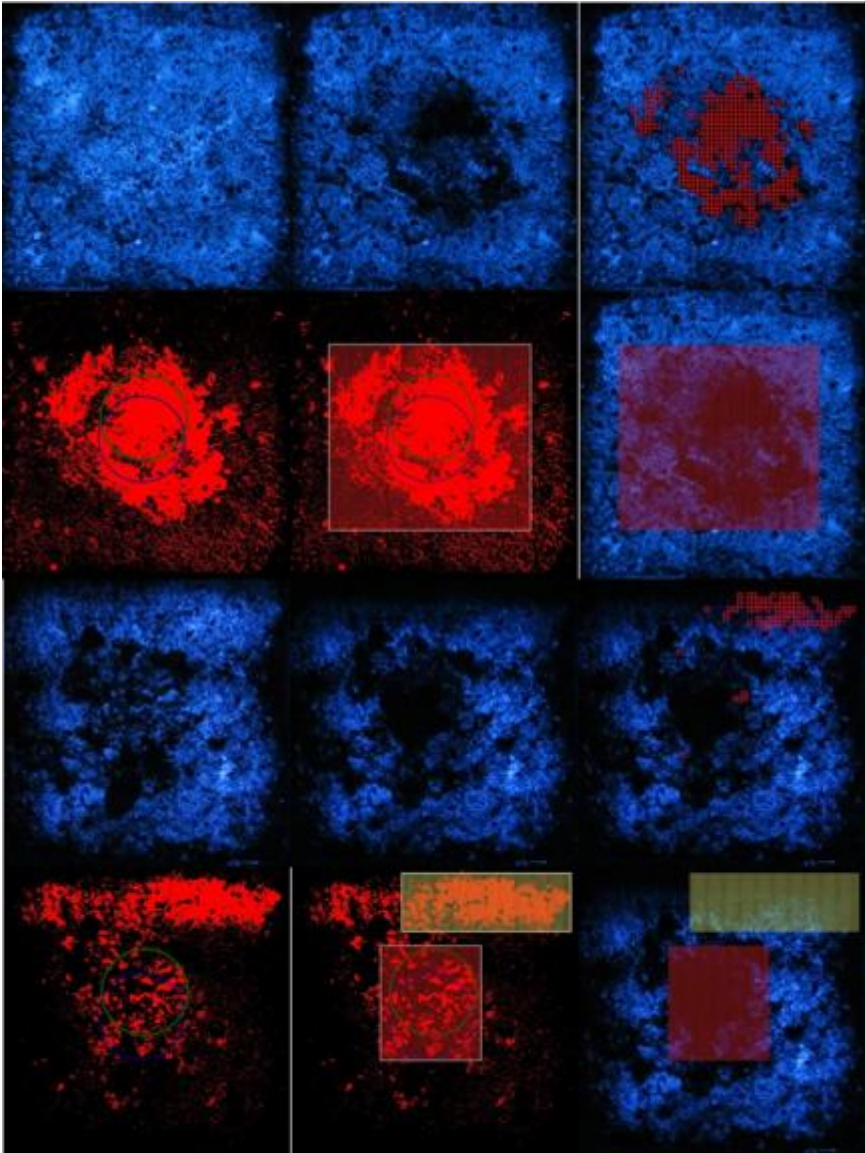


## UV Tagged Loam

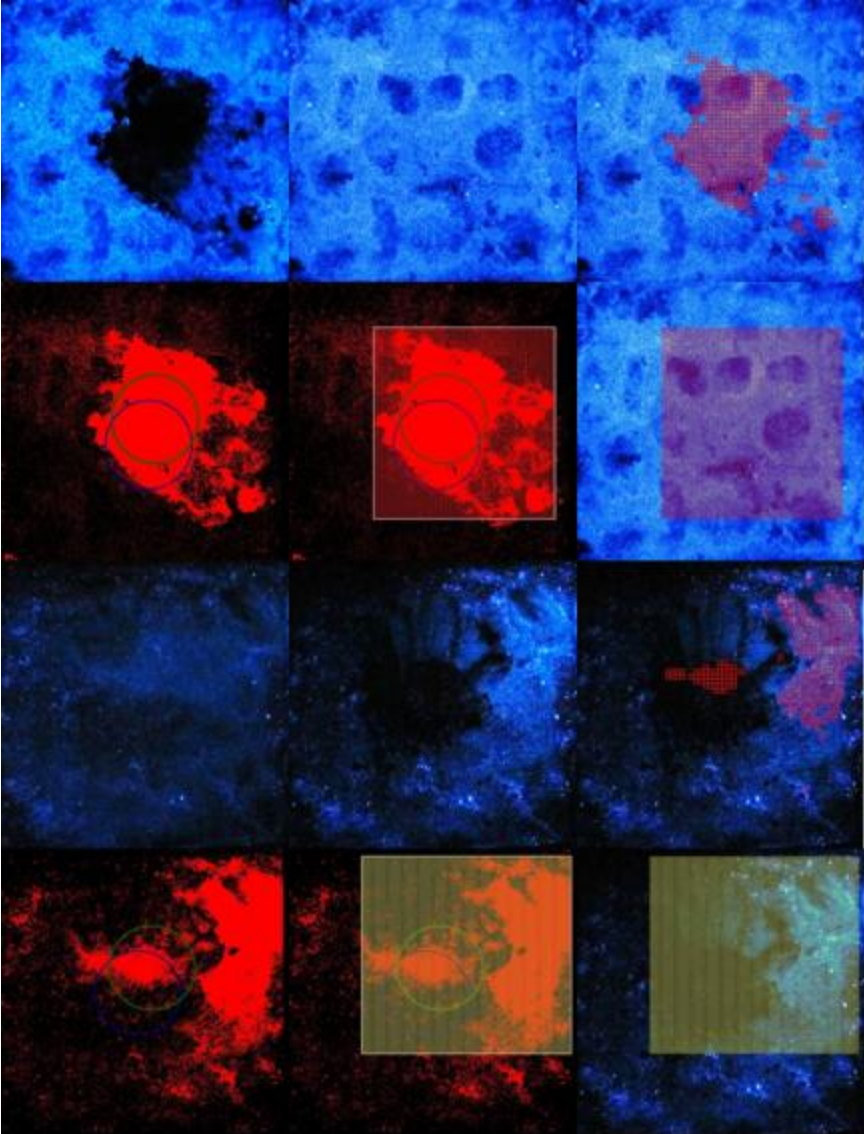




## UV Tagged Sand

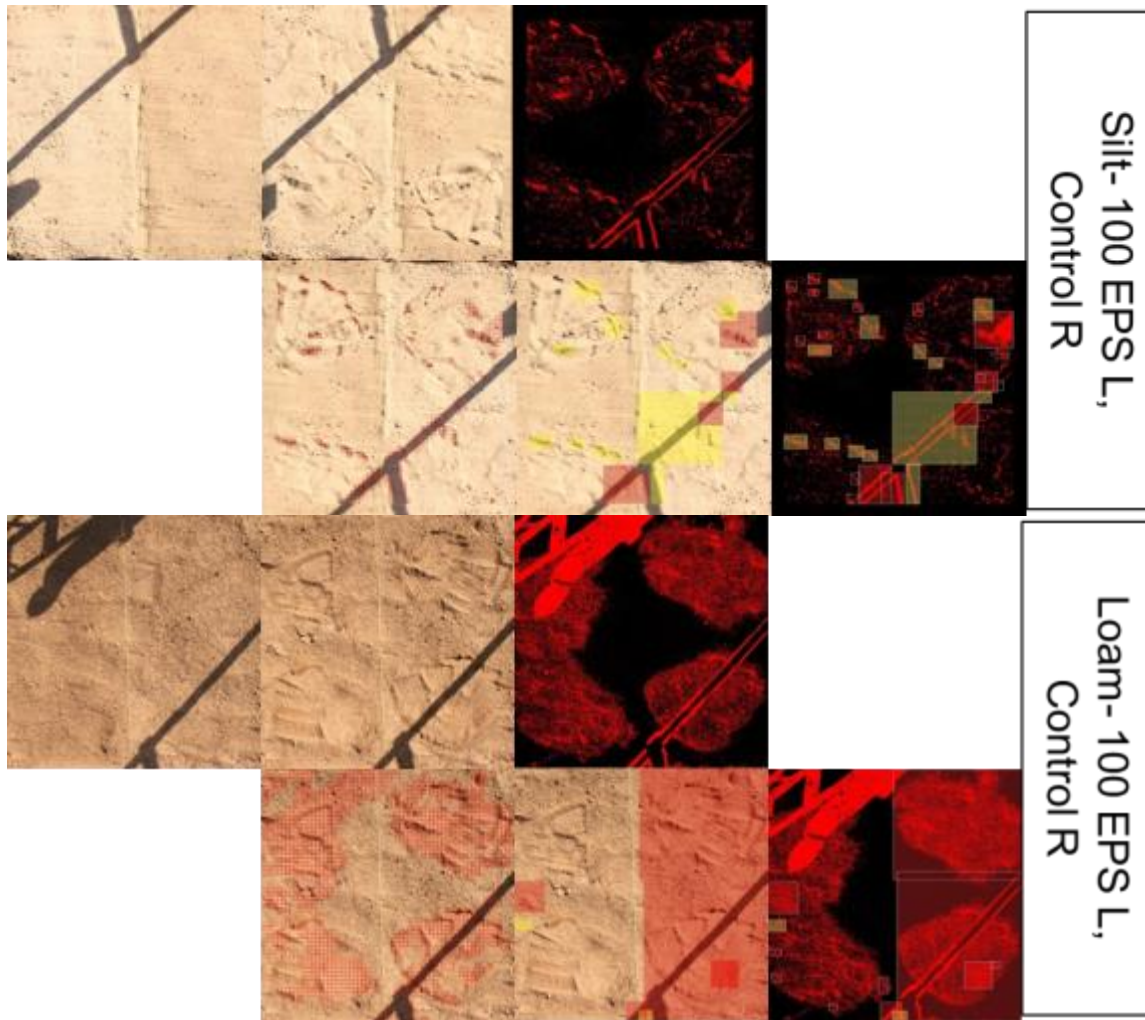


UV Tagged Silt

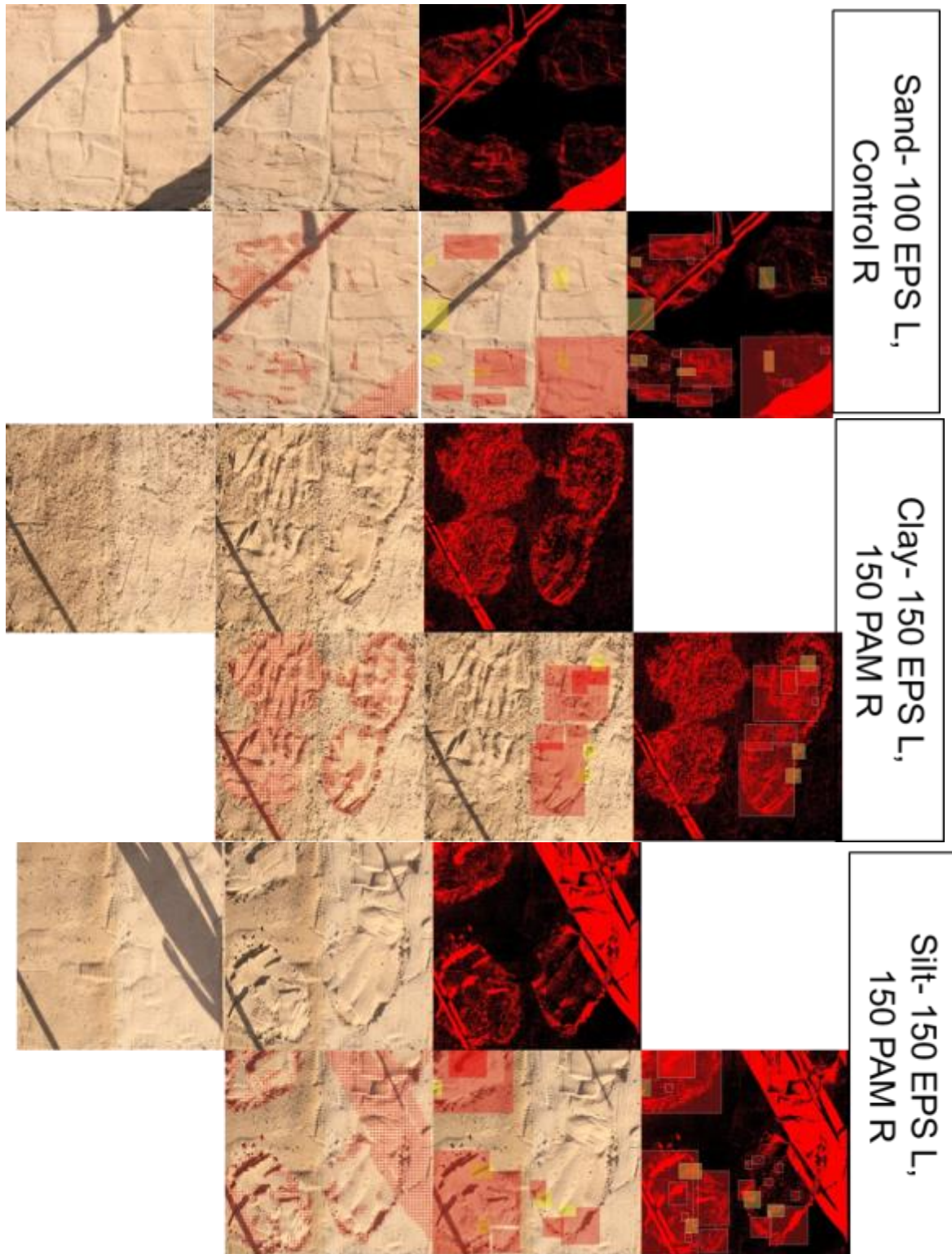


*w. Appendix F- Large Plot Testing Results*

Large scale testing plots where two materials are applied to an individual plot, one on the left and one on the right. The first image is the pre-disturbance or implanted image, the second image is the disturbed or implanted image, the third image is the change difference between the first two images, the fourth image is the post disturbance image with the change image overlaid, the fifth image is the post disturbance image processed by the ADDS system, and the sixth image is the change detection image with the ADDS significant interval boxes overlaid. The label on each figure identifies the soil type (either silt, clay, loam, and Arizona), the material, EPS (exopolysaccharide), PAM (polyacrylamide), chitosan (Chit), and the tagged UV material, and the rate at which they were applied in kg/acre.

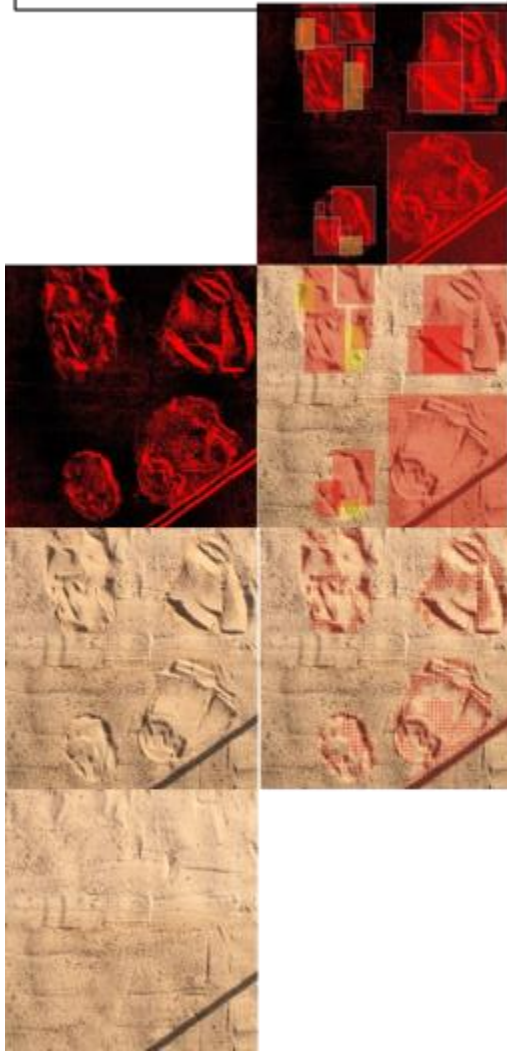




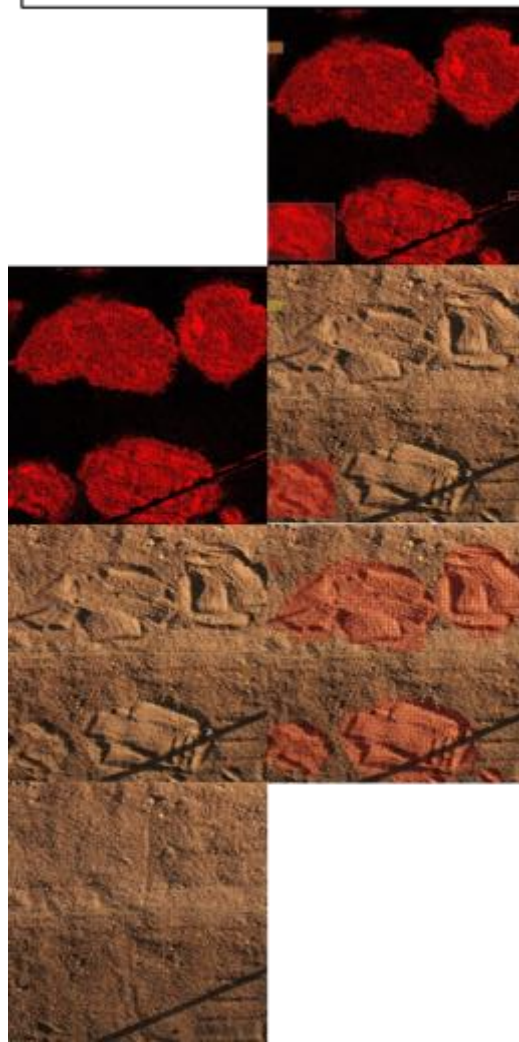


Note- A shadow introduced significant error on the PAM side

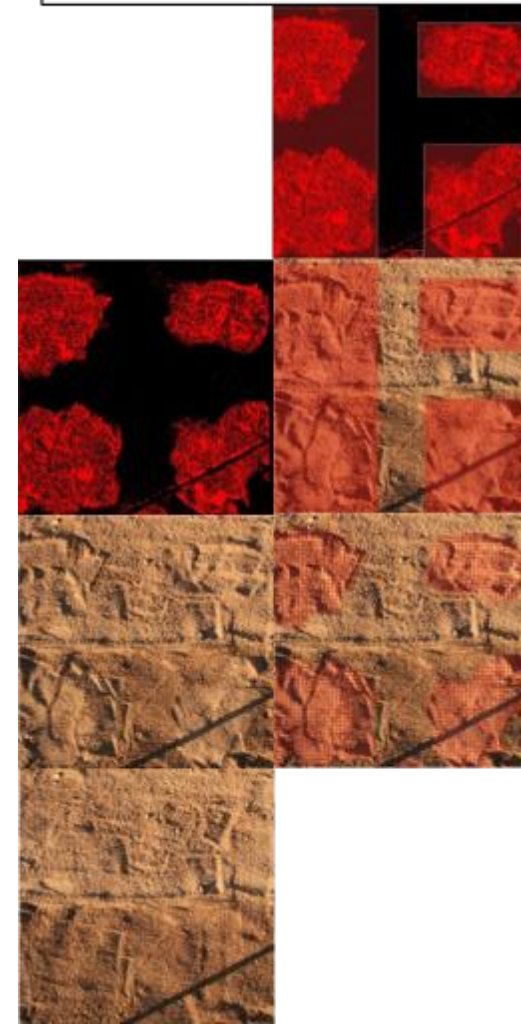
Sand- 150 EPS L,  
150 PAM R



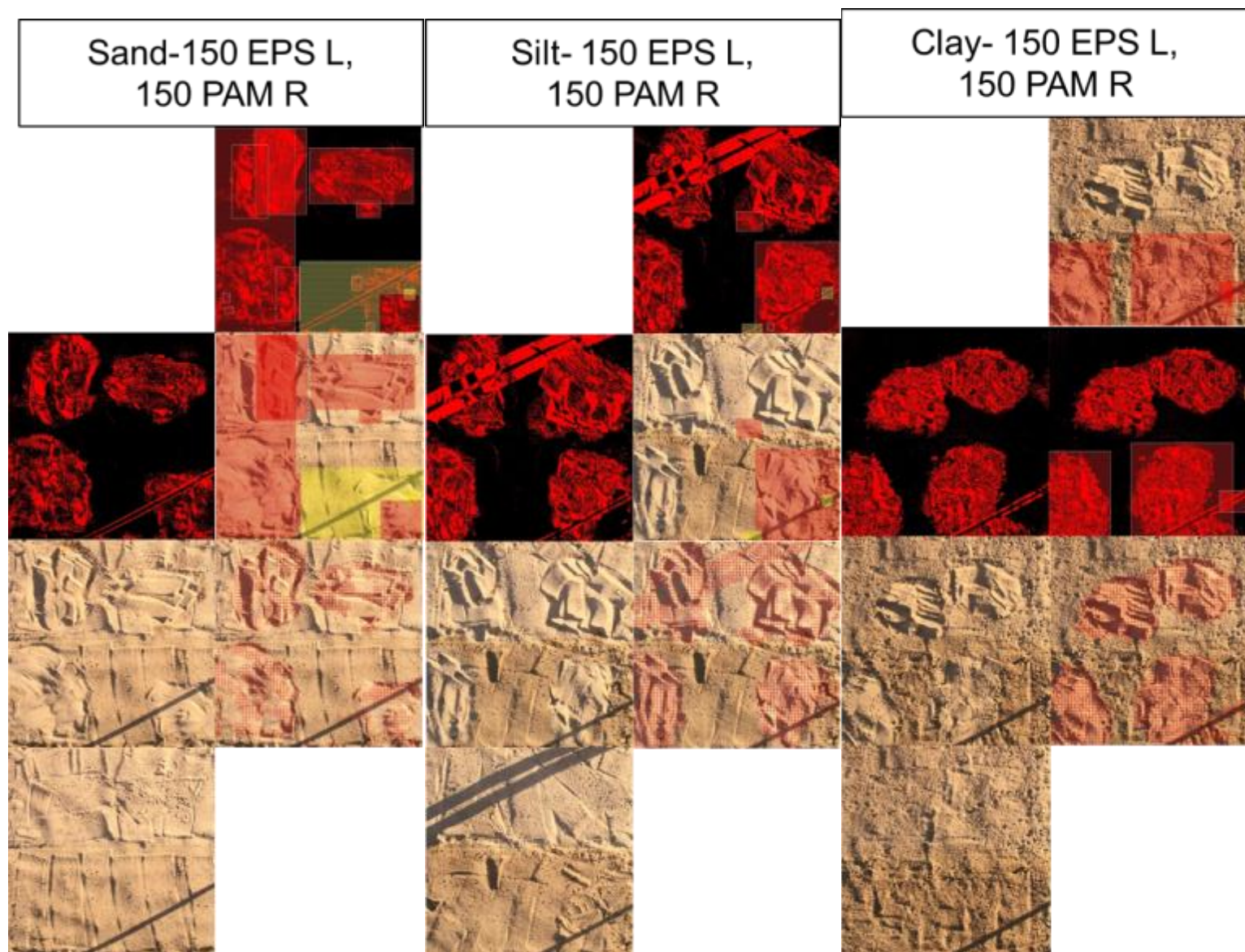
Loam- 150 EPS L,  
150 PAM R



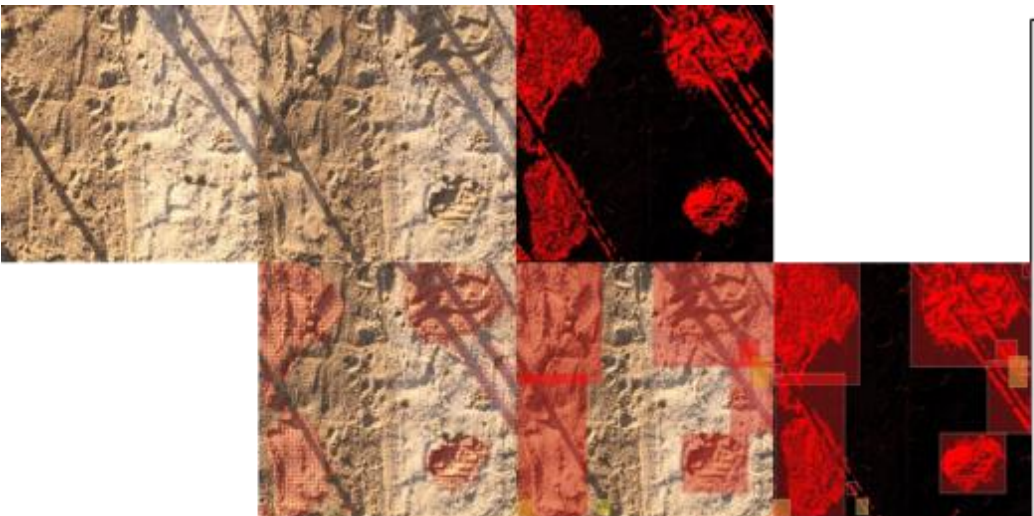
Loam- 150 EPS L,  
150 PAM R



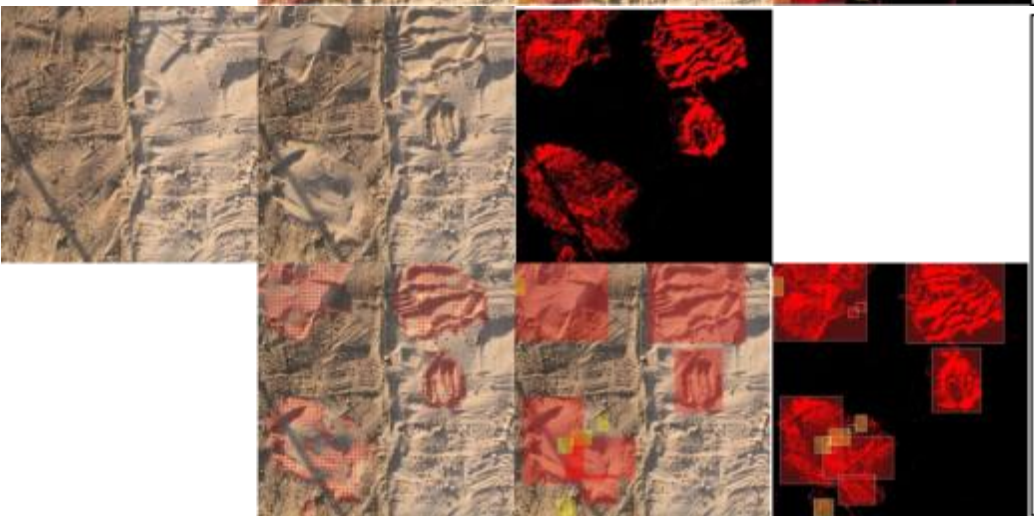




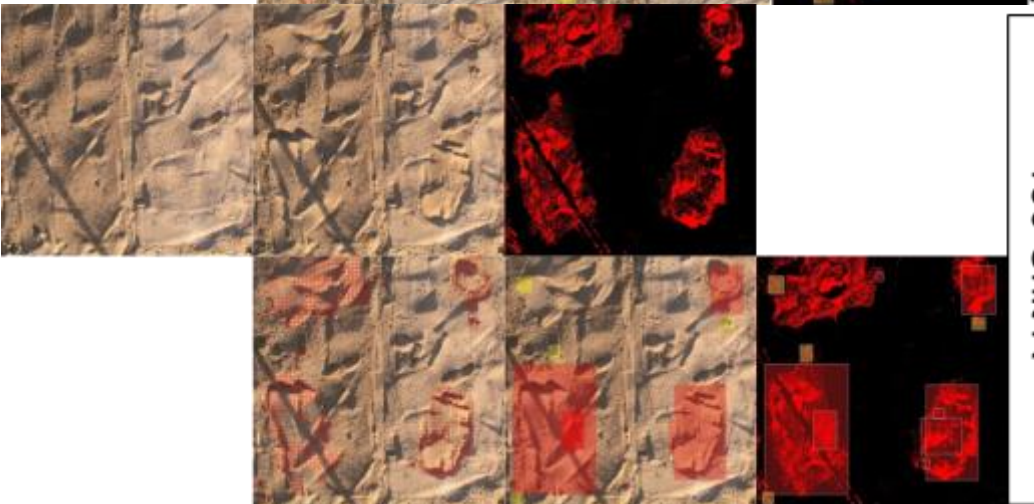
Clay- 150 EPS L,  
150 Chit R



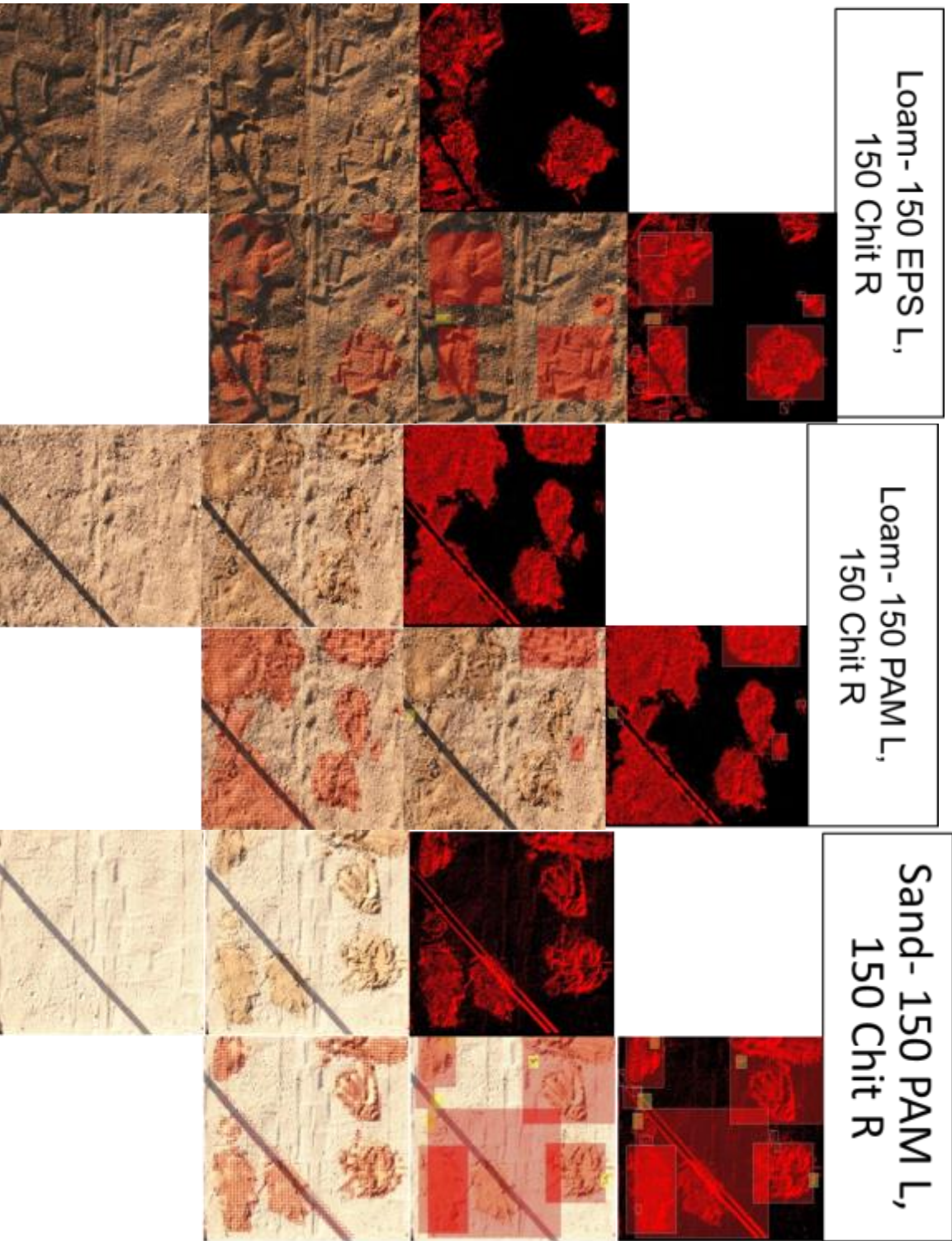
Silt- 150 EPS L,  
150 Chit R



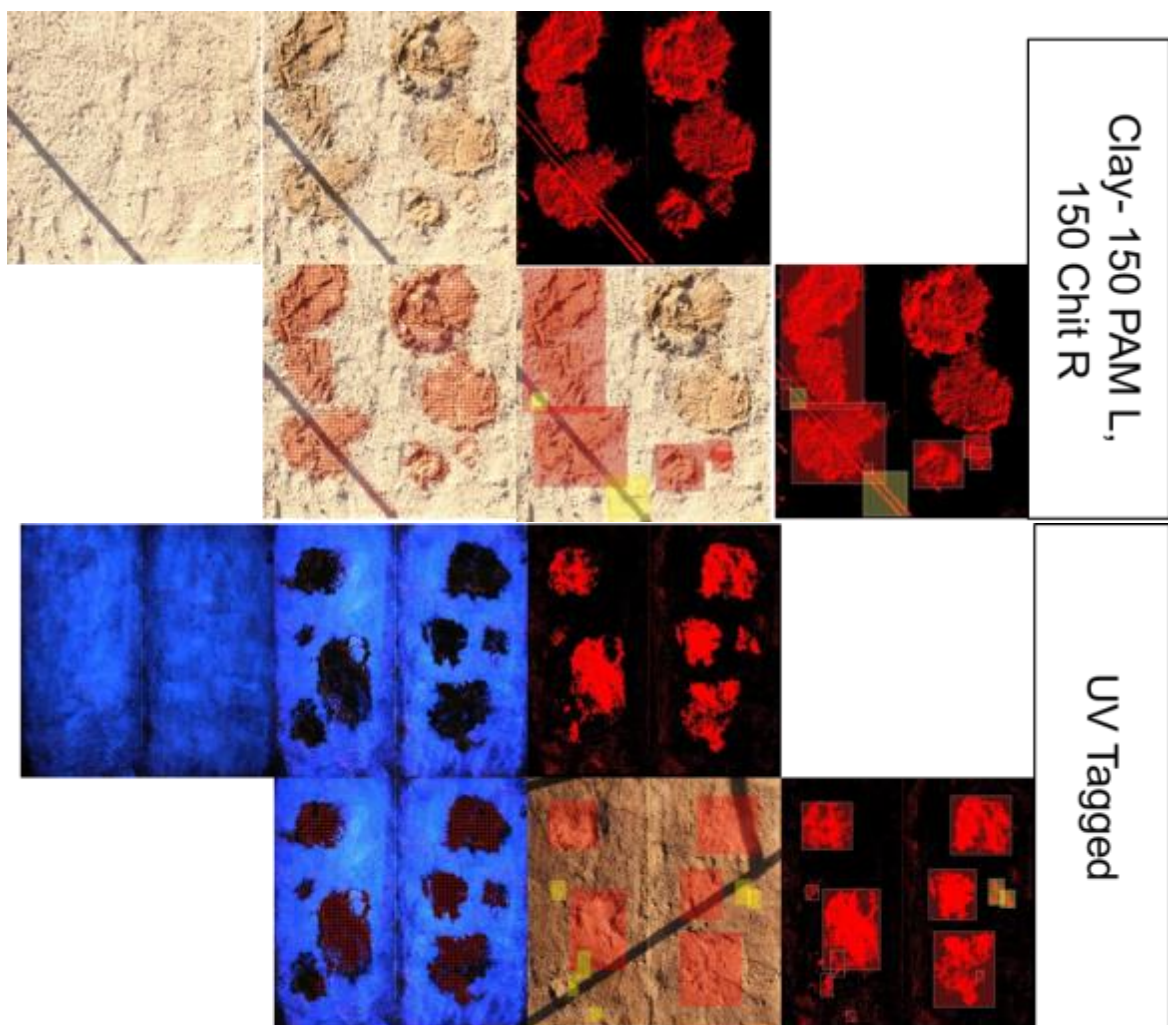
Sand- 150 EPS L,  
150 Chit R



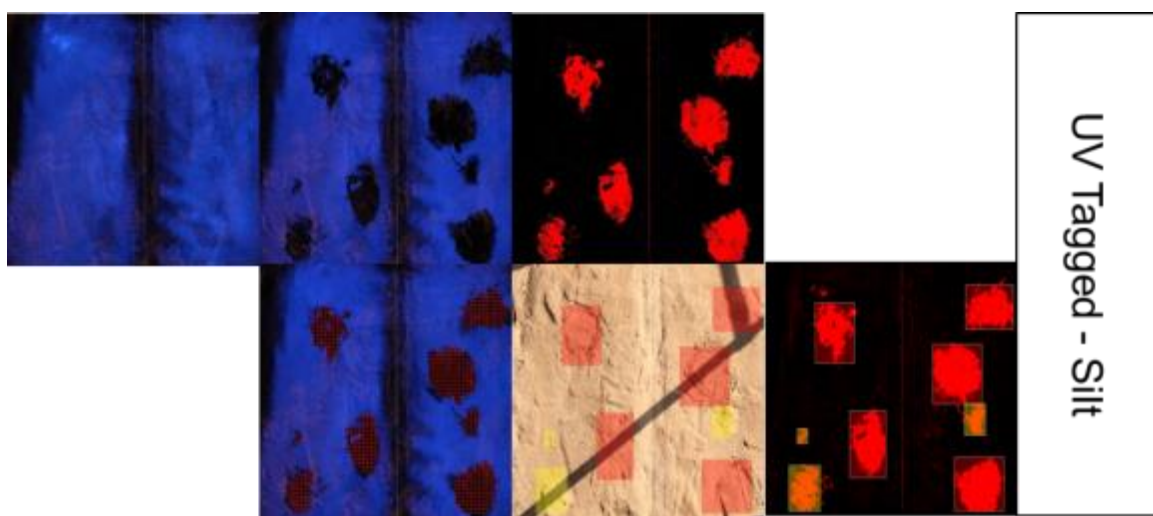


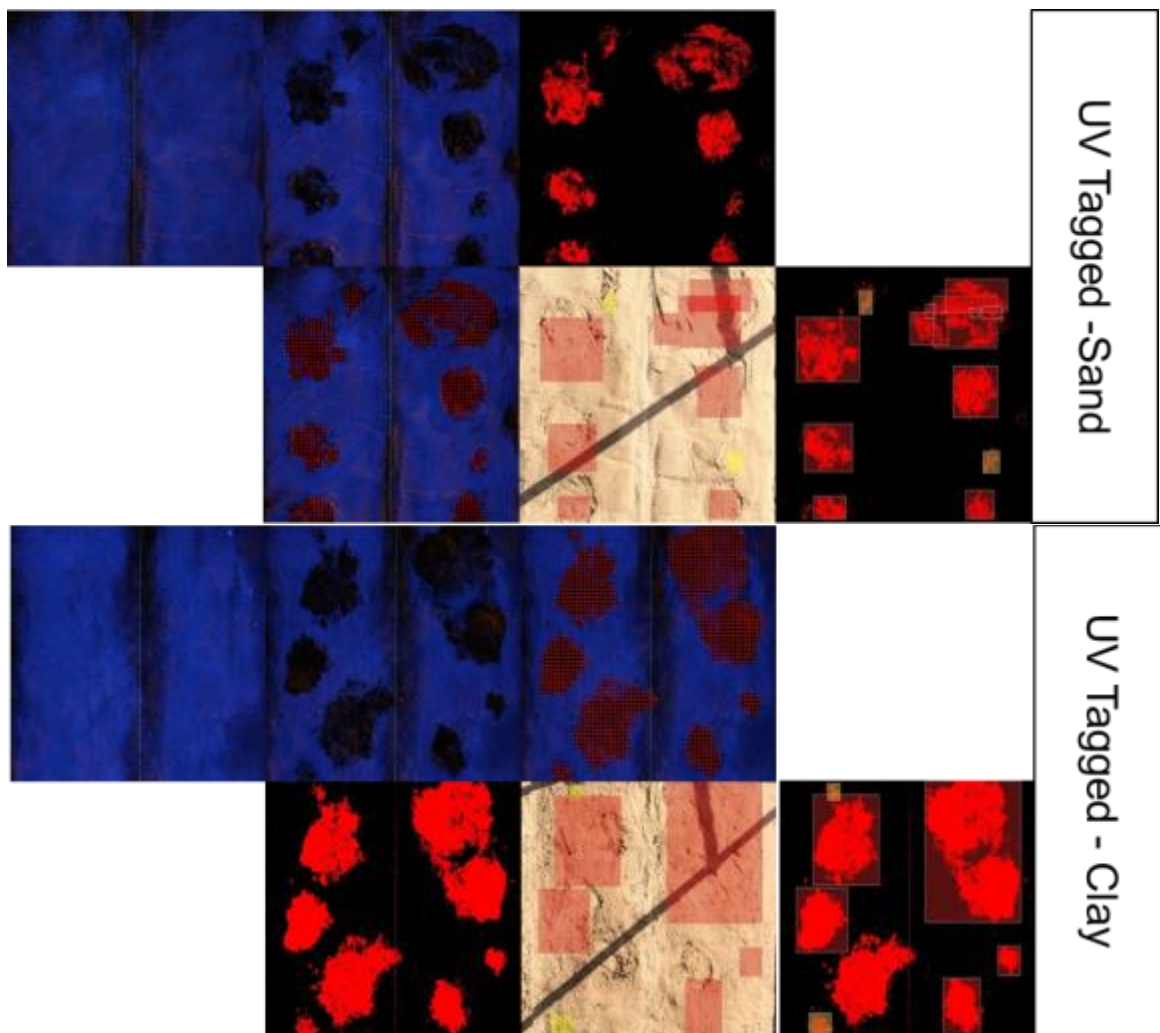






NOTE- Marked one area smaller and labeled it yellow but still registered





NOTE- Missed one object, could be due to the simplicity of the Object Recognition program